A satellite view of the North Sea region, showing the coastline of Europe and the North Atlantic. The sea is dark blue, and the land is green and brown. A color overlay on the sea indicates tidal range development, with lighter colors (yellow and orange) showing higher tidal ranges and darker colors (blue and green) showing lower tidal ranges. The text is overlaid on the sea area.

# Temporal development of the tidal range in the southern North Sea

Florenz A.P. Hollebrandse



# Temporal development of the tidal range in the southern North Sea

Florenz A.P. Hollebrandse

A dissertation submitted in partial fulfilment of the requirements for the degree of  
Master of Science in Civil Engineering, specialisation Hydraulic Engineering and Fluid Mechanics

Faculty of Civil Engineering and Geosciences  
Delft University of Technology, Delft, The Netherlands

June 2005



## Abstract

The North Sea is a shallow sea on the Eurasian continental shelf. This study focuses on the temporal development of the tidal range in the southern part of the North Sea. Records of annual tidal range data from gauging stations along the Dutch coast show in general an increasing trend perturbed by random fluctuations. Changes in tidal ranges are caused by natural (periodic) processes and anthropogenic effects.

To examine the impact of human measures on the tidal range, the natural components are separated from the recorded tidal range. The only natural cycle significantly present in annual mean tidal range records is the nodal tide with a period of 18.6 yr and amplitudes of 0.2-2.0%. The short-term (few years) fluctuations are qualitatively similar for different stations with individual peaks occurring at the same time. This indicates that the noisy signal is caused by regional processes and not by measurement errors (as is not expected using annual mean values).

The residual tidal range shows that apart from noise the tidal range remained constant from the early 19<sup>th</sup> century till circa 1955. During the period 1955-1980 a gradual increase in tidal range is observed at all stations. Although differences exist between the stations, their trends are very similar. Because the short-term and the long-term developments are similar, it is meaningful to construct an artificial average of the tidal range records from different stations. In this study the average of the Dutch stations and the average of the German stations are compared [see figure 1]. The graph shows that a similar gradually increasing trend is observed at the Dutch and German coast.

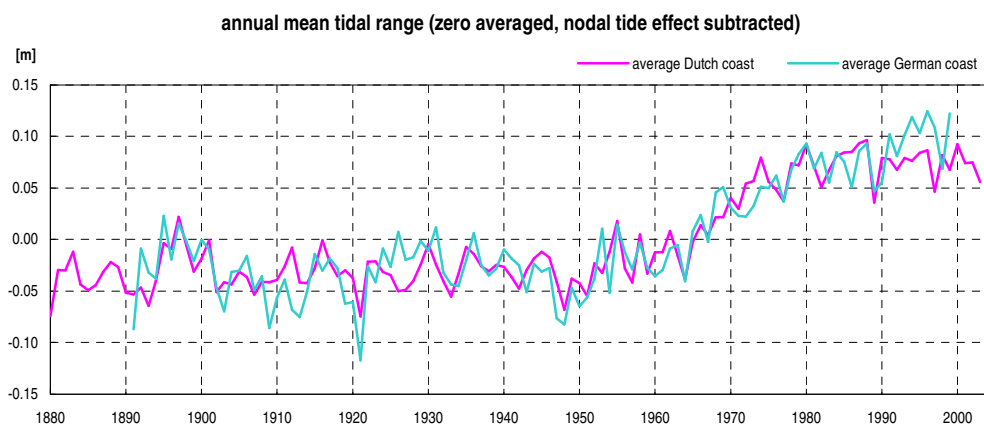


**Figure 1: Tidal range development at the Dutch and German coast. Records of individual stations are normalized to a zero-average record and the nodal tide cycle is subtracted. The average of the Dutch stations Vlissingen, Burghsluis, Hoek van Holland, Scheveningen and IJmuiden and the average of the German stations Borkum, Norderney, Lighthouse Alte Weser, Helgoland, Wittdün and List are shown.**

The hypothesis that this trend is caused by coastal engineering in the River Rhine delta, is tested. A conceptual model is applied in which the North Sea is schematised to a rectangular basin. Estuaries with tidal prisms corresponding to Zeeland estuaries are included in this model. The model shows that the tidal range increases at the mouth of the estuary when it is closed. This increase decays along the Dutch coast with a typical length with an order of magnitude of 150 km [see figure 2]. The results of the conceptual model are supported by a detailed model study incorporating the shape of the coast line and the bathymetry [Langendoen, 1987]. Both analyses suggest strong evidence that the tidal range is not significantly affected north of Den Helder after a closure of an estuary in the Zeeland delta. This implies that the observed trend at the Dutch and German coast does not have as common cause coastal engineering in the River Rhine delta.

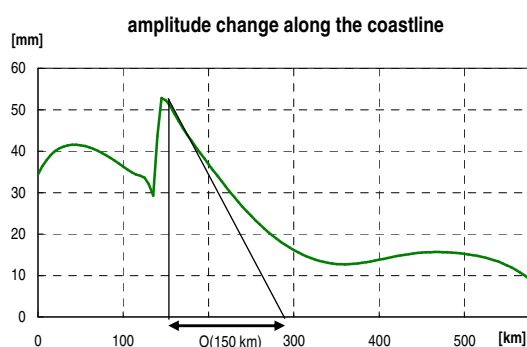


**Figure 2: Change in  $M_2$  amplitude (approximately half the magnitude of the tidal range) along the Dutch coastline after the closure of an estuary at location E. The tidal prism of this estuary is  $\sim 1.3 \cdot 10^9 \text{ m}^3$ .**

A satisfactory explanation for the trend since 1955 is not given in this report. However, our results suggest that the most likely cause is complex changes in the oceanic and the shelf sea system due to meteorological and astronomic changes. Analyses of tidal spectra based on hourly observations can give more insight into the processes involved.

# Contents

	Abstract	1
1	Introduction	6
	1.1 Background	6
	1.2 Study aims	7
	1.3 Problem approach	7
	1.4 Theoretical background and research to date	9
SECTION 1: Statistical evaluation of tidal range records		
2	Methodology statistical evaluation	14
	2.1 Visual inspection	14
	2.2 Spectral analysis	14
	2.3 Multiple linear regression analysis	15
	2.4 Short-term behaviour	16
	2.5 Long-term behaviour	16
3	Available tidal data	18
	3.1 Tide gauging stations and measurement records	18
	3.2 Accuracy and errors	19
	3.3 Data preparation for the analyses	19
4	Interpretation of the tidal range records	20
	4.1 Visual inspection	20
	4.2 Determination of the tidal constituents dominant in the mean tidal range	21
	4.3 Evaluation of the nodal tide phase	22
	4.4 Evaluation of the nodal tide amplitudes for each station	23
	4.5 High frequency residual tidal range	24
	4.6 Long-term trends	25
	4.7 Analysis of breakpoints	27
	4.8 Summary statistical analysis	29
SECTION 2: Modelling inlet closures		
5	Conceptual model of inlet closures	30
	5.1 Schematisation and model description	30
	5.2 Modelling reference case	32
	5.3 Sensitivity analysis of boundary conditions	34
	5.4 Modelling closures of estuaries	36
	5.5 Interpretation of model results	41
6	Conclusion	44
	6.1 Joint interpretation of statistical and model analyses	44
	6.2 Final conclusions	45
	6.3 Application and relevance of the conclusions	46
	6.4 Recommendations	46

References	47
------------	----

## APPENDICES:

A1	Multiple linear regression (MLR) analysis	49
A2	Spectral analysis	50
A3	Analysis of breakpoints in tidal range records	51
A4	Tidal periodicities	53
A5	Tide gauging stations	55
A6	Plots of tidal records	57
1	Vlissingen	58
2	Burghsluis	59
3	Hoek van Holland	60
4	Scheveningen	61
5	IJmuiden	62
6	Den Helder	63
7	Oudeschild	64
8	Den Oever	65
9	Kornwerderzand	66
10	Harlingen	67
11	West-Terschelling	68
12	Schiermonnikoog	69
13	Delfzijl	70
14	Euro Platform	71
15	Newlyn	72
16	Average Netherlands (Vlissingen, Burghsluis, Hoek van Holland, Scheveningen and IJmuiden)	73
17	Average German North Sea islands (Borkum, Norderney, Lighthouse Alte Weser, Helgoland and Wittdün)	74
18	All stations MTR trend anomaly	75
A7	Irregularities in tidal range records	76
A8	Phases periodicities 8.85-18.6 yr	79
A9	Results of MLR analysis of tidal ranges	80
A10	Long-term trends	81
A11	Delft3D-FLOW model description	82
A11	Delft3D-FLOW model description	83
A12	Evaluation of model adjustment time	86
A13	Wave amplification in an estuary	87
A14	Simulation results	89

With thanks to Gerben de Boer, Jelmer Cleveringa, Koos Doekes, Edwin Elias, Walter Jacobs, Elizabeth Macleod, Julie Pietrzak, Dick Rakhorst, John de Ronde, Marcel Stive and Tjerk Zitman.

# 1 Introduction

This chapter describes the background and aims of this study. Section 1.1 gives an introduction to the North Sea and the complex temporal development of the tides. The aims of this study are presented in section 1.2. In section 1.4 we outline the approach to answer the research questions. This study builds on the current scientific knowledge on tides and specific studies on the tidal regime in the North Sea, outlined in section 1.4.

## 1.1 Background

The North Sea is a shallow sea on the western border of the Eurasian shelf [see figure 1.1]. The North Sea is bounded by Great Britain in the west, The Netherlands and Germany in the south and Denmark and Norway in the east. The northern end has an open connection with the North Atlantic Ocean. The surface area of the North Sea is 750,000 km<sup>2</sup> and the depth varies between 200 m near the end of the shelf to 20 m at the south-east coastline. The tides are a dominant hydrodynamic feature in the North Sea driven by the tidal wave progressing through the North Atlantic Ocean.

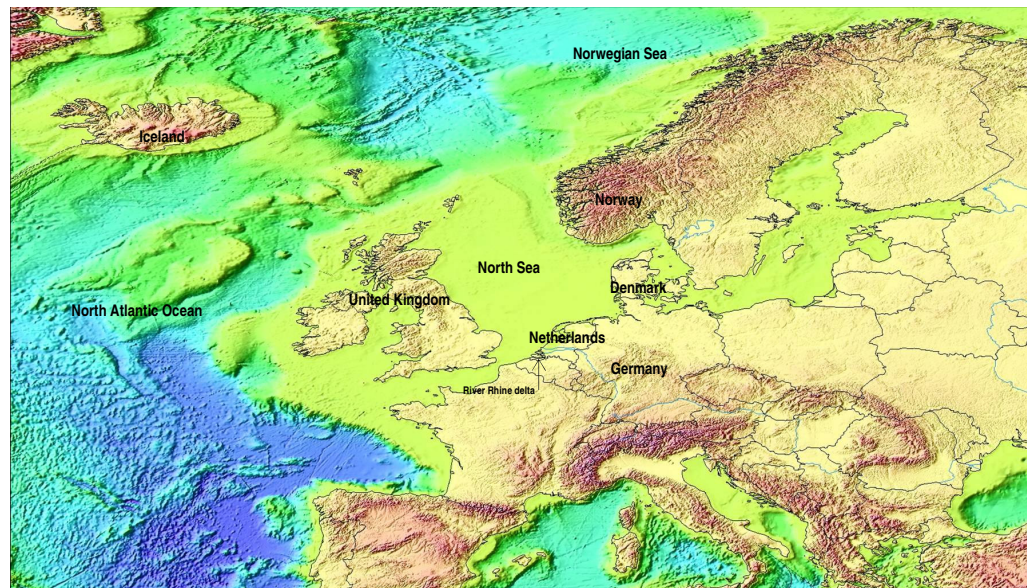


Figure 1.1: Location of the North Sea [U.S. Geological Survey, 2005]

Mean sea level changes around the world are extensively studied and well known. The rate of change of the mean North Sea level over the last century is of order 1-2 mm/yr [Woodworth *et al.*, 1991]. It is obvious that sea defences need to be improved to keep the same level of protection against storm surges. This need is increased by higher surge water levels due to more severe storms [Flather and Williams, 2000].

Beside change of mean sea level and storm surge levels, the mean high and low water levels change with time. The difference between high and low water level, the tidal range, is in general increasing along the Dutch coast. It is known that the tidal range is affected by changes in the geometry of the North Sea. This can be a consequence of human interventions e.g. dredging in river mouths, closures of estuaries and inland seas (e.g. the closure of the Zuider Sea in 1932), and other modifications of the coastline [Rakhorst, 2003b]. The geometry can change by natural processes like accretion and erosion in deltas. Beside these changes in the geometry of the shelf itself, changes in the deep ocean tides and changes in meteorological conditions can affect the tidal range [Führböter and Jensen, 1985; Woodworth *et al.*, 1991]. It is known that periodic cycles with periods from 1 year to c. 20,000 yr and larger are present in the tidal movements [Munk and Dzieciuch, 2002; Treloar, 2002], but the processes linking climate changes with the ocean tides, are not well understood.

Looking at the records of tidal range in the North Sea we observe a complex temporal development with periodic cycles, discontinuities due to human interventions and possibly non-periodic trends caused by long-term changes in the North Sea and the North Atlantic Ocean tidal system. To be able to assess what the impact is of anthropogenic effects, e.g. the closures of an estuary, we need to extract natural changes from the recorded tidal range.

## 1.2 **Study aims**

In this study the temporal development of the tidal range along the southern border of the North Sea is evaluated. The aim of this study is to identify which trends are caused by natural processes and which are a cause of anthropogenic effects. Specifically this study aims to give an indication of the distance over which the tidal range is affected after a closure of an estuary in the River Rhine delta.

## 1.3 **Problem approach**

In order to separate natural processes from anthropogenic effects we carry out a statistical analysis of records of annual mean values of the tidal range (*MTR*). Primarily, data from Dutch tide gauging stations are used. Data from the German coast and British stations are used for comparison. The first goal of this analysis is to determine which natural (astronomic, meteorological) periodic components are present in the tidal range. Subsequently, the phases and amplitudes of the significantly present periods are quantified. Subtracting this from the tidal range record reveals both short-term fluctuations and long-term trends which are not cyclic with periods that can be identified from the records. Short-term fluctuations of various stations are mutually compared to assess whether these fluctuations are caused by local processes or are common for a larger region. Coastal engineering works and other human interferences can result in a sudden changing tidal range. To determine these breakpoints, the energy spectra of sub-intervals of a whole record are compared.

The fact that a similar trend is observed at stations which lie far apart, does not necessarily mean that this trend is caused by a change of the whole system or part thereof. One can imagine that coastal works at a certain location affect the tides over a large distance. To determine what the magnitude of order of this distance is for a typical intervention, the closure of an estuary, a conceptual model is applied. In this model the North Sea is schematised as a rectangular basin. The northern boundary is forced by a simple semidiurnal tide which propagates as a Kelvin wave trough the basin. Estuaries with various sizes are added at different locations at the southern border and are subsequently closed. The changes in the tidal range after the closure are computed and the distance of influence evaluated.

## 1.4 Theoretical background and research to date

### Theory of equilibrium astronomic tide

Time series of sea water levels contain many periodic components. The orbits of the planets are the cause of a continuously changing gravity field. This changing gravity field is the driving force of the ocean tides. Examples of periodic components are the solar and lunar tides with periods of circa 12 and 24 hrs. The well known spring-neap tide cycle has a period of circa 30 days. Long-term periodic components with periods larger than 1 year also exist. The long-term period with the greatest impact is the nodal tide with a period of 18.6 yr. This cycle is called the nodal tide because it is caused by the changing positions of the nodes of the moon's orbital plane [see figure 1.2].

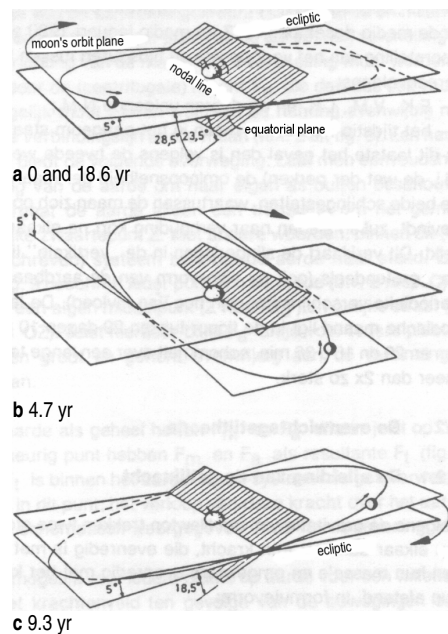


Figure 1.2: The rotation of the moon's nodes in 18.6 yr [adapted from Holthuysen]

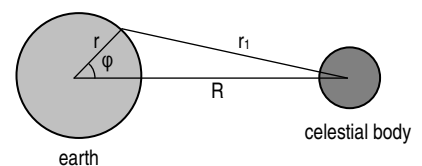
Mathematically, the tides can be described as a superposition of a finite number of cosine functions:

$$h(t) = h_0 + \sum_m a_m \cos(\omega_m t - \varphi_m) \quad [1]$$

In equilibrium tide theory we assume the globe is covered completely with oceans and friction, inertia and currents do not play a role. The tide generating potential from a celestial body (e.g. the moon) on earth is given by [Stewart, 2002]:

$$V_M = -\frac{\gamma M}{r_1} \quad [2]$$

$$\text{with } r_1^2 = r^2 + R^2 - 2rR \cos \varphi \quad [3]$$



where  $\gamma$  is the gravitational constant and  $M$  is the mass of the celestial body, distances and angle  $\varphi$  are shown in the figure.

Combining equations 1 and 2 gives:

$$V_M = -\frac{\gamma M}{R} \left[ 1 - 2 \left( \frac{r}{R} \right) \cos \varphi + \sqrt{\frac{r}{R}} \right]^{-\frac{1}{2}} \quad [4]$$

This can be expanded in powers of  $r/R$ :

$$V_M = -\frac{\gamma M}{R} \left[ 1 - \left( \frac{r}{R} \right) \cos \varphi + \frac{1}{2} \left( \frac{r}{R} \right)^2 (3 \cos^2 \varphi - 1) + \dots \right] \quad [5]$$

Only the gradient of the potential, term 3 in equation 5, generates tidal forces. The second term is the centripetal force keeping the earth in its orbit. The tide generating potential is:

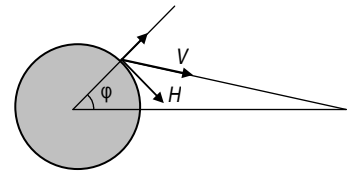
$$V = -\frac{\gamma M r^2}{2R^3} (3 \cos^2 \varphi - 1) \quad [6]$$

The vertical component of the potential (perpendicular to the earth's surface) is balanced by pressure on the sea bed, only the horizontal component (tangential to the earth's surface) drives the tides:

$$H = \frac{2G}{r} \sin(2\varphi) \quad [7]$$

with

$$G = \frac{3}{4} \gamma M \frac{r^2}{R^3} \quad [8]$$



where  $\varphi$  is the latitude and  $G$  is Newton's constant of gravitation.

The celestial bodies generating the tidal potential are moon and sun mainly, each with a different gravitational constant. The relative contribution of sun and moon to the tidal potential is:

$$\frac{G_{sun}}{G_{moon}} = 0.46 \quad [9]$$

Taking into account the changing positions of the planets due to the rotation of the earth around its own axis, the earth around the sun, the moon around the earth and the (change of) the declinations of the moon and earth, the tide generating potential can be computed at any time and place on earth. The tidal potential can be separated into twice-daily, daily and long periods. Doodson [1921] expanded the tidal potential into Fourier series with six fundamental frequencies [see table 1.1].

	physical cause	period	frequency [°/hr]
1	local mean lunar time	1 lunar day	14.49205211
2	moon's mean longitude	1 month	0.54901653
3	sun's mean longitude	1 year	0.04106864
4	longitude of moon's perigee	8.847 yr	0.00464184
5	longitude of moon's ascending node	18.613 yr	0.00220641
6	longitude of sun's perigee	20,940 yr	0.00000196

Table 1.1: Fundamental tidal frequencies [Stewart, 2002]

Each tidal constituent has a frequency (or angular velocity) of:

$$f = n_1 f_1 + n_2 f_2 + n_3 f_3 + n_4 f_4 + n_5 f_5 + n_6 f_6 \quad [10]$$

where  $f_i$  are the frequencies from table 1.1 and  $n_1 = 1, 2, 3$  and  $n_{2,3,\dots,6} = -5, -4, \dots, 5$

The tidal constituents can be separated into principal tides ( $M_2$  and  $S_2$ , both semidiurnal), declination tides (e.g.  $M_f$ , fortnightly, and  $S_{sa}$ , semi-annual) and elliptic tides (e.g.  $Q_1$ , diurnal lunar, and  $N_2$ , semidiurnal lunar). An example of a sea level record showing different tidal constituents is given in figure 1.3.

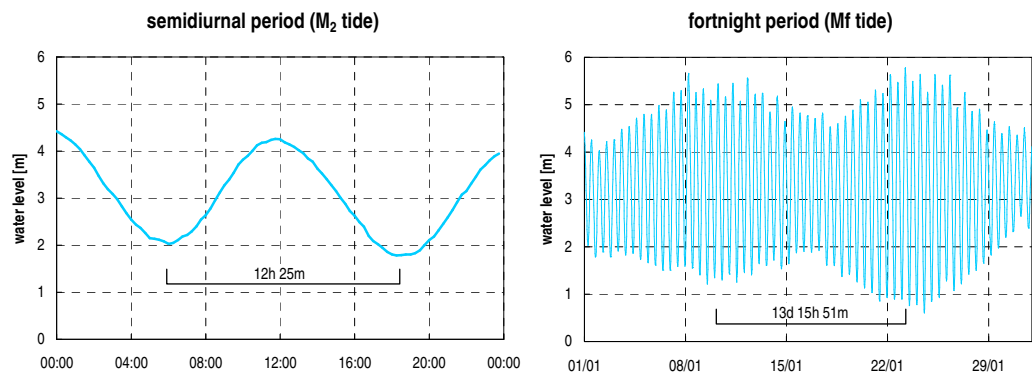


Figure 1.3: Semidiurnal and fortnightly period in sea water level at Newlyn, south east England [data obtained from POL, 2005]

### Non-equilibrium tides

The above description of the tide is the equilibrium astronomic tide. The theory of the equilibrium tide can be used to estimate water levels in deep oceans. In reality, however, the continents, inertia and currents will deform the tidal wave. The tides are even more disturbed in coastal areas due to bottom friction [Kalkwijk, 1976]. This will induce non-linear effects. In these regions the equilibrium tide does not describe the real tides accurately.

Although the tides in shallow seas do not satisfy the equilibrium astronomic tides, many of the tidal constituents can still be perceived in the sea level records. In fact, many more constituents with higher frequencies are present due to non-linear processes. The frequencies of the tidal constituents are equal to the frequencies of the equilibrium tide. The amplitudes and phases are different and need to be determined empirically by a harmonic or a spectral analysis. The astronomic tides can be described with the formula:

$$h(t) = h_0 + \sum_n f_n H_n \cos(\omega_n t + V_n + u_n - g_n) \quad [11]$$

where  $h$  is the water level at time  $t$ ,  $H_n$ ,  $V_n$  and  $\omega_n$  are the amplitude, phase and frequency of the tidal constituent and  $f_n$  and  $u_n$  are corrections for the nodal tide which is the only commonly considered constituent with a period longer than 1 year [see for more detail appendix A4].

### Long-term variability in the tides

Long-term changes in the ocean tides can be caused by different physical processes. Climate changes, like temperature rise and atmosphere pressure oscillations, have an effect on mean sea level and possibly the tidal range [Führböter and Jensen, 1985]. Many researchers have tried to prove the existence of various natural periodic components in water levels.

The effect of the sunspot cycle on sea water levels has been studied by Currie [1981] and Woodworth [1985], amongst others. The mechanism connecting solar variability with climate changes and water levels is not well understood. There is, however, evidence of a statistical significant solar cycle in mean sea level. Currie's [1981] estimate of the period of the solar cycle in mean sea level is  $10.9 \pm 0.6$  yr and the amplitude is roughly 9 mm. Woodworth [1985] carried out a world-wide search for the solar cycle in mean sea level. He confirms the results by Currie with slightly different numeric results. Furthermore, Woodworth discovered that the phase of the solar cycle depends on the latitude. Apart from in Europe, the author finds no convincing evidence for an 11-yr cycle in mean sea levels.

Searching for the existence of the solar cycle in surface data, Currie and Woodworth discovered periodic components with different periods. Besides the astronomical cycles of 8.85, 11 and 18.6 yr, there are cycles with periods of 7.5, ~6.3 and ~4.5 yr present in sea level records [see appendix A4 for overview of long-term cycles and references]. Possible explanations are the North Atlantic pressure oscillation (7.6 yr) and El Niño effects (4.4 yr) [Treloar, 2002]. More long-term cycles caused by moon-sun interaction are outlined in [Treloar, 2002] and are of great importance for studies on tide-climate interaction. It should be noted that in most studies records of mean sea level are analysed. The only mentioned long-term periods in tidal range record in literature are the 18.6-yr cycle and the 4.4-yr cycle [Gordon, 1968; Cartwright, 1974].

In this study an assessment is made which of the mentioned tidal constituents are present in the tidal range in the southern North Sea in order to construct a residual tidal range.

### Research on tidal regime in the North Sea

Several researchers have studied the tidal regime in the North Sea [see figure 1.4] to assess whether short-term or long-term changes occur. Of particular interest are studies on the changing tidal range along the different coastlines. Long-term records of high and low water levels exist for the Dutch, German and Danish coast and several stations in Great-Britain. Many records of coastal stations are affected by human interventions, which complicates the study of the natural system. Langendoen [1987] has studied the change of tidal range at Vlissingen and other stations along the

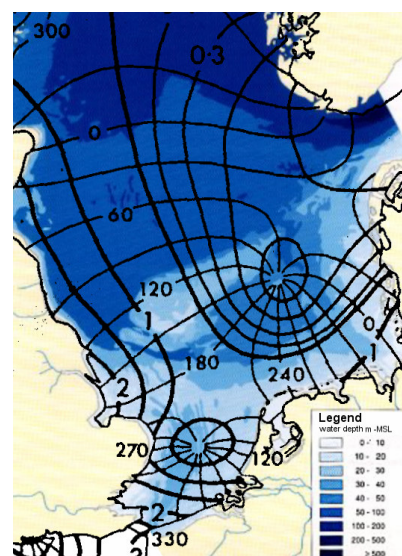


Figure 1.4: Co-tidal and co-range lines (bold lines) of the M2 tide in the North Sea. Adapted from [Pingree and Griffiths, 1987] and [Rijkswaterstaat Directie Noordzee, 2005].

Western Scheldt, south Netherlands. Langendoen has estimated the contribution of different factors to the increase of the tidal range in the mouth of the Western Scheldt. He concludes that the tidal range has increased with c. 1.5 mm/yr (4.0% per century) during the last century and that this is mainly caused by changes in the geometry of the estuary and its mouth (c. 75%) and partly by sea level rise (c. 25%). Furthermore, Langendoen has examined the effect of (real and hypothetical) closures of estuaries in the Rhine delta area. According to model simulations, the tidal range increases with an order of magnitude of 50 mm at the location of closure. This increase decays asymptotically in space with a typical length of ~50 km [see figure 1.5]. Rakhorst [2003a; , 2003b; , 2005] has made an extensive analysis of tidal range records of all Dutch tidal stations to identify anthropogenic effects such as the different closures, but also river runoff regulations and harbour modifications. His conclusion is that apart from natural periodic variability in the tidal range, most changes can be explained as anthropogenic effects.

To identify secular trends and natural variability in the tidal range along the Dutch coast, records need to be compared with those observed along other coastlines in the North Sea. The tidal regime at the German coast has been studied by Jensen and others [Führböter and Jensen, 1985; Jensen *et al.*, 1992; Jensen and Mudersbach, 2002]. The researchers observed an extraordinary increase in mean tidal range since 1956. This coincides with an increase in frequency and duration of storm surges in the same period. Before this period, the tidal range stayed relatively constant – apart from noise and an 18.6-yr periodic component.

An extensive study of the tidal range records of the British stations has been done by Woodworth *et al* [1991]. The aim of this research was to identify secular trends in mean tidal range. Since many stations at the British coast have short or unreliable records, general long-term trends are difficult to evaluate. The only station with a continuous and long record is Newlyn, south west England. At this station a small but significant trend in the tidal range of  $0.34 \pm 0.09$  mm/yr has been observed. This change is primarily due to a change in the  $M_2$  tidal constituent. Since the tide recorder at Newlyn is located in deep water and hardly influenced by human effects, it indicates that a real secular trend in the tidal range of the ocean tides exists.

In this study we build on the various studies from the Netherlands, Germany and Great Britain. Especially to assess long-term, common trends we will compare the trends from the different stations.

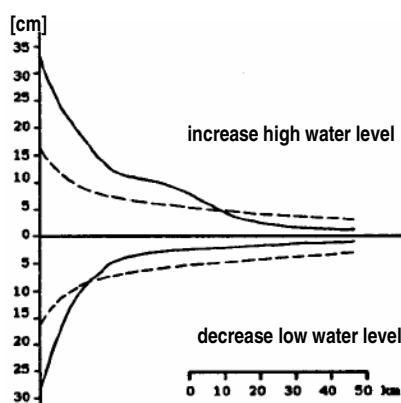


Figure 1.5: Modelled change of extreme water levels after closure of the Western Scheldt estimated with a numerical model (solid) and an analytical calculation (dotted). [Figure adapted from Langendoen, 1987]

## 2 Methodology statistical evaluation

This chapter describes which methods are used to assess the development of the tidal range in the North Sea. First of all a visual inspection is needed to assess the record roughly (section 2.1). Since we know that the tidal forces are caused by astronomic processes with different cyclic periods, a spectral analysis and a multiple linear regression analysis are used to quantify the periodicities (section 2.2 and 2.3). Section 2.4 describes how both these methods are used to separate short-term fluctuations of the tidal range from the observed records. This chapter concludes with a description how long-term trends are evaluated.

### 2.1 Visual inspection

A first assessment of the tidal range records is made with a visual inspection. This first inspection is used to determine whether data records need to be split into different sections (if obvious breakpoints are present) or data need to be omitted (in case of strongly deviating data points). For each station the tidal range and the high and low water levels are plotted and inspected for clearly recognisable patterns or trends, discontinuities and gaps in the data.

### 2.2 Spectral analysis

After a visual evaluation of the data a spectral analysis is used. The purpose of this analysis is to examine the cyclic behaviour of the tidal range. It is expected that cycles like the nodal tide (with a period of 18.6-yr) can be recognised in the tidal range. However, the question is whether more meteorological or astronomical cycles affect the tidal range and what their relative importance is. Periodic components can be extracted from a record with a spectral or Fourier analysis. Joseph Fourier showed that almost any function over the interval  $\langle -\infty, +\infty \rangle$  can be decomposed into an infinite number of sine and cosine functions. In case of a function with a limited domain, the sine and cosine series have harmonic frequencies ( $m \cdot f$  with  $m=0,1,2,\dots$ ) of the fundamental frequency ( $f=1/T$  with  $T$  is the record length) [Stewart, 2002]. In this study we use a fixed record length of 93 yr. This length is close to the record length of most stations and enables us to determine both the 18.6-yr ( $93/5$ ) and the 4.4-yr ( $93/21$ ) cycle accurately. If a record length is greater than 93 yr we compute the average of the spectrum of the first 93 yrs and the last 93 yrs. If a record length is smaller than 93 yr the record is padded with zeros.

A discrete Fourier transform algorithm is used to compute the amplitudes of the harmonic components [Oppenheim *et al.*, 1999]. A commonly used algorithm is the Fast Fourier Transform (FFT) algorithm. The algorithm implemented in MATLAB [Mathworks, 2003] is used in this study. With this algorithm an energy

density spectrum of the fundamental frequencies can be constructed. See for more details on the used spectral analysis appendix A2.

### 2.3 Multiple linear regression analysis

To quantify the dominant physical periodic processes accurately, a multiple linear regression (MLR) analysis is used. With an MLR analysis the shape (e.g. a sinusoidal function with given frequency) of the components can be set beforehand. For this study we use an MLR analysis of the following form:

$$MTR(t) = MTR_0 + s \cdot t + \sum_{m=1}^M a_m \cos\{\omega_m (t - t_{0_m})\} \quad [12]$$

where  $MTR(t)$  is the approximation of the observed mean tidal range. This trend line – what it actually is – is composed of a linear trend and a limited number of cyclic trends. The linear parameters are calculated with the least squares method [see appendix A1]. The linear parameters are  $MTR_0$  (offset value),  $s$  (linear slope) and  $a_m$  (amplitude of cyclic trend  $m$ ). The angular velocities ( $\omega_m$ ) are given by the periods of the natural cycles ( $\omega_m = 2\pi/T_m$ ) of which values are available in literature [Godin, 1972].

Although it is known that many long-period constituents are present in the tidal range (e.g. 4.4, 8.85, 11 and 18.6 yr), they cannot always be discriminated significantly. Non-tidal variability introduces large errors in the calculations of the weaker constituents [Stewart, 2002]. One way to test whether the results are possibly related to a natural phenomenon is to compare the phases computed at various stations.

The phase of periodic components with very long periods is expected to be the same for all stations. This is because the distance between the stations at the North Sea coast can be ignored relative to the wavelength corresponding to the tidal constituent. The wavelength of the nodal tide in 100 m deep water, for example, is c. 20 million km. Therefore the phase of the constituents is not used as a linear parameter in the MLR analysis but set as a constant value. This reduction in degrees of freedom of the MLR increases the accuracy of the calculated amplitude.

Although most researchers [e.g. Woodworth *et al.*, 1991; Jensen *et al.*, 1992] use a linear regression ( $s \cdot t$  in equation 12) in their analysis of the tidal range, it is not clear if there is a physical explanation for such a trend. At this stage the linear trend is mainly used to calculate the amplitudes of the cyclic trends as accurate as possible. While evaluating long-term trends, it needs to be assessed whether found trends are constant in time or whether accelerations and periods of zero-trends occur [see section 2.5].

## 2.4 Short-term behaviour

Short-term fluctuations in the tidal range are of interest because we want to know whether the observed variability is caused locally or is caused by regional changes. In this study short-term is defined all trends with a smaller period than the nodal tide cycle (18.6 yr). Two different methods are used to calculate a residual tidal range.

1. With the first method a signal is constructed containing the higher Fourier frequencies. The computed spectrum of a record is cut off at the frequency  $f = 5/93 = 1/18.6$  and using an inverse Fourier transform, converted into an artificial record. Hence, this records includes all components with periods between  $T = 93/46 = 2.02$  and  $T = 93/2 = 46.5$  yr .
2. The second method uses the results of the MLR analysis. Here the trend line (periodic trends only) calculated in the MLR analysis is subtracted from the observed tidal range record. This residual tidal range includes short term fluctuations and long-term trends of unknown origin.

The first method, based on the spectral analysis, represents the short-term behaviour better, because the second method's residual includes cyclic trends with periods not evaluated in the MLR analysis. The second method at the other hand has a more direct physical explanation than the first method.

The residuals are examined on patterns and irregularities. Different stations are mutually compared to asses whether short-term behaviour is caused by local or larger scale (North Sea, Atlantic Ocean, global) processes.

## 2.5 Long-term behaviour

Not only the short-term trends, but also gradual developments over intervals larger than 18.6 yr and sudden jumps of the tidal range are of interest. To assess gradual changes a moving average of the tidal range is constructed for each station. The moving average is calculated over intervals of 19 yr. As annual data are used, the moving average cannot be calculated for 18.6-yr intervals. Since the interval is not equal to the 18.6-yr periodic component, which dominates the variability of the tidal range, this can introduce periodicities in the moving average. If, for example, a tidal range of the following form is assumed:

$$MTR(t) = C + \sin(\omega t) \quad [13]$$

The moving average over interval lengths  $T$  at time  $t = \tau$  is given by:

$$\overline{MTR}(\tau) = \int_{\tau-T/2}^{\tau+T/2} [C + \sin(\omega t)] dt = C + 2 \sin\left(\frac{1}{2}\omega T\right) \cdot \sin(\omega \tau) \quad [14]$$

This moving average has a constant value  $C$  only when  $\frac{1}{2}\omega T$  is a multiple of  $\pi$ . This is not the case since the interval of the moving average ( $T=19$  yr) is different from the period of the tidal constituent ( $2\pi/\omega = 18.6$  yr). However, since the chosen interval  $T=19$  yr is close to the nodal tide period, the periodicity accompanying the moving average is small.

A disadvantage of the moving average technique is that together with the high frequencies, sudden jumps are filtered out. What might look like a gradual change could be a jump that is smoothed out by the averaging technique. Therefore another method is also used to specifically find locations with jump-type irregularities. In this method the entire tidal range record is split into intervals and for each interval the tidal spectrum is computed. The spectra of two adjacent intervals are compared and the difference expressed in a single parameter, here called the Euclidian distance. The Euclidian distance between two amplitude spectra with frequencies  $m$  is defined as the square root of the sum of the squared distances between the two spectra, or in formula form:

$$L_2 = \sqrt{\sum_m (S1_m - S2_m)^2} \quad [15]$$

where  $S1$  and  $S2$  are the two compared amplitude spectra with frequencies  $m$ .

This is repeated for the whole time domain and a plot is made of the Euclidian distance versus time. This parameter is a measure of the change in spectrum at a breakpoint in between two intervals and can be read as a discontinuity parameter. The interval length is varied between 10 and 20 yrs to find an optimum value between a very noisy signal and a smoothed signal. See appendix A3 for more details on this method.

As with the short-term behaviour the long-term trends of different stations are mutually compared to evaluate common and divergent trends.

## 3 Available tidal data

This chapter describes the observations that can be applied to the evaluation methods as described in chapter 2. Section 3.1 summarizes at which locations and what time period the tidal range is known. Section 3.2 discusses how reliable and accurate these data are.

### 3.1 Tide gauging stations and measurement records

The Dutch tide gauging network consists of a number of stations along the Dutch coast and on the Wadden islands. Their records go back to as early as 1827 (Delfzijl). For this study data from 14 Dutch stations have been used [see appendix A4 for details and locations]. The length of the records and the density of the network make it possible to assess common trends for the North Sea region. However, as noted by Jensen and Mudersbach [2002], the stations need to be uninfluenced by human activities. This is not likely the case since extensive works have been carried out since the beginning of the records. This makes interpretation of the data difficult because unknown natural changes need to be distinguished from human interferences. Therefore not only data from Dutch gauging stations are used but also data from the 6 stations on the German North Sea islands, the gauging station Euro Platform in the North Sea and the gauging station at Newlyn, south west England [see appendix A4 ].

For most stations the records till 1920 or 1936 are obtained by registrations of the high and low water levels by local port authorities or 4 or 8 readings per day. The recent records have been measured at hourly or 15 mins. intervals with fully automatic recorders [POL, 2005]. When the water level is recorded at a fixed time interval, the exact moment and the level of the high and low waters need to be approximated with Interpolation techniques. Annual mean values of the high waters (MHW), low waters (MLW) and the tidal range (MTR) for all gauging stations used are given in appendix A6. These data are obtained from the national coastal management institutes. In this study we limit ourselves to annual average only. Considering within-year variability would increase the amount of data and the processing time considerably.

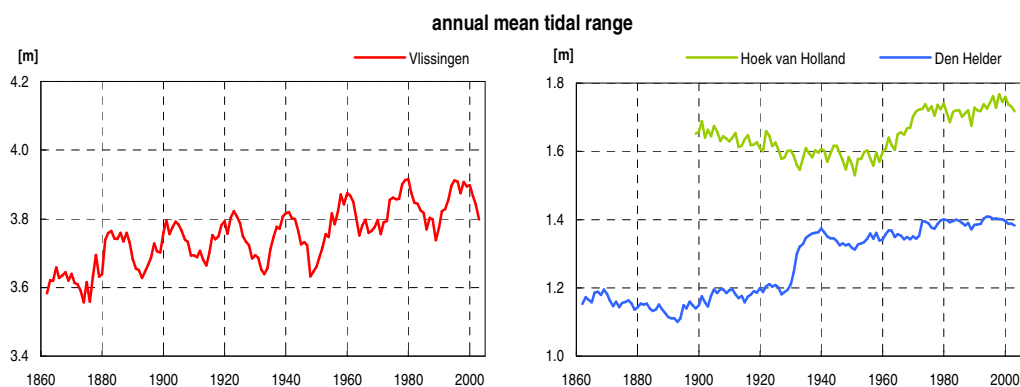


Figure 3.1: Mean tidal range for Vlissingen, Hoek van Holland and Den Helder

### 3.2 Accuracy and errors

Before the data are applied to the analyses we need to know if they are reliable and of sufficient accuracy. There are several causes for errors in the measurements of the tides. Random errors, for instance, are caused by incidentally wrongly recorded or registered water levels. Random errors are not important for this study because only annual mean data are used. Random errors in individual high and low waters barely influence the annual mean values of the high and low waters and the tidal range. Individual errors of a few centimetres result in an millimetre accuracy of the annual values [Woodworth *et al.*, 1991].

Bias is of more importance since it can influence the annual average values systematically. High and low waters can be systematically over (or under) estimated. Although this will affect the annual values of the high waters and the low waters, this does not affect the tidal range since the computation of the tidal range cancels out these types of errors. The same holds for land subsidence or the mere displacement of a gauging station [Jensen and Mudersbach, 2002]. However, the location of the gauging station is important since the low waters (more than the high waters) are affected by the water depth, remaining water at (very) low tides or discharges of nearby sluices. In coastal systems with barrier islands and tidal basins large volumes of water are discharged through the inlets at ebb tide. Hence, the water levels at those locations will be higher than if measured at open sea. This effect is stronger at ebb tide than at flood tide [Jensen and Mudersbach, 2002].

Systematic errors can be introduced when the interpolation techniques to determine the high and low water levels systematically overestimate the high water level while underestimating the low water level or the other way around. This has been noticed with the Newlyn record which gave different tidal ranges when computed from hourly or 15 mins water level time series [Doekes, personal communication].

### 3.3 Data preparation for the analyses

To be able to mutually compare individual stations, the deviations from the entire record's mean value are considered:

$$\Delta MTR_n = MTR_n - \overline{MTR} \quad [16]$$

where  $\Delta MTR_n$  is the departure of the tidal range from mean value  $\overline{MTR}$  and  $n$  is a time-index.

And to obtain percentage values [Woodworth *et al.*, 1991; Jensen and Mudersbach, 2002]:

$$\Delta PMTR_n = \frac{MTR_n - \overline{MTR}}{\overline{MTR}} \quad [17]$$

Especially the percentage change is helpful since the magnitude of the tidal range depends highly on the location and therefore the absolute values of for example the amplitude of the nodal tide can be different for each station.

## 4 Interpretation of the tidal range records

The results of the analysis of tidal range records with the methods described in chapter 2 are given in this chapter. Interpretations of the results are given at the end of each section. The first section gives a rough assessment of trends and irregularities based on a visual inspection of the data. In section 4.2 it is analysed which tidal constituents are dominant in the records. Since only the nodal tide can be observed on a significant level this constituent is further quantified in the sections 4.3 (evaluation of its phase) and section 4.4 (evaluation of its amplitude). The short-term behaviour of the tidal range is given in section 4.5 and the long-term trends are presented in section 4.5. Section 4.6 presents an analysis of discontinuities in the tidal range records. As a conclusion, section 4.7 gives a summary of the main observations and interpretations.

### 4.1 Visual inspection

The records of all stations, except Scheveningen, are continuous and without gaps. The stations of the Texel inlet (Den Helder, Oudeschild, Den Oever, Kornwerderzand and Harlingen) show a sudden increase in tidal range around 1930. This is caused by the closure of the former Zuider Sea which reduced the area of the basin of the Texel inlet with c. 85%. After the closure the tidal wave is amplified at the closure dam which increases the tidal range at Den Oever, for example, with almost 100 percent! In the analysis of the tidal range records the records before and after the closure are analysed separately. The data between 1928 and 1943 are not used to omit the affects of quick morphological changes during and immediately after the construction of the dam. The tidal range at West-Terschelling is also affected by the closure of the Zuider Sea although the timescales of the adaptation are larger than at Den Helder and the other stations of the Texel inlet. West-Terschelling is located in an adjacent tidal basin. A slow

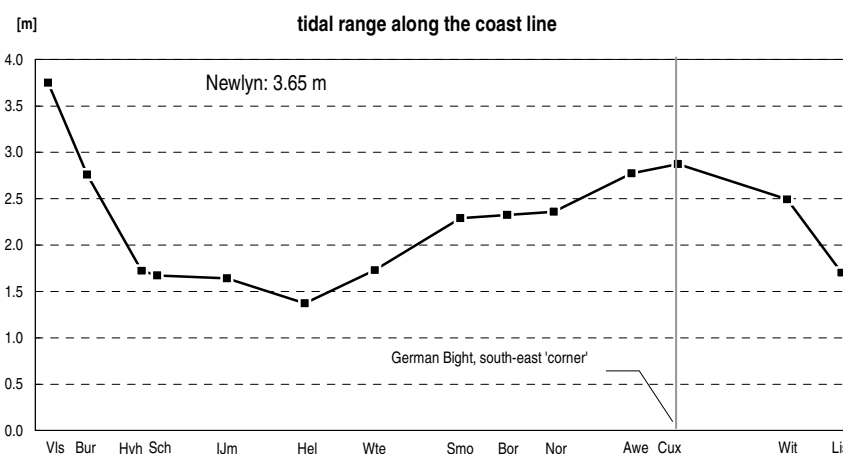


Figure 4.1: The average tidal range of each stations entire record along the Dutch and German coastline. The horizontal axis suggests the location of the stations along the coastline. Station name abbreviations are given in appendix A5.

process of accretion in the Texel inlet basin reduces the surface area of the Terschelling basin, resulting in a gradually increasing tidal range at West-Terschelling.

The station Vlieland Haven is not analysed in this study since the first part of the record shows a decreasing trend which deviates from the nearby station West-Terschelling. An accretion of the channel near this station influenced the recordings of the low water levels and made it necessary to relocate the gauging station [Rakhorst, 2003a].

At first glance all stations show that the tidal range increases gradually with time. Many of the stations have a periodic fluctuation with a period of 18.6-yr (nodal tide), which makes it difficult to see whether sudden changes occur or whether increasing trends are constant in time. The nodal tide has a larger amplitude for the stations in the Zeeland delta area and the station in the north Netherlands and the German Bight. Along the Holland coast it is more difficult to identify the nodal tide. Remarkable is the decreasing trend of the tidal range at Hoek van Holland until 1960. This is correlated to an increasing river discharge at the gauging station, which raises the low water levels. A description of each station's trend and main irregularities are given in appendix A7.

#### 4.2 **Determination of the tidal constituents dominant in the mean tidal range**

The aim of a multiple linear regression (MLR) analysis is to evaluate the tidal constituents. First of all we want to know which tidal constituents are dominant in the tidal range records. From the spectral analysis it is clear that the nodal tide with a period of 18.6 year is significantly present at all stations. To assess whether other tidal constituents can be observed, a MLR analysis is carried out with the periods 18.6, 13.3, 11 and 8.85 yr. These three periods are the most studied [e.g. Currie, 1976; Woodworth, 1985; Woodworth *et al.*, 1991; Jensen *et al.*, 1992; Braker, 1994] long-term tidal cycles with a clear physical cause. Gerritsen [1989] mentions many more long-term periodicities with typical periods like 55.84, 88.5 and 93 yr, but many of these periods lack a clear explanation and they have not been applied to analyses of tides before. Furthermore, the records of the Dutch gauging stations have lengths with an order of magnitude of 100 yr; hence constituents with periods larger than 50 yr cannot be evaluated accurately.

To test which constituents are significantly present, we calculate the phase of each possible period at each station. The standard deviation of the calculated phases is a measure of the accuracy of the constituent's phase since each station should give almost exactly the same phase [see section 2.3]. Moreover, we test if a combined MLR for the 4 components together gives the same phase as 4 individual MLRs. The combined and the individual MLRs are applied to 6 stations, namely Vlissingen, Burghsluis, IJmuiden, Den Helder (1944-2003), West-Terschelling (1944-2003) and Delfzijl (1833-1960). These stations have the longest records limitedly affected by human interventions. Figure 4.2 shows the standard deviation of the phase and the difference between the combined and the individual MLRs for the periods 8.85, 11, 13.3 and 18.6 yr. The phase is defined as the year with a maximum tidal range [see equation 12].

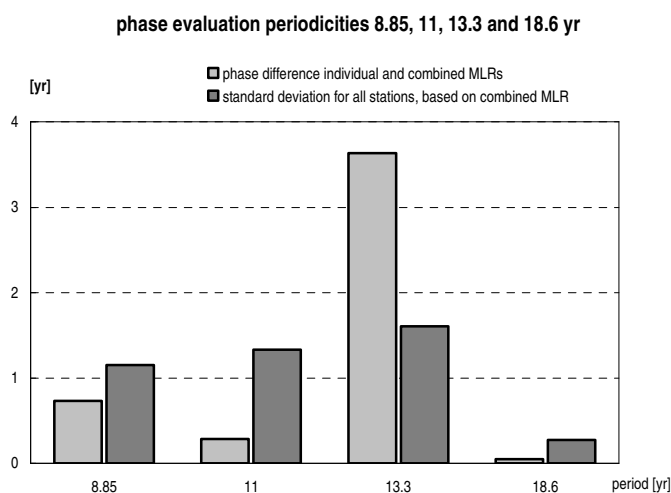


**Figure 4.2: Evaluation of the phase [yr with maximum] for different tidal constituents. The variance for 6 stations is shown and the difference between the average phase of a MLR for each period individual and a MLR with the 4 periods together. See appendix A8 from numerical values.**

The conclusion can be drawn that only the 18.6-yr cycle can be determined accurately since its phase is nearly the same for the different stations. For the other constituents the calculated phases are highly variable, this makes it impossible to determine whether the real physical process is evaluated or some other noise with an as yet unidentified cause.

#### 4.3 Evaluation of the nodal tide phase

The phase of the nodal tide is determined as the mean value of the phases determined for a set of selected stations. MLR analyses are applied to each station's record to calculate the phase of the nodal tide. Only the records with a good fit ( $R^2 > 0.75$ ) are used in this section. The stations with a good fit are West Terschelling, Vlissingen, Den Helder, Oudeschild and the Euro Platform [see table 4.1]. The mean value of the 18.6-yr phase is 1978.4 yr, defined as the year with a maximum. This value will be used in the final MLR analyses to construct residual tidal ranges.

station	trend fit ( $R^2$ )	phase
	[-]	[yr modulo 18.6 yr]
West-Terschelling (1944-2003)	0.93	1977.9
Vlissingen	0.84	1977.8
Den Helder (1944-2003)	0.83	1978.1
Oudeschild (1944-2003)	0.77	1979.5
Euro Platform	0.64	1978.4
standard deviation		<b>0.70</b>
<b>mean</b>		<b>1978.4</b>
astronomical calculation		1978.5

**Table 4.1: Determination of the nodal tide phase.  $R^2$ -values are from MLR (including linear trend and 18.6 cycle). Phases are year with a maximum.**

The calculated phase corresponds accurately with the astronomic tide, observations at the Euro Platform and observations along the British and German coast. Computations of the moon's orbit show that the distance moon-earth has a minimum on 19 July 1978 which means that the tidal forces are maximum at that time point [Boon, 2004] [see appendix A4]. The Euro Platform is located c. 50 km off the Dutch coast at 30 m water depth and is hardly influenced by human interferences and local geometry changes. The noise in this tidal range record is very small and therefore the phase can be determined very accurately. It should be noted that its record length is limited (since 1984), which decreases the accuracy. Woodworth *et al.* [1991] find for the British Isles an average phase of  $1978.8 \pm 0.61$  yr. And for the German North Sea stations the phase has been evaluated as 1978 [Jensen *et al.*, 1992].

#### 4.4 Evaluation of the nodal tide amplitudes for each station

With the calculated phase, a MLR is carried out for all stations with the only parameters a constant value ( $MTR_0$ ), a linear slope ( $s$ ) and the amplitude of the nodal tide ( $a_{18.6}$ ). A table with these parameters for each station is given in appendix A9. The 18.6-yr amplitude varies from 1.7% of the mean tidal range at Schiermonnikoog to 0.3% at Scheveningen and has a mean value of 1.0% or 21 mm. The Euro Platform has an amplitude of 2.1% and Newlyn 2.8%. Figure 4.3 shows the amplitudes of the stations at the Dutch coastline. The graph in figure 4.3 makes clear that both the absolute but also the percentage amplitude values are not constant. The stations in the south and the north show the largest amplitudes and the Holland coast stations (Hoek van Holland, Scheveningen, IJmuiden and Den Helder) show relatively small amplitudes.

The fact that the tidal range is identical for different stations is caused by the geometry of the shallow North Sea which leads to a complex non-linear propagation pattern of the tidal wave. This local variation have been simulated with numerical models [for example in De Ronde, 1986; Pingree and Griffiths,

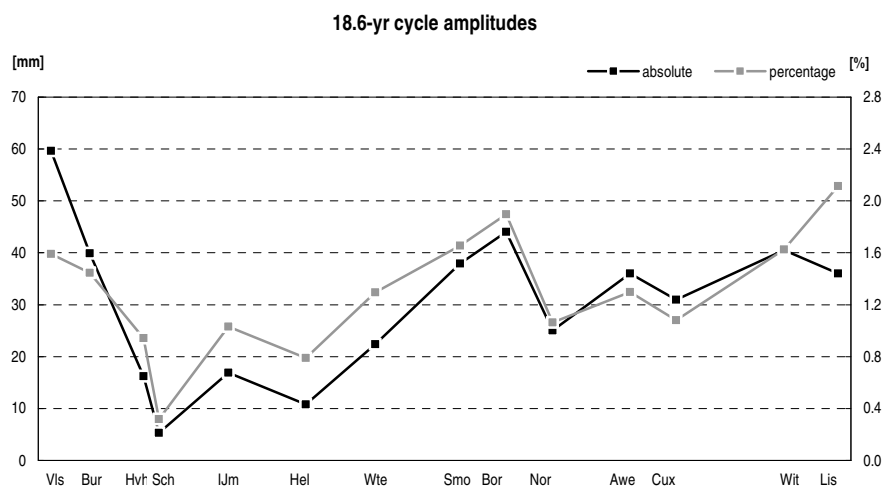


**Figure 4.3: Absolute and percentage amplitudes of the nodal tide along the Dutch and German coast. The horizontal axis suggests the location of the station along the coastline. Percentage values (right axis) are a percentage of the mean MTR of the entire record.**

1987]. Furthermore, local geometries can have significant effects on the tidal wave near the coast. Especially recorded low waters are dependent of the local situation.

The theoretical amplitude of the 18.6-yr cycle of the equilibrium tide is 3.7% [Pingree and Griffiths, 1987]. This amplitude is damped out when the ocean tide propagates through the North Sea under influence of bottom friction. This can explain why the observed amplitudes at the Dutch coast are much smaller than the astronomic equilibrium tide.

#### 4.5 High frequency residual tidal range

The tidal range records show a large variance. The residual of the tidal range after subtracting the 18.6-yr cycle evaluated with the MLR analysis, is shown in graphs in appendix A6 ['trend anomaly' line, figure c]. The high frequency residual signals as calculated from the amplitude spectra are plotted in figure 4.4 [see also appendix A6, figure c, 'periods<18 yr' line]. In this figure The Zeeland and Holland stations, the Texel inlet stations and the Northern stations are grouped together to assess if the residual signals are comparable. The peaks in the residual signal have a magnitude of 50 mm, roughly 2% of the mean tidal range. This is in the same order of magnitude as the amplitude of the strongest tidal constituent, the 18.6-yr cycle.

The Zeeland and Holland stations have the largest variance. Although these station's tidal ranges are highly variable, most peaks correspond. Only during the period 1935-1960 the peaks become larger and do not correspond with each other. The residuals are very similar since the 1980s.

The Texel inlet stations stand out for their small variance and the highly similar signals. The similar trends can be explained by the fact that the stations are located close to each other. After the closure of the Zuider Sea the residuals are nearly the same for these stations. This can be explained by the fact that by the reduction of the basin area the tidal wave has changed from a progressive to a standing wave in a basin with a characteristic length small compared to that of the tidal wave. Hence all stations experience the same water levels at the same moment.

The stations West-Terschelling, Harlingen and Schiermonnikoog to a certain extend, are similar but do not correspond very much with the Texel inlet stations. Apparently the noise has different causes. The Delfzijl fluctuations are large and do not match the signals of the Wadden stations. However, the similarity with the Zeeland and the Holland stations is striking.

The findings strongly indicate that the noisiness of the mean tidal range is not caused by measurement errors neither by purely local variability. Instead, the fluctuations for the stations are similar and likely to have a common cause.

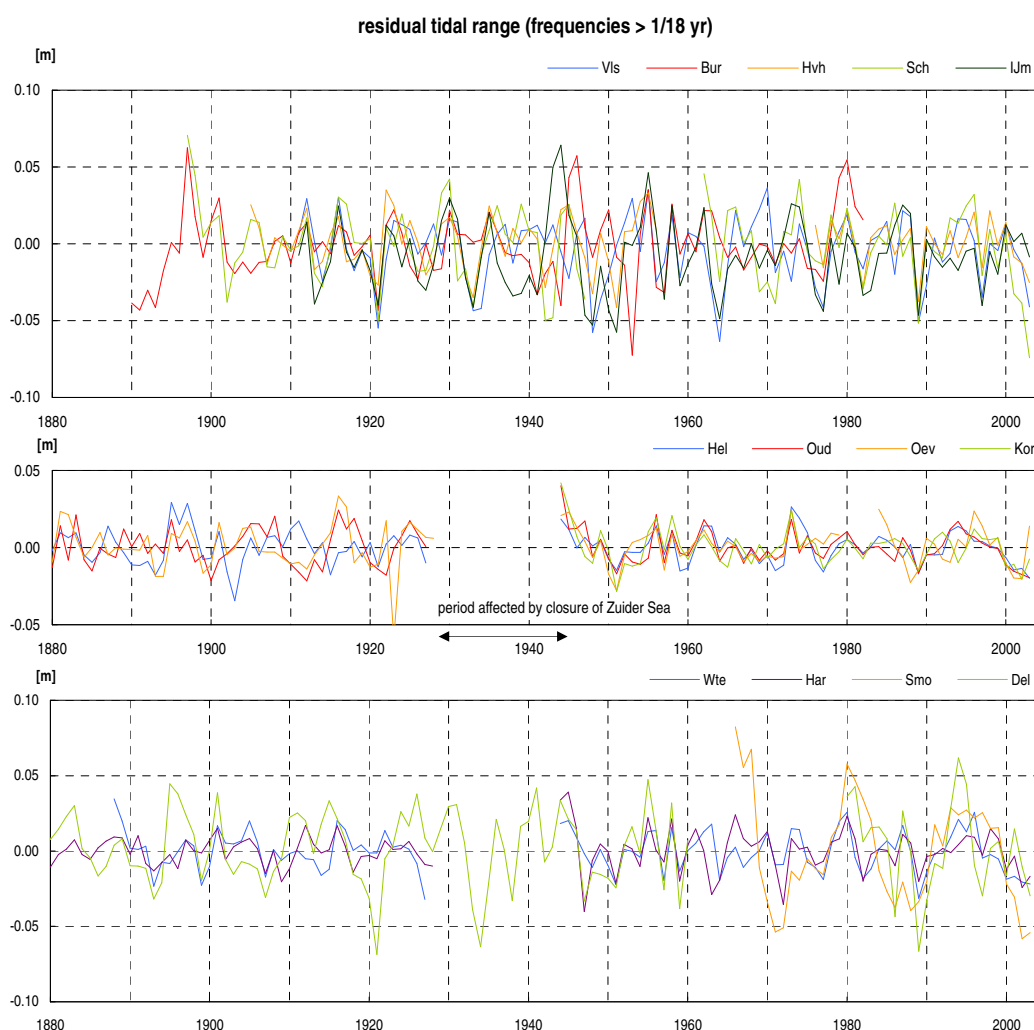


**Figure 4.4: Residual tidal range for all stations grouped per region [see appendix A5 for station name abbreviations]**

## 4.6

### Long-term trends

In this section the long-term trends are examined. The main points of interest are changes in the tidal range not within the strong 18.6-yr cycle and the occurrence of sudden jumps. To assess the long-term trends we construct moving averages with a time interval of 19 yr. The average value is assigned to the centre of the interval. Graphs of each station's moving average are shown in appendix A6. Beside a high correlation in the short-term fluctuations between the various stations, the 19-yr average shows also similar trends. In general, most Dutch and German stations show a relative flat course until the 1950s, or 1930 for the Wadden Sea stations. The latter stations show an evident sharp rise, which is actually the smoothed jump caused by the Zuider Sea closure. After the closure the trends for the Wadden Sea stations stabilize but rise again after c. 1955. After c. 1980 the trends level again for all stations, except that a rise can be observed during the past few years at the German stations [see appendix A10]. To illustrate the general trend an artificial average of different stations is constructed. This is meaningful

since both the long-term trends and the short-term fluctuations are similar for the individual stations. Here we have constructed averages of the Zeeland and Holland stations (Vlissingen, Burghsluis, Hoek van Holland, Scheveningen and IJmuiden), of the Texel inlet stations and of the stations of the German North Sea islands and are shown in figure 4.5. Graphs of a MLR and a spectral analysis of the Dutch and German averages are given in appendix A6.16 and A6.17. The station Den Oever is not included in the stations of the Texel inlet because of its divergent trend in the 1980s caused by the relocation of the harbour entrance.

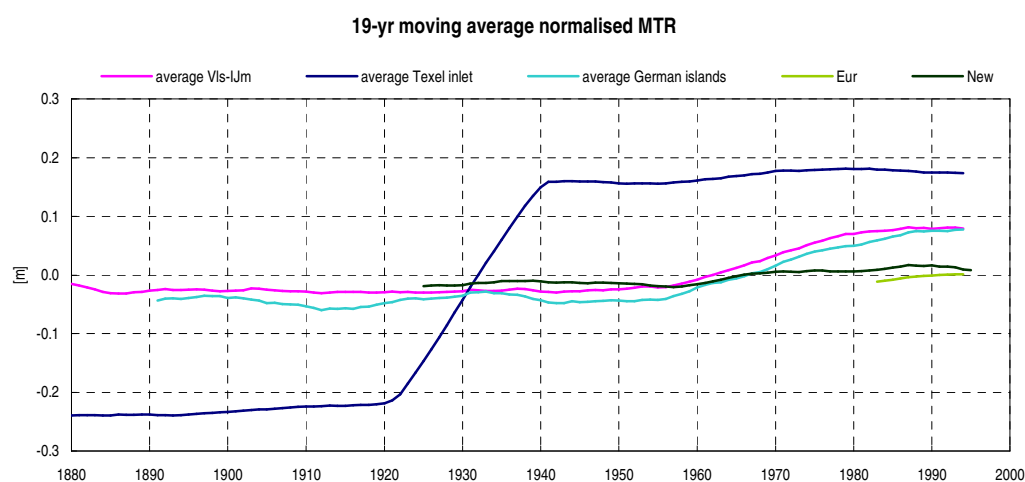


**Figure 4.5: Long-term trends for the Zeeland and Holland coast (Vls-IJm), the Texel inlet, the German North Sea islands and the Euro Platform (Eur).**

Figure 4.5 shows that the average trend of the Dutch stations is very similar to the average trend of the German stations. The tidal range increases gradually between 1955 and 1980 with c. 0.10 m (~5%). To assess if the trends are similar merely due to the 19-yr averaging, we test if the original annual data show a similar correlation. Therefore the annual tidal ranges of the artificial average of the Dutch stations and the German stations are expressed as a percentage deviation of their mean value and plotted together [see appendix A10]. This shows that not only the long-term trend is highly similar, but also the amplitude of the nodal tide and other fluctuations. The correlation coefficient of the two data sets is 0.92. The 19-yr average of the tidal range record at Newlyn indicates a changing trend after 1955. This increase, however, is much smaller (less than 1% till 1990) and it is not clear if this trend stabilises.

There are several stations with slightly deviating trends. First of all, it should be noted that the increasing trend between 1955 and 1980 is not exactly the same for all the stations. Some stations show a steeper and higher increase than others or start later. Vlissingen's trend is rising during more time intervals and the strong rise starts already in c. 1945. Here we observe a combination of local effects [see appendix A7] and the general trends as described before. Hoek van Holland is different too, because at this location the discharge of the Nieuwe Waterweg affects the low water levels such that the tidal range decreased between 1900 and 1955. The Wadden Sea the station Den Oever need to be interpreted with

care because discharges of the sluice affect the low waters significantly since 1980 [Doekes, personal communication]. Furthermore at West-Terschelling it is difficult to distinguish between the effects of the closure of the Zuider Sea and the general observed increasing trend between 1955 and 1980. Since the adjustment to the closure takes longer than at Den Helder for example, it looks as if there is a long time interval with an increasing trend which gradually levels out, but this trend is caused by two different phenomena. This can be seen from the discontinuity graph [see figure 4.6] and the changing trends of the high and low water levels [see appendix A6.11].

#### 4.7 Analysis of breakpoints

Not only is the general long-term behaviour of the tidal range of interest, but also sudden changes caused by human interference. To identify breakpoints in the records, we use the spectral analysis as described in section 2.6 and appendix A3. Plots of the discontinuity parameter, the Euclidian distance, are given in appendix A6 and figure 4.6 shows four examples]. In this study two different types of spectra are compared. The first type of spectrum contains all Fourier frequencies with a fundamental frequency of 1/10 yr and includes the zero-frequency amplitude ( $A_0$ ), the mean value. The second type does not include the zero-frequency amplitude.

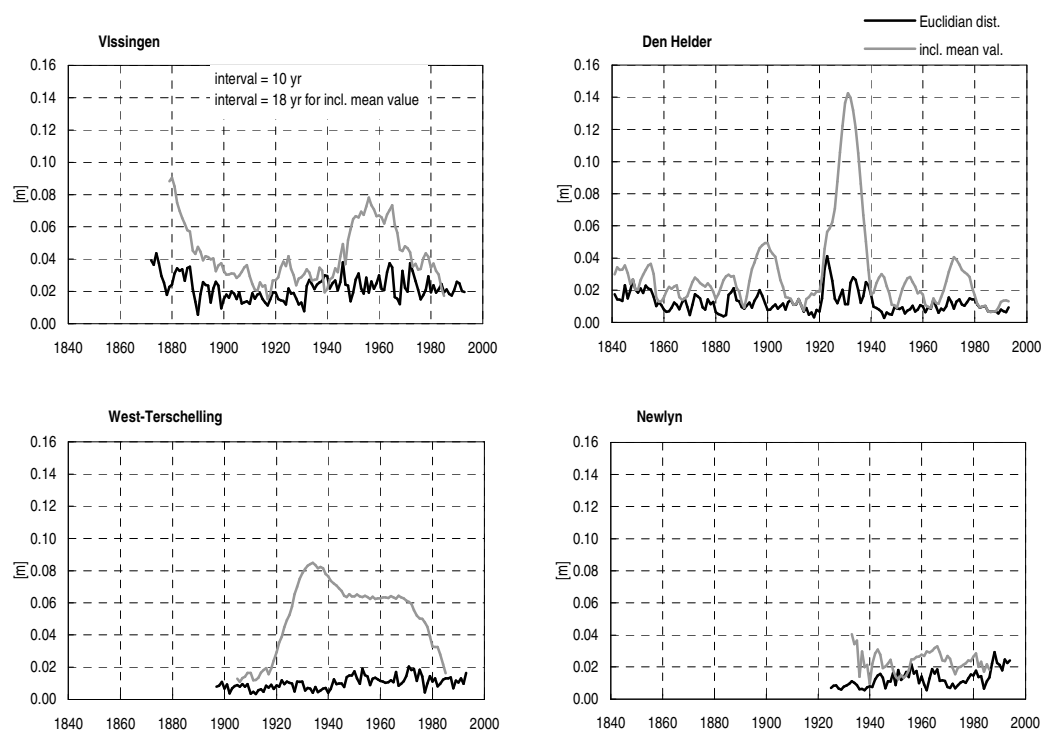


Figure 4.6: Discontinuity parameters for Vlissingen, Den Helder, West-Terschelling and Delfzijl. A time interval length of 10 yrs is used except for Vlissingen.

The Euclidian distance including the mean value of the interval, supports the interpretation of the moving average value since they both incorporate a vertical shift of tidal range. Most stations show a quite calm course between 1880 and 1950 or 1930 for the Wadden Sea. Breakpoints that can be identified with help of this parameter are shown in Table 4.2. In each case the discontinuity parameters are compared with the tidal range record and the record for high and low water levels to be able to identify and explain changes. The most obvious breakpoint is the closure of the Zuider Sea in 1932 which is observed at the Texel inlet stations and West-Terschelling. The graph of West-Terschelling [Appendix A6.11] reveals the strong increase of the tidal range after the closure which tries to level but is followed by another period of increase till c. 1970. From then on the tidal range becomes constant again. The graph shows also that this station has a very low Euclidian distance (excluding mean value) for the entire record. This means that the tidal range record is very homogenous and stable with constant frequencies and amplitudes. The opposite occurs at IJmuiden, between c. 1930 and 1960. During this time period the tidal range is very fluctuating without an identifiable change in mean value. The cause of these fluctuations is not well understood.

year	affected station(s)	cause	changes
1833	Delfzijl	unknown	jump in LW, increase TR
1880	Vlissingen	separation Scheldt into Eastern and Western Scheldt	decrease HW and LW, increase TR
1880	Hoek van Holland	construction Nieuwe Waterweg finished	LW stops increasing
1885	Den Oever and Harlingen	unknown	small drop in HW and LW, variability in HW and LW reduced and water levels start increasing
1885-1900	Den Helder	changes in outer delta	LW increases stronger than HW
c. 1890	IJmuiden	harbour entrance modifications note: measurements changed from staff gauge to recorder in 1883	HW and LW stop decreasing, TR stays constant
1905	Hoek van Holland	waterway network modifications	LW starts increasing
1930	Hel, Oud, Oev, Kor, Har, Wte	closure Zuider Sea	HW and LW more extreme, increase TR
1930-1960	IJmuiden	harbour modifications, unreliable records during WWII	high fluctuations HW and LW
1950-1980	Vls, Bur, Hvh, IJm, Hel, Har, Wte, Del	unknown, non-local cause likely, local perturbations possible	increase HW, constant LW
1960-1980	Hoek van Holland	harbour modifications	gradual increase HW, LW constant
1970-1980	Delfzijl	harbour modifications	decrease LW
1980	Den Oever	harbour modifications	increase LW
1984	Burghsluis	partial closure Eastern scheldt	increase LW, decrease HW, drop in TR

**Table 4.2: Breakpoints in tidal range records. LW=low water levels, HW=high water levels, TR=tidal range, see appendix Axx for station name abbreviations.**

#### 4.8 Summary statistical analysis

The following summarising items are presented to conclude the statistical analysis of tidal range records from the Dutch and German coast.

- Spectral analyses and a multiple linear regression analyses are applied to annual data of the tidal range at the Dutch tidal stations to determine which tidal constituents are present. It has been shown that only the nodal tide with a period of 18.61 yr can be identified on a significant level.
- The phase of the nodal tide has been evaluated as 1978.4 (year with a maximum) and the amplitude varies between 0.3% and 1.7% along the Dutch coast. The equilibrium ocean tide has an nodal tide amplitude of 3.7%. The fact that the observed tidal range is smaller and not identical for all stations is caused by friction in the North Sea basin.
- The short-term fluctuations have been assessed by constructing a residual signal from the tidal range spectra's high frequencies. The short-term fluctuations show a high similarity between the various stations. This indicates that the large variability in the tidal range is mainly caused by larger scale processes, not by measurement errors or local changes in geometry.
- Long-term trends in tidal range have been assessed by subtracting the 18.6-yr cycle from the measured tidal range and by constructing 19-yr moving averages. The 19-yr average tidal range shows that there is a positive trend in most of the records although this trend is not constant with time. The tidal range stayed constant from early 19<sup>th</sup> century till circa 1955 – apart from the nodal tide fluctuation and other random fluctuations. Only from then on does the tidal range increase with circa 5% till around 1980 and becomes constant again. This trend has been observed along the Dutch coast and the German coast, although recent data suggest that the tidal range is again increasing since 1993 at the German station. The tidal range at Newlyn shows a very small but significant trend. The 19-yr average indicates that the trend before 1955 is almost zero and increases after that year. An assessment of the individual high and low water levels in the period 1955-1980 show that the increase in tidal range during that period is caused by a changing trend in the low water levels.
- Breakpoints in tidal range records have been assessed by a spectral analysis, and a visual assessment of high and low waters, the tidal range residual signal and the moving average. The most evident change is the sudden increasing tidal range after the closure of the Zuider Sea in 1932. This has affected the stations of the Texel inlet and West-Terschelling. Other changes caused by anthropogenic effects have only a very local effect (e.g. river discharge regulations affecting the tidal range at Hoek van Holland, and harbour modifications in Delfzijl resulting in several breakpoints in the tidal range).

## 5 Conceptual model of inlet closures

In the previous chapter we found that highly similar tidal range developments are observed at the Dutch and German coast in the period 1955-1980. In this chapter the hypothesis is tested that this trend is caused by one common cause, being (partial) closures of inlets in the Zeeland delta area, south Netherlands. A conceptual model is applied to evaluate the spatial scale of influence of the closure of an estuary on the tidal range along the adjacent coastline.

Section 5.1 describes the model and the schematisation of the North Sea. In section 5.2 the numeric results of the reference case, a closed estuary, are presented. A sensitivity analysis of the boundary conditions is carried out to test how the tides in the North Sea basin are affected by disturbances in the Atlantic Ocean. The results are presented in section 5.3. The effects of closures of different estuaries are evaluated in section 5.4 and the interpretation of the results of the model is discussed in section 5.5.

### 5.1 Schematisation and model description

To verify the hypothesis that the tidal range along the German coast can be influenced by local changes at the Dutch coast, we are interested in the order of magnitude of the spatial scale of influence of a closure. This length scale is evaluated by using a conceptual model of the North Sea.

The model comprises a rectangular basin with roughly the dimensions of the North Sea [see figure 5.1]. The northern border is an open boundary with a connexion to the North Atlantic Ocean. In the model this boundary is forced with a simple semidiurnal ( $M_2$ ) tide. The other boundaries represent the British, Dutch, German, Danish and Norwegian coastline. These boundaries are closed (no cross current) and frictionless. Two reference scenarios are modelled, one with a constant bed level at 100 m below mean sea level and one with a sloping bed to examine friction effects.



Figure 5.1: Rectangular basin representation of the North Sea [map source: Wolters-Noordhoff, 2001]

In a basin with the dimensions of the North Sea, the rotation of the earth affects the tides. The importance of the earth's rotation can be estimated with the Rossby deformation radius [Pedlosky, 1987]:

$$R = \frac{c}{f} \approx \frac{\sqrt{gh}}{f} \quad [18]$$

where  $c$  is the wave velocity and  $f$  the Coriolis parameter ( $f = 1.2 \cdot 10^{-4} \text{ s}^{-1}$ ). The Rossby radius is a length scale at which the Coriolis accelerations become as important as accelerations due to pressure gradients. The Rossby radius for the North Sea is c. 270 km. Therefore Coriolis accelerations need to be included in the hydrodynamic equations [see appendix A11]. The tide generating potential within the basin is negligible; hence the tides are only driven by the incoming ocean tidal wave generated in the oceans. The wave progresses counter clockwise through the basin under the influence of Coriolis accelerations [Taylor, 1921]. Inertia and friction attenuate the tidal wave when it progresses through the shallow basin.

At the southern boundary various estuaries are added and subsequently closed at the inlet point. In this study the focus is on an estuary with variable size in the south-eastern corner which represents the Zeeland delta area. The size of the estuary will be chosen such that the tidal prism of the estuary is in the order of magnitude of  $10^9 \text{ m}^3$  as are the prisms of the Zeeland estuaries.

The calculated water level time series at each grid cell are transformed into the frequency domain which enables us to present graphs of co-range and co-tidal lines. Although bed friction will generate shallow-water tides with frequencies deviating from the  $M_2$  constituent, these will not be considered in the analysis. Inspection of the time series at various locations shows that the error in estimating the tidal range with the  $M_2$  constituent is small [see appendix A12]. This is not valid inside the estuary where friction has a much larger effect, but we are mainly interested in the change of tidal range outside the estuary.

The model is implemented using the software package Delft3D [WL | Delft Hydraulics, 2004]. The hydrodynamic equations used in this package are outlined in appendix A11. In this study a 2-dimensional, depth-averaged flow model is used.

There are several advantages of a conceptual model in comparison to a detailed model with accurate descriptions of the entire geometry and many external forces like complex tide and climatic conditions.

- A limited amount of data is required. Only the approximate dimensions of the North Sea and one typical ocean tidal constituent needs to be known.
- Calibration is almost unnecessary. The model results are qualitatively interpreted rather than quantitatively, so exact numbers are not important as long as they have realistic magnitudes.
- Short implementation time. Since a very small amount of data is used and almost no calibration is required, the model can be implemented in a relatively short time period.
- Easier to verify. In a model with a strongly schematised geometry and other input variables, only a few physical processes are simulated. The output data therefore, are less complex and easier to recognise and verify.

- Short simulation and data processing time. The use of less detailed data increases the calculation speed and results are processed more quickly. This gain in time can be used to evaluate a larger number of scenarios.

A disadvantage of a conceptual model, on the other hand, is that the interpretation of the model results is less straightforward than in a more realistic model. Many processes – of which some might dominate the actual tides – are not taken into account in the model. Therefore the model results need to be interpreted with care.

## 5.2 Modelling reference case

First of all two reference cases are modelled, representing the North Sea with a closed estuary. All input variables are presented in table 5.1. After simulation the time series of a few grid points are plotted to check when a stable situation has established free from initial condition effects. This is the case after 4 days or less [see appendix A12]. For extra safety and to allow for a longer adaptation time in case of an open estuary, only the last 4 days out of 11 are used in the analysis. The times series of these 4 days (with 8 cycles with  $f=30^\circ/\text{hr}$ ) are transformed into the frequency domain with a Fourier analysis. Co-range and co-tidal lines of the reference cases with a constant bed level and a sloping bed are shown in figure 5.2 a and b. The scenario with a constant bed level has a single amphidromic point in the centre of the southern half of the basin. The second reference case shows two amphidromes, one closer to the southern boundary and one closer to the eastern boundary. This latter scenario satisfies much more the actual tide in the North Sea [see also figure 5.9]. In the conceptual model the amplitudes are too large. The amplitude in the area representing the Zeeland delta, for example, is c. 50% larger than the actual value. The phase difference between the north-west corner and the south-west corner is c. 10 hr in the model and c. 14 hr in reality. The phase difference between the south-west and south-east corner is c. 8 hr in the model and 12 hr in reality. This indicates that the depth and the bed friction are not accurately included in this model, but the qualitative similarity is sufficient to use this model as a reference case.

property	value
length	940 km
width	580 km
depth	simulation 1 100 m
	simulation 2 100 m at open boundary, 25 m at southern boundary, linear slope
Chézy bed smoothness coefficient, $C$	65 $\text{m}^{1/2}\text{s}^{-1}$
Coriolis parameter, $f$	$1.2 \cdot 10^{-4} \text{ s}^{-1}$ , corresponding with LAT $55^\circ\text{N}$
grid size	5000 x 5000 m, rectangular
open boundary	$M_2$ tide (approximated with $f=30.0^\circ/\text{hr}$ ) with amplitude 1 m around zero-level
initial condition	water level = 0 for each grid cell
simulation time	7 days of which last 4 days used for analysis
simulation timestep	15 mins
analysed frequency	$M_2$ ( $30.0^\circ/\text{hr}$ )

Table 5.1: Input variables simulations 1 (constant depth) and 2 (sloping bed)

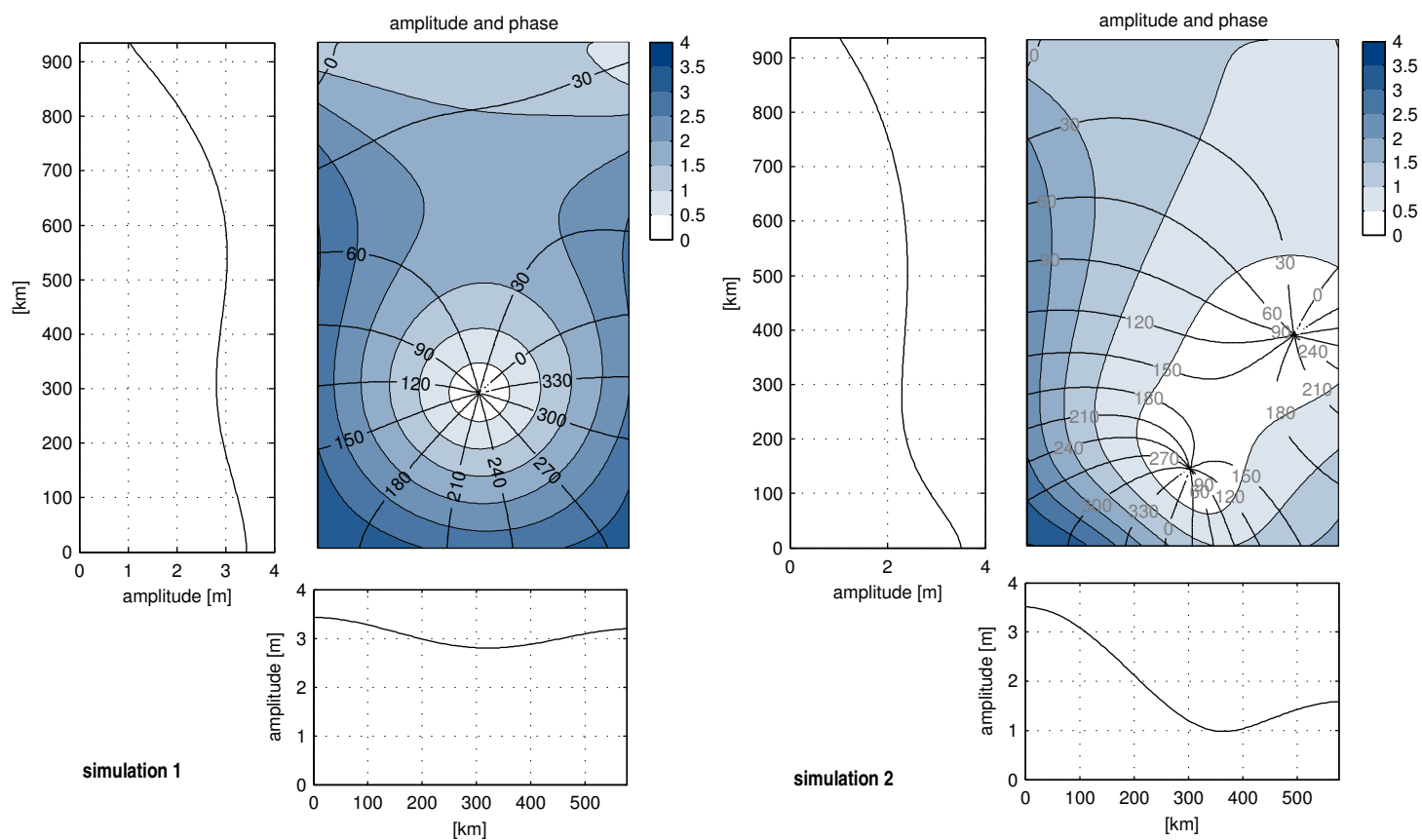


Figure 5.2: Co-tidal [°] and co-range [m] lines for two reference cases: a. constant depth of 100 m (simulation 1), b. depth decreasing from 100 to 25 m (simulation 2). Graphs at sides and bottoms show amplitude along the boundary

### 5.3 Sensitivity analysis of boundary conditions

To evaluate how disturbances in the North Atlantic Ocean tidal conditions influence the tides in the North Sea, a sensitivity analysis to the model boundary conditions is carried out. In the first case it is examined how an increased tidal range at the boundary affects the tidal range in the whole North Sea basin. In the second case the mean sea level at the boundary is increased. This certainly increases the mean sea level in the whole basin, but of interest in this study is whether and how this affects the tidal range in the basin. The input parameters are shown in table 5.2.

property	value
depth	100 m at open boundary, 25 m at southern boundary, linear slope
open boundary	simulation 3 M <sub>2</sub> tide with amplitude 1.05 m (+5%) around zero-level
	simulation 4 M <sub>2</sub> tide with amplitude 1 m around level 0.20 m (MSL rise)

Table 5.2: Input variables simulations 3 (tidal range increase) and 4 (sea level rise). All other variables are equal to the reference case (simulation 2).

The percentage change in amplitude relative to the reference case (simulation 2) is given in contour plots in figure 5.3 and 5.4. Figure 5.3 shows that an increase in tidal range at the boundary with 5% leads to a smaller increase the further the tidal wave progresses through the basin. Near the amphidromic points the relative increase is larger and decreases occur also. This means a slight shift in the location of the amphidrome. The displacement of the amphidromes is smaller than the grid size of 5000 m.

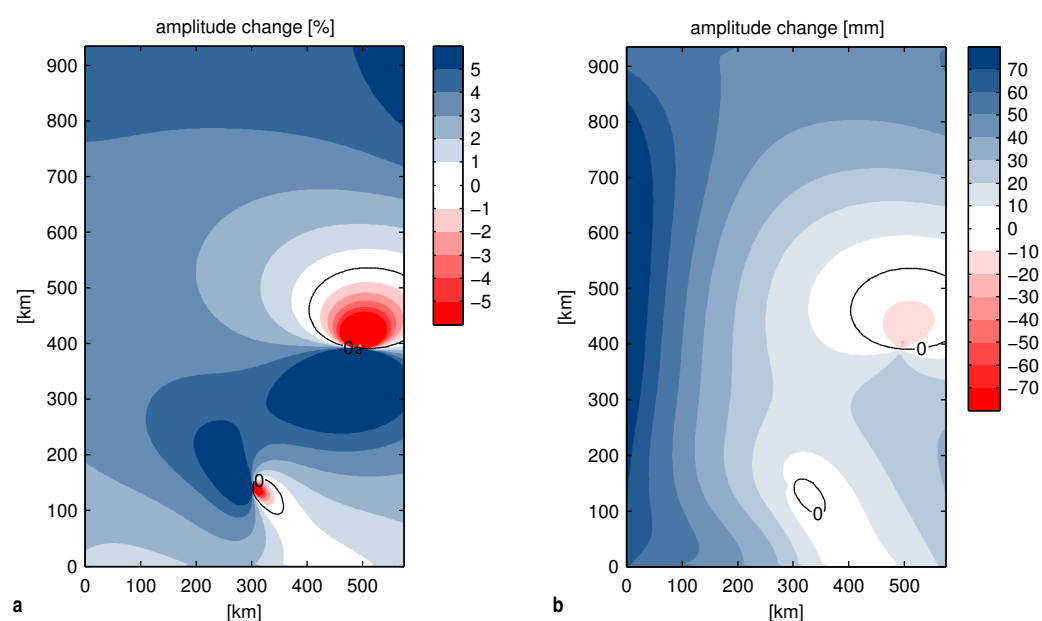


Figure 5.3: Percentage (a) and absolute (b) change of the M<sub>2</sub> amplitude after an amplitude increase of 5% at the open boundary (simulation 3)

A mean sea level rise of 0.20 m affects the tidal range varying from -38 to +33 mm. The percentage change shows high peaks of much more than  $\pm 5\%$  near the amphidromes. For most of the basin area the change lies within -2 to +2%. The general pattern is that the tidal range decreases at the west side of the basin and increases in the south east corner.

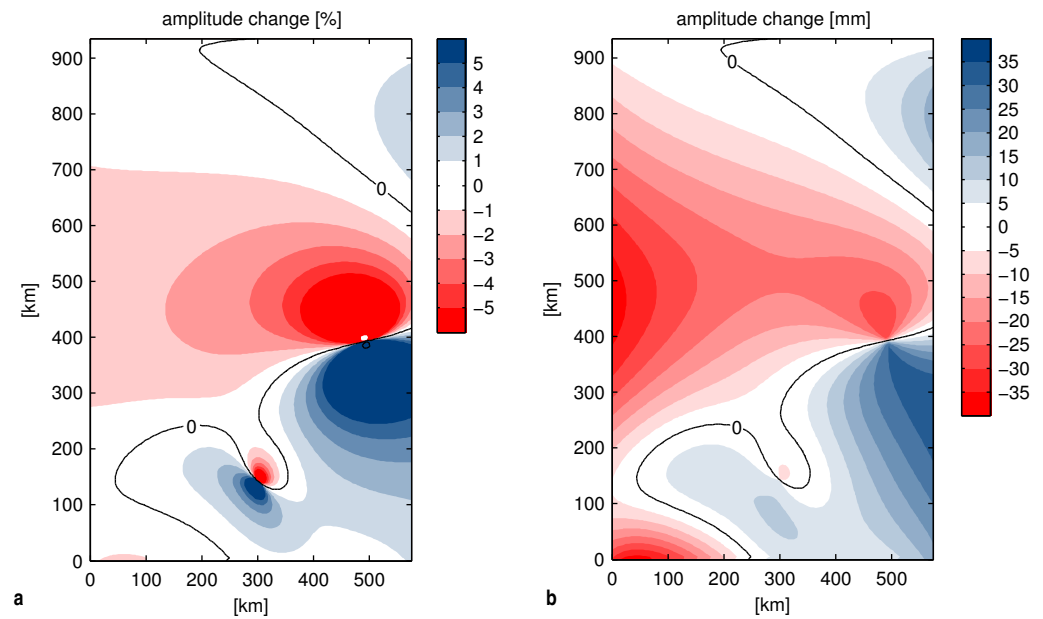


Figure 5.4: Percentage (a) and absolute (b) change of the  $M_2$  amplitude after a mean sea level rise of 0.20 m (simulation 4)

#### 5.4 Modelling closures of estuaries

The scenario modelled in section 5.2 is the situation after the closure of an estuary. In this section the situation before the closure of an estuary is evaluated. First, we examine the influence of the size of an estuary at a fixed location. The estuary is added to the basin near the south west corner, which represents an estuary in the Zeeland delta area. The width of the estuary is 5 or 10 km and the length is varied between 50 and 200 km [see table 5.3 for the input parameters]. To avoid reflection and amplification at the closed end of the estuary, the depth inside the estuary is reduced to 10 or 5 m and the bed smoothness reduced to  $C=45 \text{ m}^{1/2}\text{s}^{-1}$  [see for discussion on reflection appendix A13].

The water volume stored inside the estuary during a tidal cycle is called the tidal prism. This prism attenuates the tidal wave outside the basin. The tidal prism is therefore a better measure for the impact on the tides outside the mouth than the length and the width of the estuary. After each simulation the tidal prism is estimated as the area under the tidal range curve inside the estuary. This is not exactly the tidal prism when the tidal wave inside the estuary is not a standing wave but a propagating wave. This means that the actual prisms are slightly smaller. The estimated tidal prisms of the simulated scenarios are  $3.3 \cdot 10^9$ ,  $1.3 \cdot 10^9$  and  $0.7 \cdot 10^9 \text{ m}^3$ . The latter two scenarios (simulation 6 and 7) are closest to a real estuary in the Zeeland delta. The change in  $M_2$  amplitude after the closure of the estuary in simulation 6 is shown in figure 5.5. The results of the other scenarios are given in appendix A14.

property	value
depth basin	100 m at open boundary, 25 m at southern boundary, linear slope
estuary dimensions	simulation 5 width W=10, length L= 200 km, depth D=10 m, tidal prism P~ $3.3 \cdot 10^9 \text{ m}^3$ <sup>1 </sup>
	simulation 6 W=5, L=100 km, D=10 m, P~ $1.3 \cdot 10^9 \text{ m}^3$
	simulation 7 W=5, L=50 km, D=5 m, P~ $0.7 \cdot 10^9 \text{ m}^3$
estuary location	southern boundary, x=150 km
boundary condition closed end estuary	Q=0
<sup>1 </sup> prism estimated from model results	

Table 5.3 : Input variables simulations 5, 6 and 7. All other variables are equal to the reference case (simulation 2).

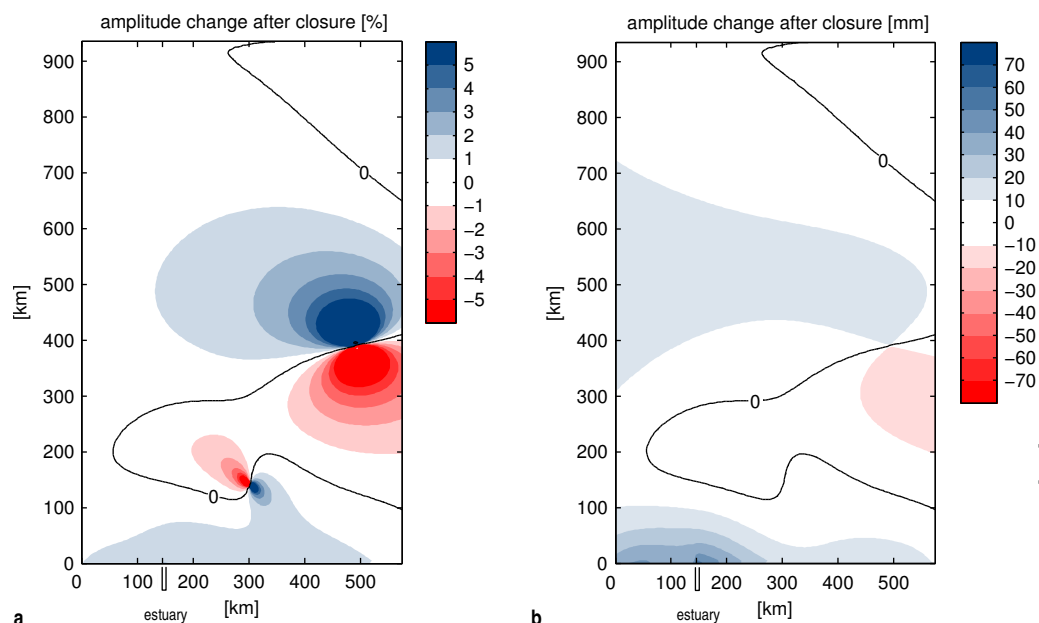


Figure 5.5: Percentage (a) and absolute (b)  $M_2$  amplitude change after closure of an estuary with  $P=1.3 \cdot 10^9 \text{ m}^3$  (simulation 6)

The tidal range increases with circa 1.9% or circa 100 mm (twice the amplitude) near the closed inlet. The further away from the inlet, the smaller the increase. The change in the tidal wave amplitude along the southern coastline is shown in figure 5.6 for the different scenarios. The graph shows that there is a peak at the (former) mouth of the estuary which decreases asymptotically along the coastline.

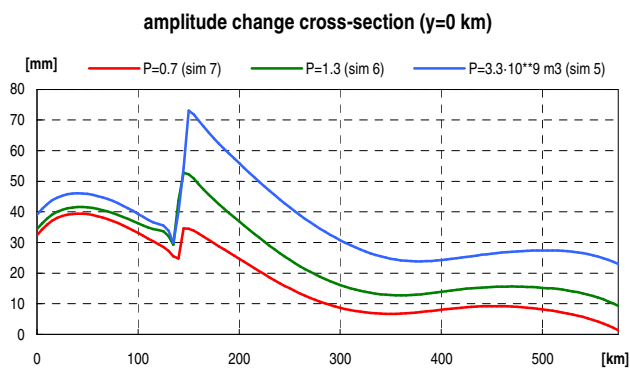
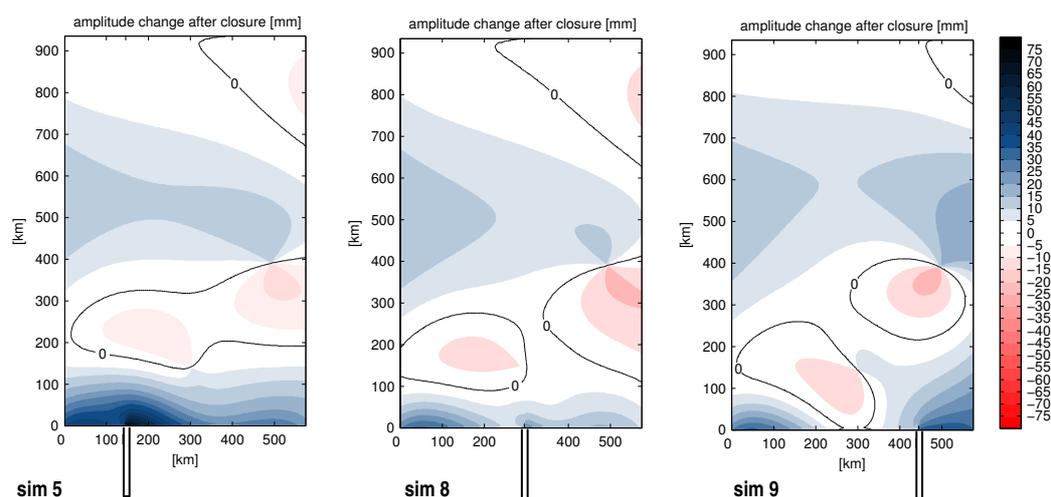


Figure 5.6:  $M_2$  amplitude change along the southern boundary for various estuary dimensions (simulations 5, 6 and 7)

Now we examine the influence of the location of the closure. For that purpose the estuary is shifted along the southern border of the basin at  $\frac{1}{4}$ ,  $\frac{1}{2}$  and  $\frac{3}{4}$  of the border length. Figure 5.8 shows patterns of the absolute change in amplitude throughout the basin. Relative changes are shown in appendix A14.

property	value
depth basin	100 m at open boundary, 25 m at southern boundary, linear slope
depth estuary	10 m
estuary dimensions	W=10, L=200 km
estuary location	simulation 5 southern boundary, x=150 km simulation 8 x=300 km simulation 9 x=450 km
boundary condition closed end estuary	Q=0

**Table 5.4: Input variables simulations 5, 8 and 9. All other variables are equal to the reference case (simulation 2).**



**Figure 5.8 :  $M_2$  amplitude change after closure of estuaries at different locations (simulation 5, 8 and 9)**

The results shown in figure 5.8 illustrate that the change in tidal range is more complex than a simple asymptotic decay along the coastline. Locally the tidal wave is amplified after a closure but the tides are affected over a large distance. There are even locations where the tidal range decreases after a closure. An alternating pattern of increasing and decreasing tidal ranges can be recognised throughout the basin. The amphidromes are the dividing points between zones with increasing and zones with decreasing tidal ranges.

A second observation is that the peak at the location of a closure is smaller when the estuary is located closer to an amphidromic point. Not only the absolute but also the percentage changes are smaller in the case of a closure nearer to an amphidrome (3% in simulation 5 and 2% in simulation 8). This indicates that the results are sensitive to the location of the inlet that is closed.

As mentioned before, computational results obtained with a conceptual model can be difficult to interpret and translate to a realistic situation. The conceptual model shows that the tidal wave is amplified when an estuary is closed and that this amplification diminishes away from the mouth of the estuary with exponential-type decay. This has also been shown in detailed model studies [e.g. Langendoen, 1987]. The magnitude of the increase is not very sensitive to the estuary dimensions but it does depend on the location of the closure and most likely also on the local geometry. To obtain more insight into the spatial behaviour of the tidal range after a closure we apply a slightly more detailed model. In this model the shape of the coastline of the southern North Sea is included schematically. The rectangular shape of the northern part of the basin is maintained since we want to avoid a boundary that is too close to the area of interest and at the same time we are not interested in the detailed spatial pattern in the northern part. In this model a rectangular estuary with dimensions c. 10 x 200 km is added at the location of the Western Scheldt. Co-tidal and co-range lines for the  $M_2$  tidal constituent in the more detailed model are shown in figure 5.9.

property	value
depth basin	50 m
depth estuary	50
estuary dimensions	W=9.6, L=201.6 km, P=0.8·10 <sup>9</sup> m <sup>3</sup>
estuary location	x=235 km , y=55 km (Western Scheldt location)
boundary condition closed end estuary	Q=0
coast shape	coarse approximation of ZUNOWAK model [see Langendoen, 1987]
grid size	3200 x 3200 m

Table 5.5 : Input variables simulation 10

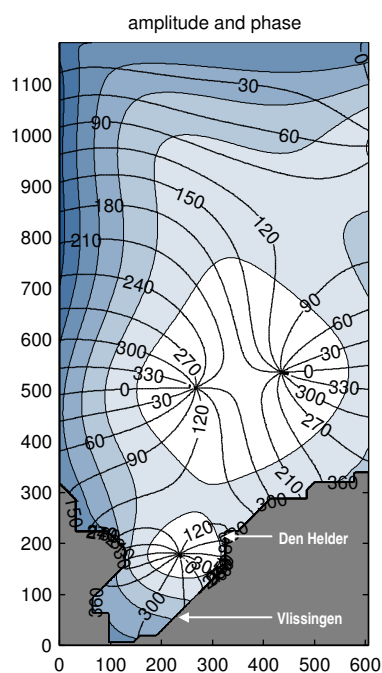


Figure 5.10:  $M_2$  co-tidal [°] and co-range [m] lines for model with detailed coastline in southern North Sea

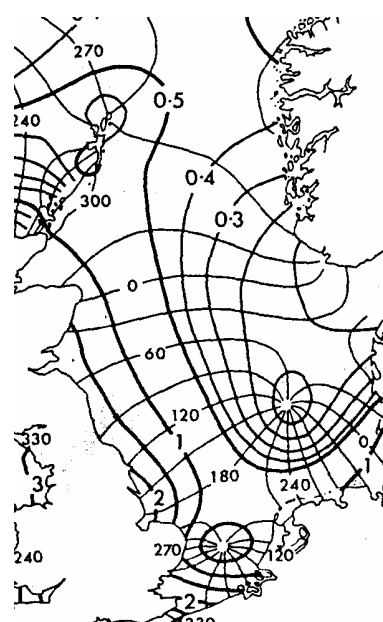
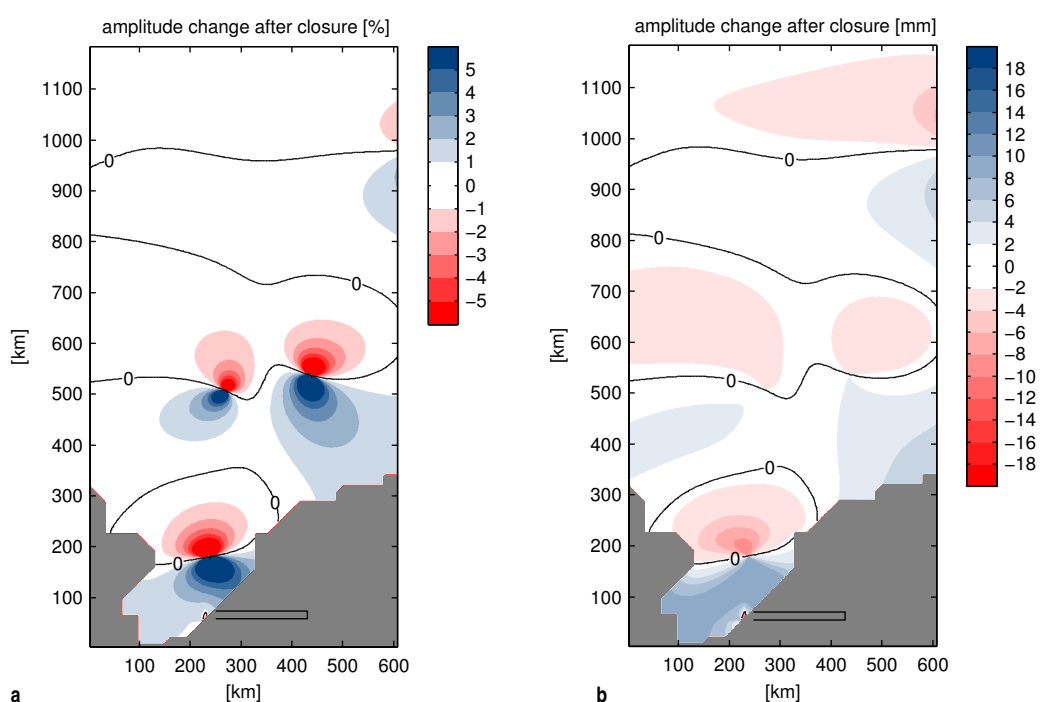


Figure 5.9:  $M_2$  co-tidal [°] and co-range (bold, [m]) lines in the North Sea [Pingree and Griffiths, 1987]

Specification of the coastline causes the amphidromic points shift to more realistic positions. The two simulated amphidromic points in the centre of the basin are in reality a single amphidromic point which is located slightly closer to the German and Danish coast. But the amphidrome in the area between the Dutch and English coast has a realistic position. This allows us to evaluate in more detail the spatial response to a closure at the Dutch coast. The absolute and percentage  $M_2$  amplitude change after closure are shown in figure 5.11.



**Figure 5.11: Percentage (a) and absolute (b)  $M_2$  amplitude change after closure of an estuary with  $P=0.8 \cdot 10^9 \text{ m}^3$  (simulation 10)**

This model with a more accurate representation of the coastline shows that the closure of an estuary results in an amplitude increase of circa 20 mm near the point of closure. This increase is smaller than in the conceptual model but that is because the tidal range is smaller in this basin: the percentage increase is similar to c. 2% for this estuary with a prism of  $1.3 \cdot 10^9 \text{ m}^3$ .

In this model the zone of increasing tidal ranges stretches out till Den Helder, circa 200 km from the closure point. The decay, however, is not exponential decaying as in the model without coastline specification. Here the geometry in combination with the position of the amphidromic point apparently limits the length scale over which the tides are affected. The change throughout the basin is a pattern of alternating increasing and decreasing tidal ranges with very small changes north of the centre amphidromes (2-4 mm in amplitude change).

## 5.5 Interpretation of model results

The results of the conceptual model with a rectangular basin show that the tidal range increases in the vicinity of a tidal inlet when it is closed. This is consistent with the theory that an estuary acts as a storage basin. The tidal wave progressing along the coast seaward of the mouth is attenuated by the storage capacity of the estuary. After closure of the inlet there is no attenuation any longer and the tidal range increases. The estimated increase of amplitude of the  $M_2$  tidal constituent is c. 50 mm (or 100 mm for the tidal range) when closing an estuary with a typical tidal prism of  $10^9 \text{ m}^3$ . This corresponds to a percentage increase of c. 1.9%. Langendoen [1987] estimated the increase in tidal range after the closure of the Wester Scheldt by 60 mm or 1.6%. This shows that the conceptual model gives a good estimate of the peak increase at the location of the closure. The results of Langendoen's study are more accurate because his model incorporated a more detailed geometry, including coastlines and bathymetry.

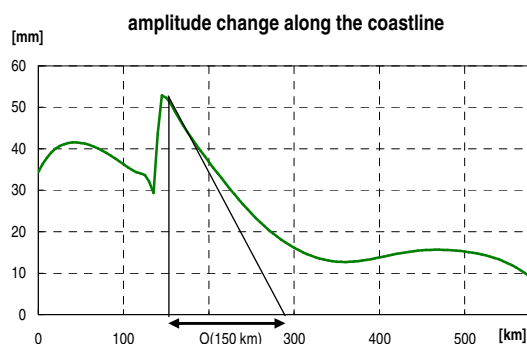


Figure 5.12: Asymptotic decay of the tidal range increase along the coastline

The conceptual model shows that the peak increase near the closed inlet diminishes along the coastline. This decay is asymptotic with a typical length scale of 150 km [see figure 5.12]. The graph shows that the tidal range increases over the entire southern boundary. There is a small increase in tidal range in the south east corner of the basin, representing the German Bight. This is visible in both the conceptual model and the more detailed model. Apparently the tidal range changes over the entire basin which raises the question whether there is a limited spatial scale of influence. The following three arguments show that the length scale derived from the rectangular basin model is a good indication of the actual length scale of influence:

1. Changes further away from the location of the closure are much smaller than at the adjacent coast line. This can be seen in the graphs of absolute changes in amplitude throughout the basin. While the change at the inlet varies from c. 50-70 mm, the changes further away remain under 10-20 mm for most of the simulations. The most significant changes are due to the cancelled tidal wave attenuation in the vicinity of the estuary and stretch out over a distance derived from rectangular basin simulations. Secondary changes are due to a small shift in the tidal system which is driven back by the closure of the estuary. This results in the alternating pattern of increasing and decreasing tidal ranges and a small shift of the amphidromes.

2. This influence over a large distance can be artificial and only arise in this conceptual model. In reality the erratic coastline and bathymetry are likely to damp out the changes over a shorter distance [Elias, personal communication]. In the model with the schematised coastline the long-distance effects are much smaller than in the rectangular basin model. It is likely that these effects are further reduced when a detailed geometry of the coastlines and the sea bed is applied. The used conceptual model and the model with the schematised coastline are not sufficiently detailed to assess these changes accurately.
3. The results of the conceptual model are supported by the more detailed model and Langendoen's simulations, indicating a significant influence till Den Helder (~200 km).

The simulations with a changed boundary condition show that changes in the North Atlantic Ocean are damped inside the North Sea basin. This means that disturbances at the ocean are not amplified when the tidal wave progresses through the basin. For example a 5% tidal range change in the Atlantic Ocean results in a change of only 1 to 3% along the Dutch coast. The consequence is that changes at the Dutch coast can only be explained by oceanic tidal changes when the changes in the ocean have the same magnitude or larger.



## 6 Conclusion

This chapter gives conclusion of the research on the tidal range in the North Sea. Section 6.1 presents a combined interpretation of the main sections of this report, the statistical analysis and the simulations of estuary closures. Section 6.2 presents the final conclusions of this study and section 6.3 shows the relevance of these conclusions. Recommendations are given in section 6.4.

### 6.1 Joint interpretation of statistical and model analyses

The statistical analysis of Dutch and German tidal range records revealed a highly similar trend between the two coastline sections. The short-term fluctuations show a similar pattern of peaks and troughs but especially the long-term trends are similar showing a gradual increase in tidal range in the period 1955-1980. The hypothesis that these trends have a common cause, namely inlet closures in the Zeeland delta, has been tested with a computational flow model. This conceptual model shows that the tidal range increases near the inlet that is closed and that these effects decay along the adjacent coastline. The length scale of this asymptotic decay is circa 150 km. This is in agreement with Langendoen's [1987] findings that closures in the Zeeland delta enlarge the tidal range along the adjacent coast up to Den Helder. In the conceptual model the tides are affected beyond this location with a pattern of increasing and decreasing tidal ranges. These changes are much smaller than close to the estuary and possibly result of the idealised geometry in the conceptual model [see section 5.5]. The observed trend at the German North Sea islands, however, is quantitatively identical to the trend at the Zeeland and Holland coast. Therefore the hypothesis that the tidal range trend at the German coast is caused by changes in the Zeeland delta area, is rejected.

In the process of setting up the model we have examined how changes in mean sea level affect the tidal range. The typical 0.20 m increase of mean sea level over the past century has an effect of less than + 1% in tidal range along the Dutch coast in the conceptual model. This has been evaluated with detailed models by Austin [1988] and De Ronde [1989] [both cited in Woodworth *et al.*, 1991]. Both researchers concluded that only several metres mean sea level change affect the tidal range significantly. Therefore, it is not likely that the observed trends in tidal range (with changes of c. 5%) are caused by an increasing sea level.

There are several possible explanations for the observed trends at the Dutch and German coast.

1. The trends are coincidentally similar and caused by individual coastal engineering at the River Elbe in Germany and the delta works in the southern Netherlands as has been suggested by Woodworth *et al.* [1991]. New data shows that the tidal range developments are very similar and are both accelerating since 1955. Furthermore, this explanation leaves the question unanswered why the increase is gradual,

as is shown by both the 19-yr averages and the tidal range residuals, and not with sudden and explainable jumps.

2. The tidal regime in the North Sea has changed due to global climatic changes. Stations like Brest, France [Cartwright, 1972] and Newlyn, south west England, [Woodworth *et al.*, 1991] suggest that secular tidal changes with an oceanic origin exist. In this report we have shown that this trend is not uniform in time: the Newlyn records indicate an increasing tidal range since 1955 only. Not only the mechanisms influencing the ocean tidal range are hardly understood, but also long records from ocean tide stations are lacking. It is therefore difficult and also beyond the scope of this study to give evidence for a causal connection between the very small trend at Newlyn and large trends at the Dutch and German coast. Sea level spectra based on hourly observations from before 1955 and after 1980 can be used to give more insight in the mechanisms causing the changes and whether they are related to known phenomena.

## 6.2 Final conclusions

The following conclusions can be drawn from the statistical analysis of tidal range records and the model simulations of inlet closures:

- The tidal range has stayed nearly constant from early 19<sup>th</sup> century till circa 1955. Nevertheless, the high and low water levels have increased at a constant rate at most of the stations.
- This constant course of the tidal range is perturbed by two phenomena:
  1. The longitude of the moon's ascending node. This causes a periodic fluctuation with a period of 18.6 yr and an amplitude of 0.2 – 2%, depending on the location.
  2. Random noise due to variability in the tides in the North Atlantic Ocean and the North Sea (caused by astronomic, meteorological or geometry changes) and measurement errors. The peaks in the noise signal have a magnitude of up to  $\pm 5\%$ . The fluctuations at Newlyn are smaller than at the Dutch stations because they are more influenced by the geometry of the coastal zone.
- Other changes observed can be explained as causes of anthropogenic effects. The most clearly recognisable effect is the sudden increasing tidal range at the stations of the Texel inlet and West-Terschelling due to the closure of the Zuider Sea in 1932. Other changes are observed at, for example, Hoek van Holland where the tidal range decreased in the period 1860-1960 due to river discharge regulations and at Delfzijl where harbour modifications affected the tidal range in 1978.
- A gradual increasing tidal range is observed at all stations in the period 1955-1980. This increase is caused by a decreasing trend in low water levels. For the Dutch and German stations the tidal range increase is circa 5%. The increase at Newlyn is smaller than 1% and at this location there is no evidence of a stabilised tidal range after 1980. The tidal range at the German stations stays constant after 1980 but seems to rise again since 1993. Because a general trend is found which is observed at many stations, changes in tidal range at individual stations cannot be explained as effects of human interventions only. Therefore individual tidal range records need to be interpreted with reservation.
- Model simulations show that coastal engineering in the Zeeland delta cannot be the common and only cause of the gradual increase in tidal range at both the Dutch and German coast. The closure of an

estuary with a typical size of a Zeeland estuary causes locally a few percent increase in tidal range. This effect falls below a significant level over a distance of maximum 200 km.

The current rate of sea level rise can only account for less than 1% tidal range increase over the past century and therefore cannot explain the observed trend. A satisfying explanation for the gradual trend cannot be given within the scope of this research project.

### **6.3 Application and relevance of the conclusions**

The relevance of this study is that it adds to existing insight into the complex spatial and temporal pattern of change in tidal range in the North Sea. In this study a large set of stations along the Dutch, German and British coast is used with up-to-date time-series. This made it possible to assess long-term and general trends. The apparent long-term trend can be used as a framework to understand and explain observed temporal changes in tidal range at the various locations in the southern North Sea.

More insight into the development of the tidal range, and especially the high water levels is important because of the impact on flood defence schemes. Increasing tidal ranges need to be superimposed on the mean sea level to acquire insight in extreme water levels. This study shows that there is no evidence that high water levels are increasing with a rate larger than that of the mean sea level. Furthermore, annual variability in the tidal range [Corkan, 1934] and storm surges determine the actual extreme water levels and are normative for the required sea defence heights. The mean tidal range, as used in this study, is not of great interest in flood risk analyses.

### **6.4 Recommendations**

An explanation for the observed gradually increasing tidal range during the period 1955-1980 has not been given. A complex interaction between the North Atlantic Ocean, the North Sea and the meteorological system is the most likely (but vague) explanation. Sea level spectra based on hourly recordings can be used to assess which tidal constituents have contributed to the changed tidal range.

More data are required to make a better assessment of general trends in tidal range. Especially recordings at deep water, uninfluenced by coastal processes, are needed to separate natural changes accurately from anthropogenic effects. Data from islands like the Shetland Islands, north of the British mainland, and the Faerøer islands, between Scotland and Iceland, are of high interest. At the moment records from these locations are still too short to assess long-term trends but will be useful in the future.

## References

- BOON, J. D. (2004) *Secrets of the tide; Tide and tidal current analysis and predictions, storm surges and sea level trends*, Chicester, Horwood Publishing.
- BRAKER, J. G. (1994) *Singular spectrum analysis of North Sea mean sea level time series*, Delft, TU Delft.
- CARTWRIGHT, D. E. (1972) Secular changes in the oceanic tides at Brest, 1711-1936. *Geophys. J. R. astr. Soc.*, 30, 433-449.
- CARTWRIGHT, D. E. (1974) Years of peak astronomical tides. *Nature*, 248, 656-657.
- CORKAN, R. H. (1934) An annual perturbation in the range of tide. 536-558.
- CURRIE, R. G. (1976) The spectrum of sea level from 4 to 40 years. *Geophys. J. R. astr. Soc.*, 46, 513-520.
- CURRIE, R. G. (1981) Amplitude and phase of the 11-yr term in sea-level: Europe. *Geophys. J. R. astr. Soc.*, 67, 547-556.
- DE RONDE, J. G. (1986) *Bepaling knoofactoren harmonische analyse met het Continental Shelf Model; Notitie GWAO-86.309*, Rijkswaterstaat, Dienst Getijdewateren.
- FLATHER, R. & WILLIAMS, J. (2000) Climate change effects on storm surges: methodologies and results. IN BEERSMA, J., AGNEW, M., VINER, D. & HULME, M. (Eds.) *Climate scenarios for water-related and coastal impacts*. Climatic Research Unit, UEA.
- FÜHRBÖTER, A. & JENSEN, J. (1985) Longterm changes of tidal regime in the German Bight (North Sea). IN MAGOON, O. T. (Ed.) *Fourth symposium on coastal and ocean management*. Baltimore.
- GERRITSEN, H. (1989) *Large periodicities in the tide*, Delft, Delft Hydraulics.
- GODIN, G. (1972) *The analysis of tides*, Liverpool, Liverpool University Press.
- GORDON, D. L. (1968) Rationalisation of chart datum in the British Isles. *Int. hydrogr. Rev.*, 45, 55-65.
- HERMAN, R. (2002) *Signal and image processing*, internet: [people.uncw.edu/hermanr/signals](http://people.uncw.edu/hermanr/signals). Wilmington, University of North Carolina.
- JENSEN, J. & MUDERSBACH, C. (2002) Long-term changes of the water levels along the German North Sea coastline. *Littoral 2002, The changing coast*. Porto, Portugal.
- JENSEN, J., MÜGGE, H. E. & SCHÖNFELD, W. (1992) Analyse der Wasserstandsentwicklung und Tidedynamik in der Deutschen Bucht. *Die Küste*, 53, 211-275.
- KALKWIJK, J. P. T. (1976) *De analyse van getijden*, Delft, Technische Hogeschool Delft.
- LANGENDOEN, E. J. (1987) Onderzoek naar de vergroting van het tijverschil te Vlissingen. *Faculteit der Civiele Techniek*. Delft, TU Delft.
- MATHWORKS (2003) MATLAB. 7.0.0.19920 ed. Massachusetts, The MathWorks.

- MUNK, W. & DZIECIUCH, M. (2002) Millennial climate variability: is there a tidal connection? *Journal of climate*, 15, 370-385.
- OPPENHEIM, A. V., SCHAFER, R. W., BUCK, J. R. & LEE, L. (1999) *Discrete-time signal processing*, Upper Saddle River, N.J., Prentice Hall.
- PEDLOSKY, J. (1987) *Geophysical fluid dynamics*, New York, Springer-Verlag.
- PINGREE, R. D. & GRIFFITHS, D. K. (1987) Tidal friction for semidiurnal tides. *Continental shelf research*, 7, 1181-1209.
- POL (2005) *Permanent Service for Mean Sea Level*, internet: [pol.ac.uk/psmsl](http://pol.ac.uk/psmsl).
- RAKHORST, D. (2003a) *Verandering in het tijverschil rond de Waddenzee*, Haarlem, Rijkswaterstaat RIKZ.
- RAKHORST, D. (2003b) *Veranderingen in het tijverschil langs de Nederlandse kust*, Haarlem, Rijkswaterstaat RIKZ.
- RAKHORST, D. (2005) *Tijverschillen langs de Nederlandse kust; De invloed van menselijke ingrepen*, Haarlem, Rijkswaterstaat RIKZ.
- RIJKSWATERSTAAT (1985) *Tienjarig overzicht der waterhoogten, afvoeren en watertemperaturen; 1961-1970*, 's-Gravenhage, Rijkswaterstaat.
- RIJKSWATERSTAAT (1989) *Tienjarig overzicht der waterhoogten, afvoeren en watertemperaturen; 1971-1980*, 's-Gravenhage, Rijkswaterstaat.
- RIJKSWATERSTAAT DIRECTIE NOORDZEE (2005) *Dieptekaart van de Noordzee*, internet: [www.noordzee.org](http://www.noordzee.org).
- STEWART, R. H. (2002) *Introduction to physical oceanography*, Texas, Texas A&M University.
- TAYLOR, G. I. (1921) Tidal oscillations in gulfs and rectangular basins. *Proc. London Math. Soc.*, 20, 148-181.
- TRELOAR (2002) Luni-solar tidal influences on climate variability. *International journal of climatology*, 22, 1527-1542.
- U.S. GEOLOGICAL SURVEY (2005) *USGS CMG InfoBank Atlas*, internet: [walrus.wr.usgs.gov/infobank](http://walrus.wr.usgs.gov/infobank). Reston, U.S. Geological Survey.
- WL | DELFT HYDRAULICS (2004) *Delft3D-Flow*. 3.39.09 ed. Delft, WL | Delft Hydraulics.
- WOLTERS-NOORDHOFF (2001) *De grote bosatlas; editie 52*, Groningen, Wolters-Noordhoff bv.
- WOODWORTH, P. L. (1985) A world-wide search for the 11-yr solar cycle in mean sea-level records. *Geophys. J. R. astr. Soc.*, 80, 743-755.
- WOODWORTH, P. L., SHAW, S. M. & BLACKMAN, D. L. (1991) Secular trends in mean tidal range around the British-isles and along the adjacent European coastline. *Geophysical Journal International*, 104, 593-609.

# A1 Multiple linear regression (MLR) analysis

borrowed from [Kalkwijk, 1976; Herman, 2002; Boon, 2004]

Starting point is a discrete record of the tidal range  $MTR_n$  with a record length  $N$ .

The tide is composed of a many sinusoidal functions each with a different period (or frequency), phase and amplitude. Each sinusoidal represents an astronomical or other physical process e.g. the rotation of the moon around the earth. The length of these cycles are well known [see appendix A4 for list of frequencies]. Theoretically, all periods longer than 1 year could be found in a annual mean tidal range record. However, many of the tidal constituents have such small amplitudes that they can not be evaluated accurately because non-tidal variability introduces large errors in the calculations of these constituents [Stewart, 2002].

Beside cyclic functions a linear trend is fitted with the tidal data. This linear trend does not represent a known physical process but is supposed to account for unknown slow processes like sea-level rise, long-term morphological changes or a change in river discharge (this affects the mean low waters at Hoek van Holland for example).

The total trend line (linear +  $m$  cyclic functions) for the tidal range is:

$$MTR_n^{trend} = MTR_0 + s \cdot t_n + \sum_{m=1}^M a_m \cos(\omega_m t_n - \varphi_m) \quad [19]$$

this can be written as:

$$MTR_n^{trend} = MTR_0 + s \cdot t_n + \sum_{m=1}^M [A_m \cos(\omega_m t_n) + B_m \sin(\omega_m t_n)] \quad [20]$$

with

$$a_m = \sqrt{A_m^2 + B_m^2} \quad \text{and} \quad \varphi_m = \arctan\left(\frac{B_m}{A_m}\right)$$

where  $a_m$  is the amplitude and  $\varphi_m$  is the phase of the constituent  $m$ . [21]

The closest fit is computed with the least square method. Hence the sum of the differences  $\varepsilon_n$  between the measured MTR and the trend need to be minimized:

$$\sum_{n=1}^N \varepsilon_n^2 = \sum_{n=1}^N (MTR_n - MTR_n^{trend})^2 \quad [22]$$

in order to minimize the derivatives of the linear parameters  $MTR_0$ ,  $s$ ,  $A_m$  and  $B_m$  need to be zero:

$$\frac{\partial \sum_{n=1}^N \varepsilon_n^2}{\partial MTR_0} = 0; \quad \frac{\partial \sum_{n=1}^N \varepsilon_n^2}{\partial s} = 0; \quad \frac{\partial \sum_{n=1}^N \varepsilon_n^2}{\partial A_m} = 0 \forall m = [1, M] \quad \text{and} \quad \frac{\partial \sum_{n=1}^N \varepsilon_n^2}{\partial B_m} = 0 \forall m = [1, M] \quad [23]$$

This results in a system of  $2+2m$  equations which can be solved.

## A2 Spectral analysis

borrowed from [Stewart, 2002]

Starting point is a record of the tidal range  $MTR(t)$  with a record length  $T$ .

When the energy density spectrum of a tidal range record is evaluated, long-term trends will influence the amplitude of the fundamental frequency and the first harmonic frequencies considerably. In order to avoid this distortion of the spectrum, the tidal range is corrected with a linear trend:

$$MTR^*(t) = MTR(t) - (a \cdot t + b) \quad [24]$$

where the parameters  $a$  and  $b$  are computed with the least square method.

The tidal range record, written as a Fourier series (in complex form) is:

$$MTR^*(t) = \sum_{-\infty}^{\infty} Z_m \exp(i2\pi mft) \quad [25]$$

$Z_n$  is the Fourier transform of  $MATR^*(t)$  and can be calculated by:

$$Z_m = \frac{1}{T} \int_{-T/2}^{T/2} MTR^*(t) \exp(-i2\pi mft) dt \quad [26]$$

where  $f = 1/T$  is the fundamental frequency and  $m \cdot f$  with  $m = 0, 1, 2, \dots$  are the harmonics of the fundamental frequency.

The power spectrum  $S(f)$  of  $MTR^*(t)$  is:

$$S(mf) = Z_m Z_m^* \quad [27]$$

where  $Z_m^*$  is the complex conjugate of  $Z_m$ .

In discrete form the equations [25] and [26] are transformed into:

$$MTR_n^* = \sum_{n=0}^{N-1} Z_m \exp(i2\pi j m/N) \quad [28]$$

$$Z_m = \frac{1}{N} \sum_{n=0}^{N-1} MTR_n^* \exp(-i2\pi j m/N) \quad [29]$$

where  $N$  is the record length and  $n$  is a time index.

Several methods are available to compute an energy density spectrum. Here we use the Fast Fourier Transform method as implemented in MATLAB [Mathworks, 2003]. The energy density at each frequency is computed with equation 27 and this enables us to compute the amplitude for each constituent:

$$a_m = \frac{\sqrt{S(mf)}}{N/2} \quad [30]$$

In case the record is zero-padded to obtain a desired record length,  $N$  is defined as the original record length without zeros.

## A3 Analysis of breakpoints in tidal range records

To be able to identify breakpoints or discontinuities in the tidal range we make use of the spectral characteristics of subsets of the whole record. The amplitude spectra of two adjoining time intervals are compared and the differences between the two spectra expressed in a single parameter. This parameter is a measure for the change at the time point (t-break) between the two adjoining intervals [see figure A3.1]. The intervals are shifted over the entire record which results in a discontinuity parameter for each time value (except at the beginning and the end of the record). This makes the method suitable for the evaluation breakpoints without any hypothesis about their positions.

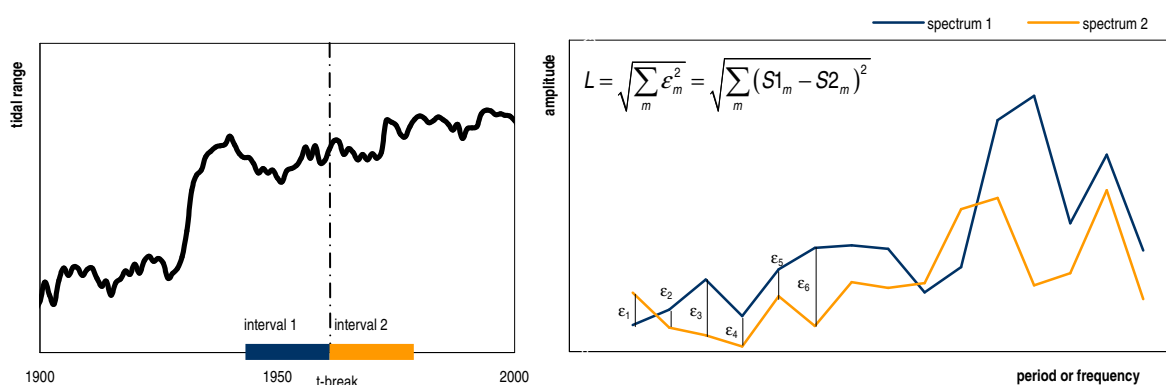


Figure A3.1: Comparison of the spectra of two adjoining intervals. t-break is varied between the start and the end of the record and the differences  $\epsilon$  are calculated for each t-break.

Two methods are used to compute and compare the spectra of the two intervals.

1. In the first method the spectra of the linear corrected tidal range is used. Here the linear trend of the interval is subtracted from the original data. This means that the calculated spectrum does not represent long-term changes but only higher frequencies within the interval.
2. The second method uses the non-corrected tidal range of the interval. Here the  $A_0$  values of the spectra deviate from zero and are included in the comparison of the two spectra. This method allows for sheer jumps in the tidal range without change of the tidal frequencies.

The parameter used to compare the spectra of the two intervals, is the so called Euclidian distance of the two spectra. It should be noted that because the two adjoining intervals are equal in length, the frequencies calculated by the Fast Fourier Transform method are the same for both intervals. Therefore,

the difference between the two spectra can be expressed by a limited number of  $\varepsilon$ -values [see figure 1]. They are combined to the Euclidian distance ( $L_2$ ) as follows:

$$L_2(t_{break}) = \sqrt{\sum_m \varepsilon_m^2} = \sqrt{\sum_m (S1_m(t_{break}) - S2_m(t_{break}))^2} \quad [31]$$

where  $S1$  and  $S2$  are the spectra of intervals 1 and 2 respectively with frequencies  $m$ .

$L_2$  has the same dimension as the spectra. Here the amplitude spectra are used, hence the dimension is [m].

## A4 Tidal periodicities

	physical cause	period	frequency °/hr
1	local mean lunar time	1 lunar day	14.49205211
2	moon's mean longitude	1 month	0.54901653
3	sun's mean longitude	1 year	0.04106864
4	longitude of moon's perigee	8.847 yr	0.00464184
5	longitude of moon's ascending node	18.613 yr	0.00220641
6	longitude of sun's perigee	20,940 yr	0.00000196

Table A4.1: fundamental astronomical tidal periods [Stewart, 2002]

Each constituent of the tide has an angular velocity (or frequency):

$$\omega = n_1\omega_1 + n_2\omega_2 + n_3\omega_3 + n_4\omega_4 + n_5\omega_5 + n_6\omega_6$$

$$\text{with } n_1 = 1, 2, 3 \text{ and } n_{2,3,\dots,6} = -5, 4, \dots, 5$$

The equilibrium astronomic tide can be calculated with the formula

$$h(t) = h_0 + \sum_n f_n H_n \cos(\omega_n t + V_n + u_n)$$

where  $h$  is the water level at time  $t$  each day starting with zero,  $h_0$  is the reference level,  $H_n$  is the amplitude of the tidal constituent,  $f_n$  and  $u_n$  are corrections for the nodal tide (only component considered with periods longer than 1 year),  $\omega_n$  the angular velocity of the tidal constituent and  $V_n$  is the uniform changing part of the astronomic argument due to the resetting of  $t$  at the beginning of each day.

To calculate real tides (non-equilibrium), the amplitude  $H_n$  is empirically determined and an empirical correction is applied on the phase. Note that the nodal tide with a period of 18.6 yr is not treated as a separate constituent with its own wave period and phase, but interpreted as slow changing amplitudes and phases of constituents with periods smaller than one year.

The correction factors for the lunar node cycle  $f_n$  and  $u_n$  are calculated as follows:

the amplification for the  $M_2$ , the  $N_2$  and  $MS_4$  constituent is:

$$f = 1 - 0.037 \cos N$$

and the phase is:

$$u = -2.1 \sin N$$

with

$$N = 259.16 - 19.3282(Y - 1900) - 0.0530(D + i)$$

where  $N$  is in degrees and  $Y$  is the year,  $D$  is the number of days after 1 January and  $i$  is the number of lap years after 1900.

For the diurnal, the 4 and 6 times per day constituents different relations hold. The annual and the semi-annual (Sa and Ssa) are not affected by the nodal tide.

physical cause	period [yr]	literature
longitude of moon's ascending node (nodal tide)	18.6	[Gerritsen, 1989; Jensen and Muddersbach, 2002; Stewart, 2002]
unknown	13.3	[Jensen <i>et al.</i> , 1992]
sunspot cycle	~ 11	[Currie, 1981; Woodworth, 1985; Jensen and Muddersbach, 2002]
longitude of lunar perigee (rotation of moon's elliptic path)	8.85	[Stewart, 2002]
North Atlantic pressure oscillations, changes in zonal (westerly) wind	~ 7.5	[Woodworth, 1985; Braker, 1994; Jensen and Muddersbach, 2002]
unknown	6.1-6.4	[Currie, 1976; Jensen <i>et al.</i> , 1992]
El Niño effects	~ 4.5	[Braker, 1994]
unknown	4.2	[Jensen <i>et al.</i> , 1992]

**Table A4.2: long-term (> 1 yr) tidal cycles with different underlying causes**

## A5 Tide gauging stations

	station	record length	remarks
	<b>Dutch coastline</b>		
Vls	Vlissingen	1862..2003	
Bur	Burghsluis	1880..1986	1984..1986 not used because of closure Eastern Scheldt
Hvh	Hoek van Holland	1864..2003	
Sch	Scheveningen	1896..1947 and 1962..2003	data not reliable
Ijm	IJmuiden	1872..2003	
Hel	Den Helder	1832..2003	
Del	Delfzijl	1827..2003	
	<b>Wadden Sea</b>		
Oud	Oudeschild	1878..2003	
Oev	Den Oever	1853..2003	
Kor	Kornwederzand	1933..2003	1933..1943 not used because of closure Zuider Sea
Har	Harlingen	1865..2003	1865..1878 not used because of deviant pattern
Vli	Vlieland harbour	1878..1921 and 1941..2003	station not used because of missing data and suspicion of strong local effects, out of trend with West-Terschelling
Wte	West-Terschelling	1887..2003	
Smo	Schiermonnikoog	1966..2003	
	<b>German North Sea islands</b>		
Bor	Borkum	1931..1999	
Nor	Norderney	1891..1999	
Awe	Lighthouse Alte Weser	1903..1999	
Hlg	Helgoland	1925..1999	
Wit	Wittdün	1937..1999	
Lis	List	1931..1999	
	<b>North Sea</b>		
Eur	Euro platform	1984..2003	1985 missing
	<b>Great Britain</b>		
New	Newlyn	1915..2004	tidal ranges compiled from hourly sea level measurements by RIKZ

**data:** annual mean values of high water levels (MHW) and low water levels (MLW)

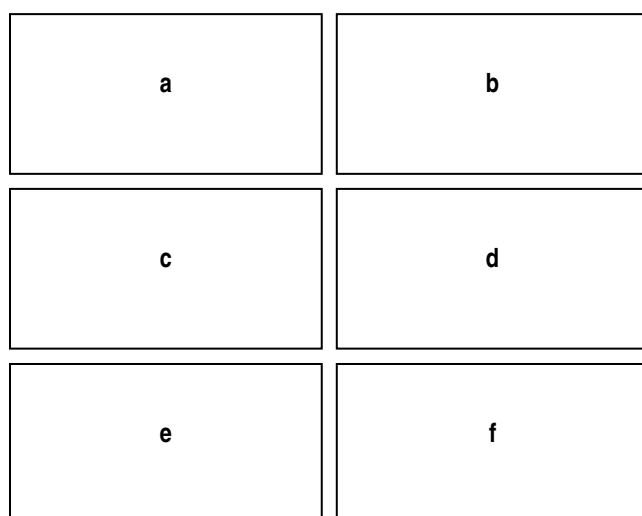
**source:** data obtained from Rijkswaterstaat Rijksinstituut voor Kust en Zee (RIKZ) (Dutch stations), Proudman Oceanographic Laboratory (POL) (British stations) and Jürgen Jensen (German stations)



**Figure A5.1: Locations of the gauging stations at the Dutch and German North Sea coast [base map adapted from Wolters-Noordhoff, 2001]**

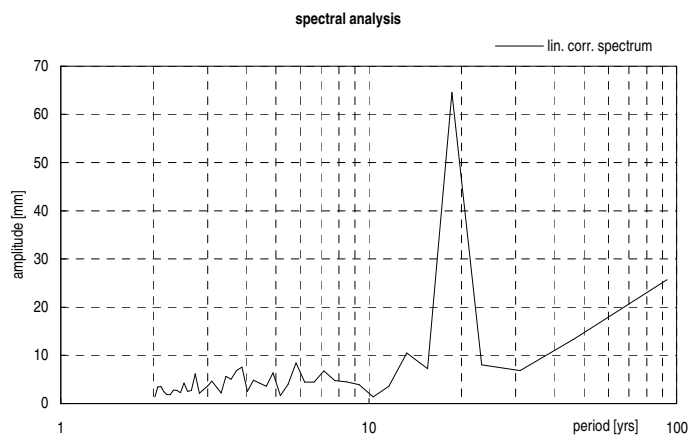
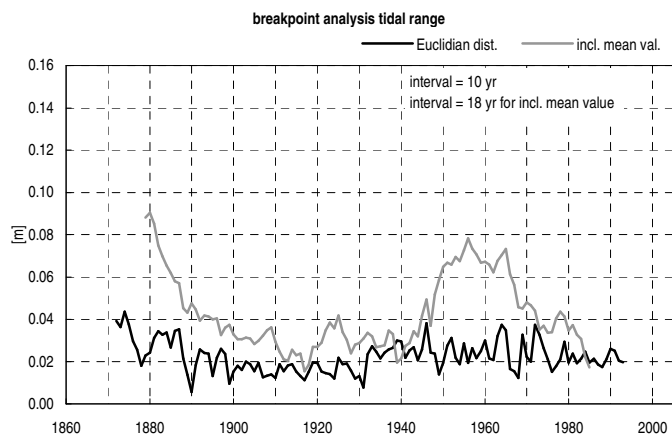
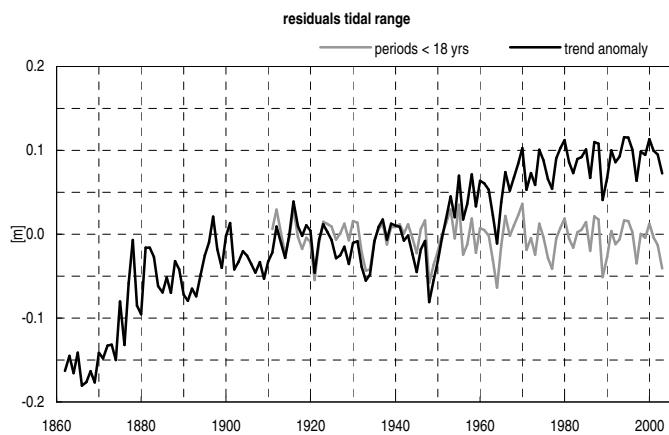
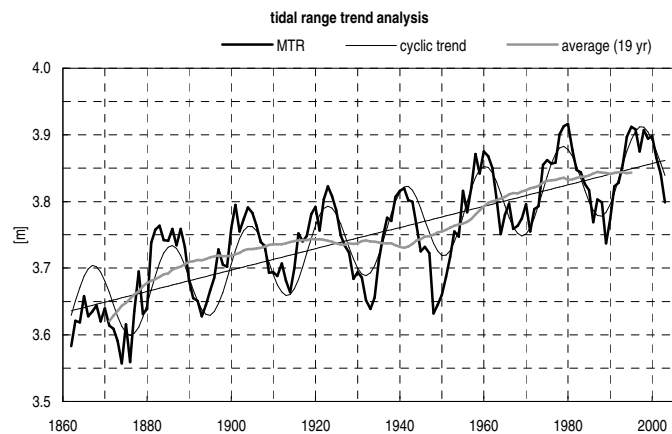
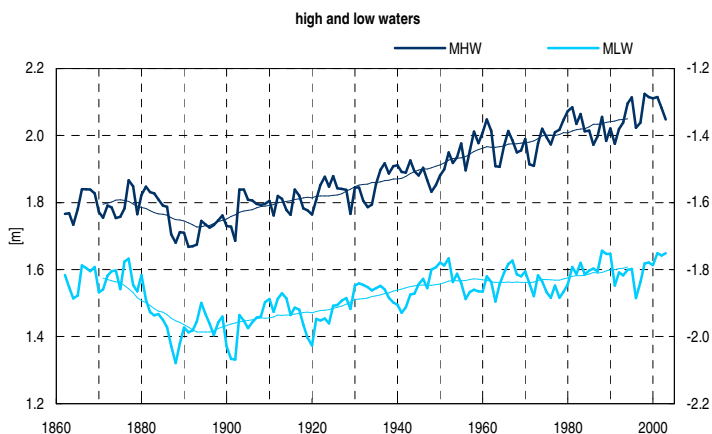
## A6 Plots of tidal records

This appendix contains graphs for high and low water levels and the tidal range and graphs with results from statistical analyses. Each station is presented on a separate page containing the following graphs:



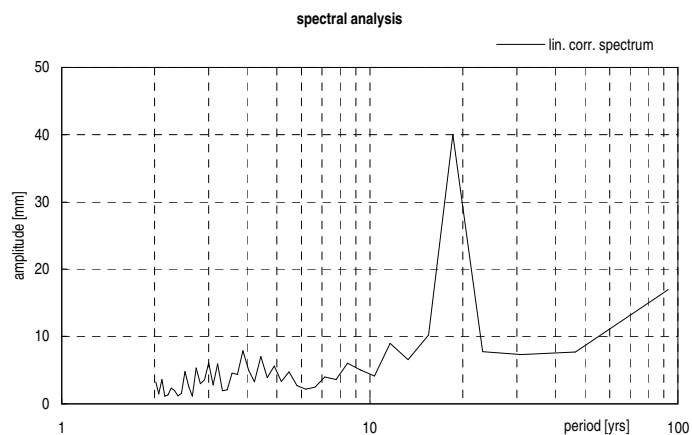
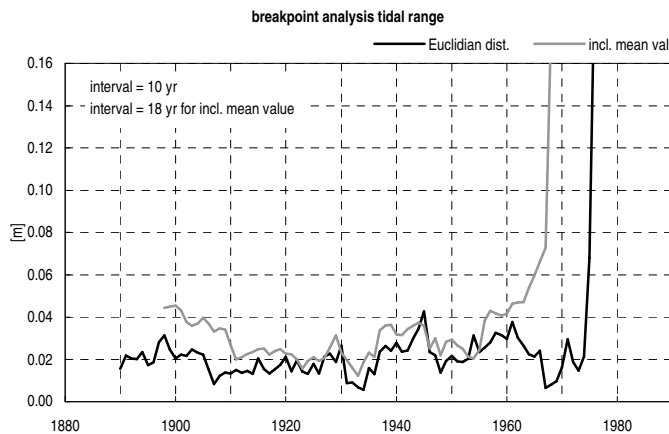
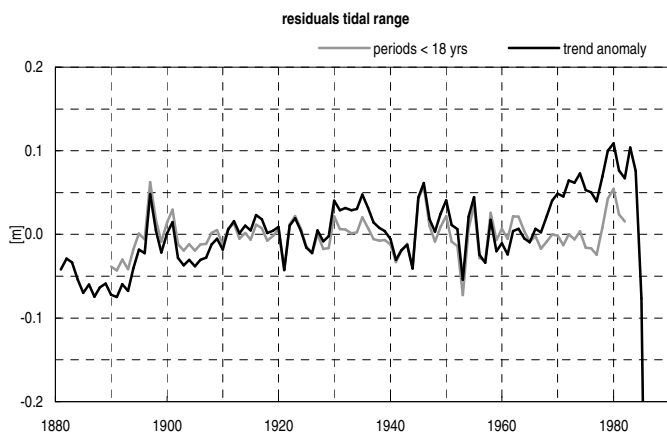
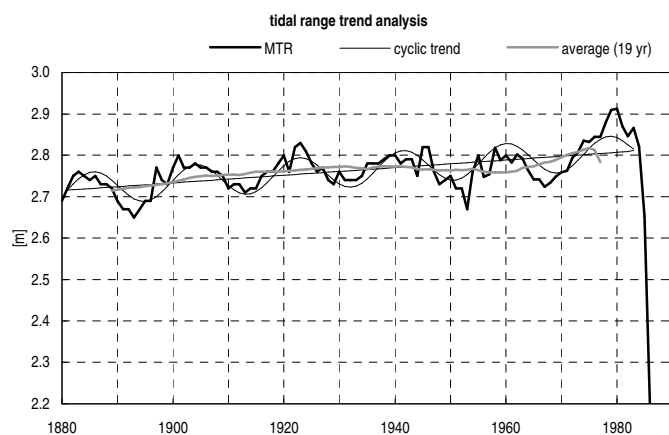
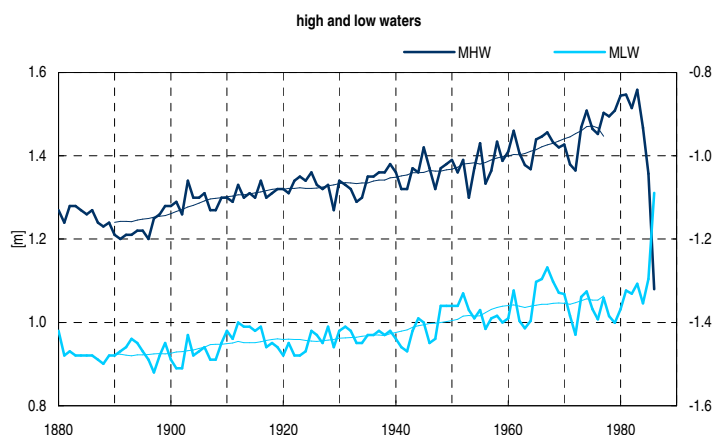
- a** 1 annual mean high water level (left axis) [m] (MHW)  
 2 annual mean low water level (right axis) [m] (MLW)  
 smooth lines are 19-yr moving averages, midpoint assigned
- b** 1 annual mean tidal range [m] (MTR)  
 2 linear trend line of MTR [m]  
 3 linear + nodal tide trend line of MTR [m] [see section 2.3 and 4.4]  
 4 19-yr moving average of MTR, midpoint assigned [m] [see section 2.5 and 4.6]
- c** 1 high frequency signal calculated from spectrum with  $f > 1/15\text{yr}$  [see section 2.4 and 4.5]  
 2 anomaly from nodal tide periodic trend (excluding linear trend line) [see section 2.4 and 4.5]
- d** 1 discontinuity parameter (Euclidian distance) excluding mean value ( $A_0$ ) [m]  
 2 discontinuity parameter including mean value [m] [see section 2.5 and 4.7]
- e** amplitude spectrum of MTR, horizontal axis: period  $T$  [yr], vertical axis: amplitude  $A$  [mm] [see section 2.2]
- f** fact sheet

1 Vlissingen



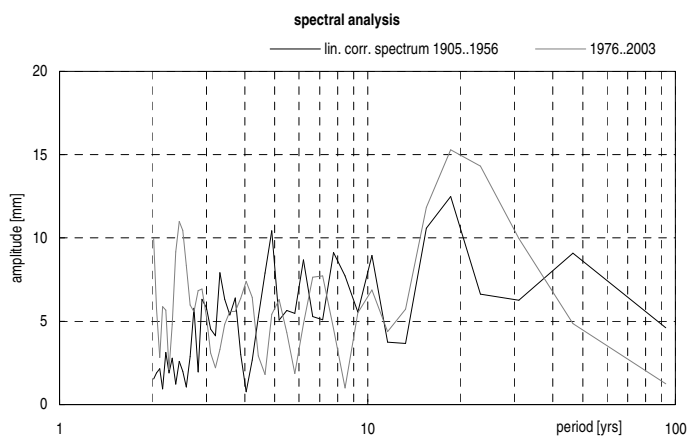
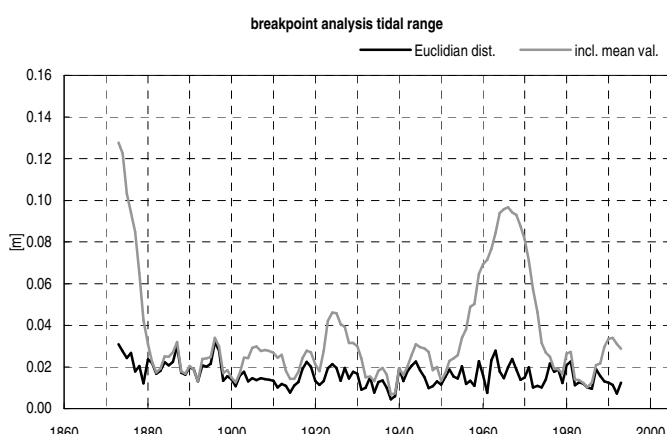
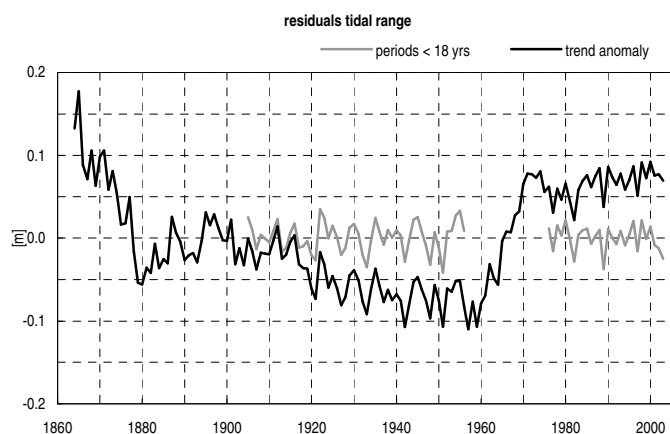
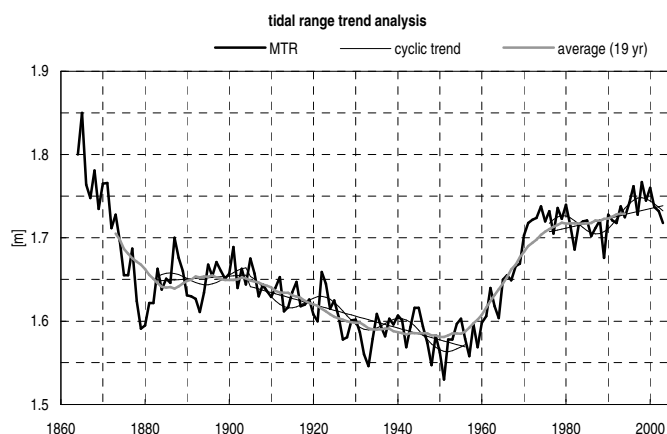
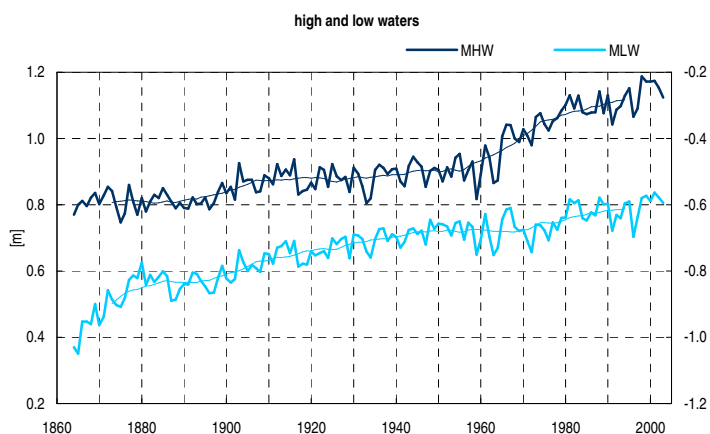
fact sheet station Vlissingen	
	1862..2003
mean tidal range [m]	3.75
linear trend [mm/100 yr]	160±7
nodal tide amplitude [mm]	59.6 (1.6%)
trend fit (R <sup>2</sup> )	0.84

2 Burghsluis



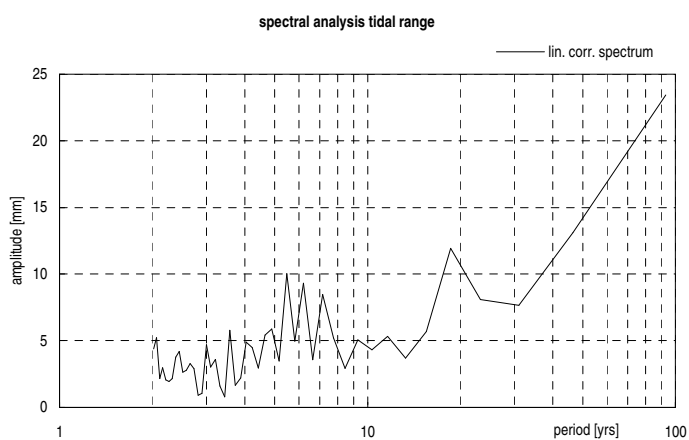
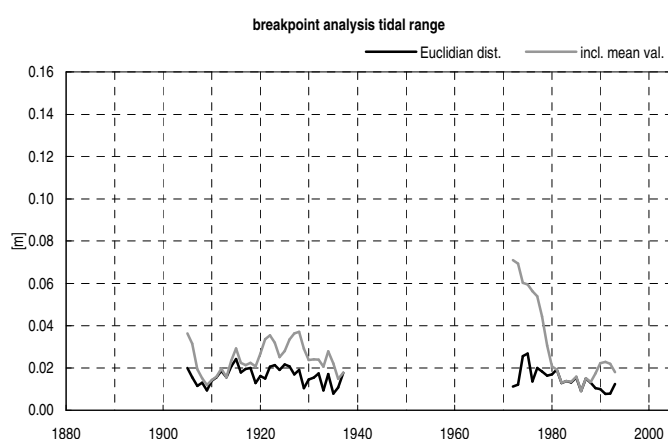
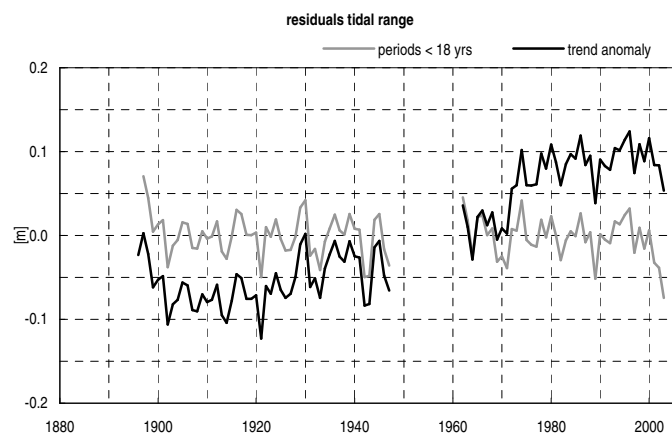
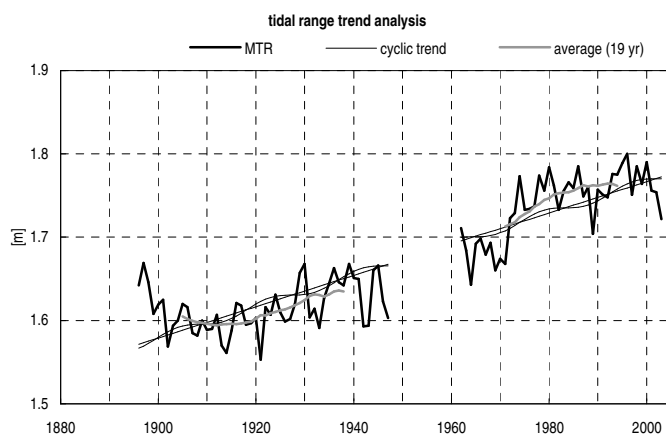
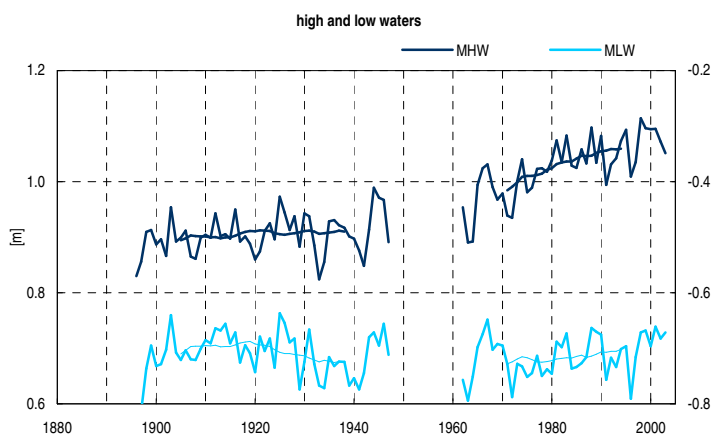
fact sheet station <b>Burghsluis</b>	
	1880..1983
mean tidal range [m]	2.76
linear trend [mm/100 yr]	92±9
nodal tide amplitude [mm]	39.9 (1.4%)
trend fit (R <sup>2</sup> )	0.67

3 Hoek van Holland



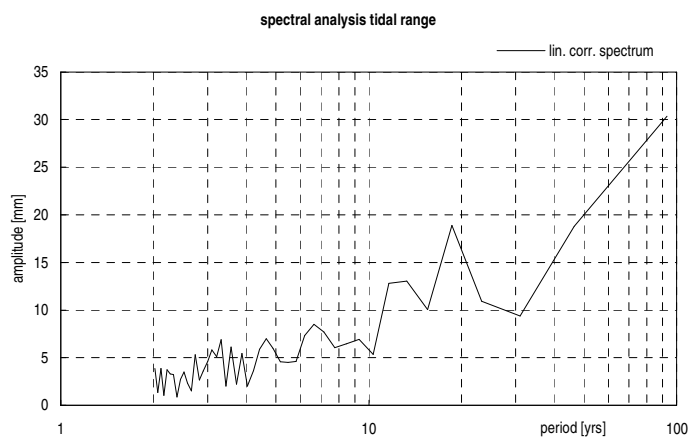
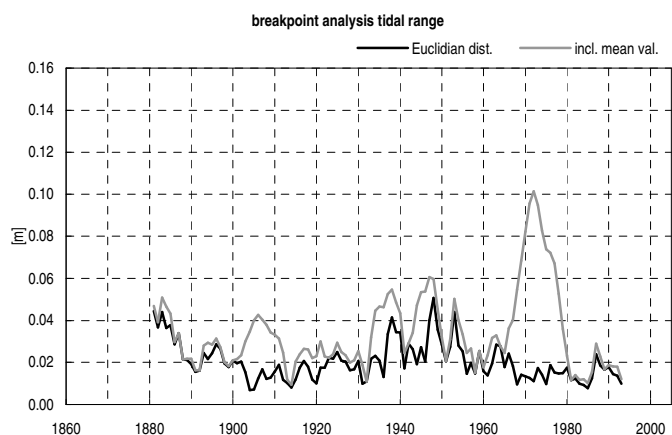
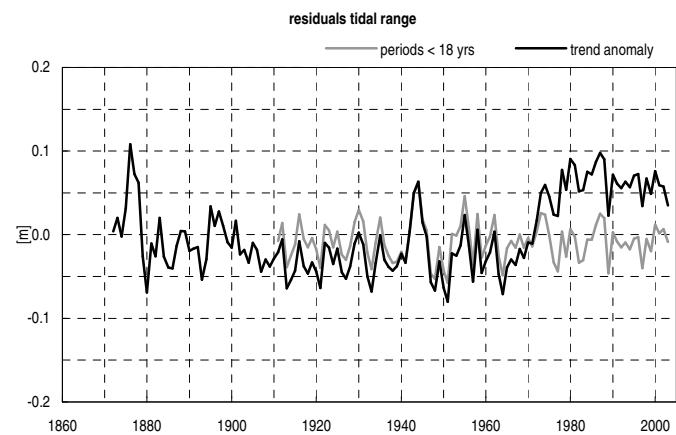
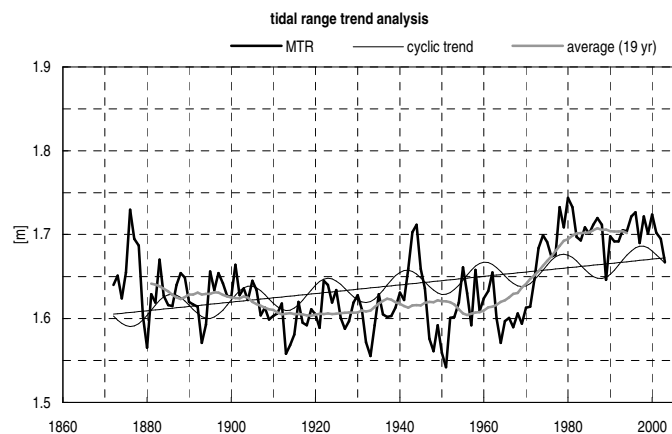
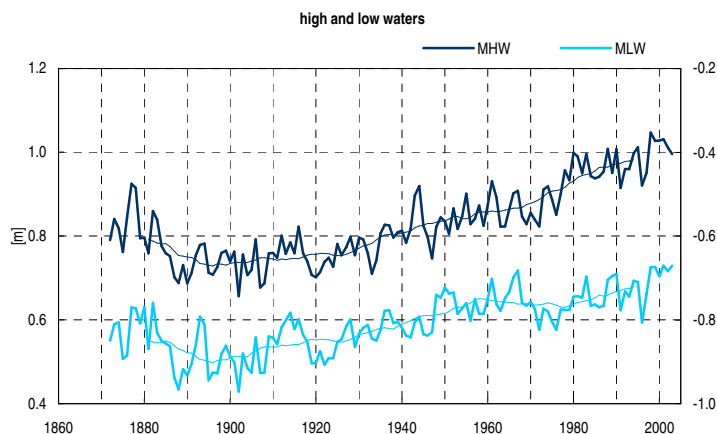
fact sheet station <b>Hoek van Holland</b>			
	1883..1904	1905..1956	1976..2003
mean tidal range [m]	1.65	1.61	1.72
linear trend [mm/100 yr]	34±69	-141±18	116±35
nodal tide amplitude [mm]	8.6 (0.5%)	12.8 (0.8%)	16.2 (0.9%)
trend fit (R <sup>2</sup> )	0.09	0.62	0.49

4 Scheveningen



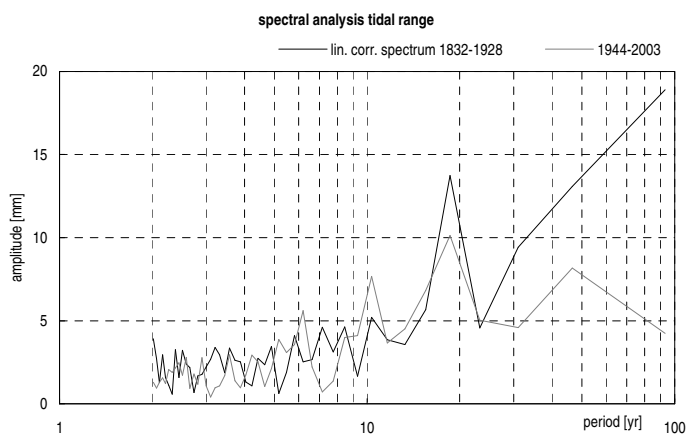
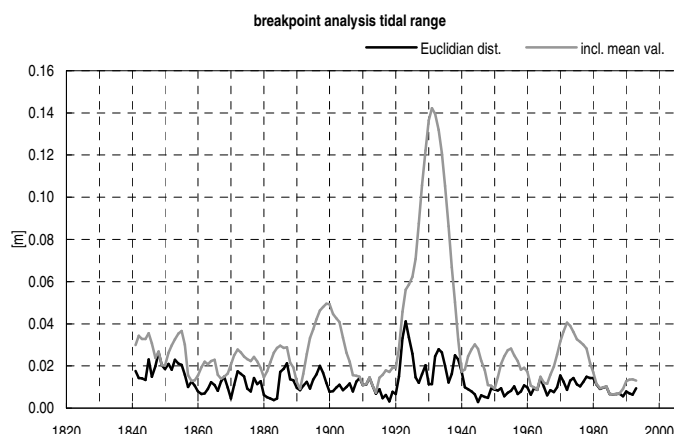
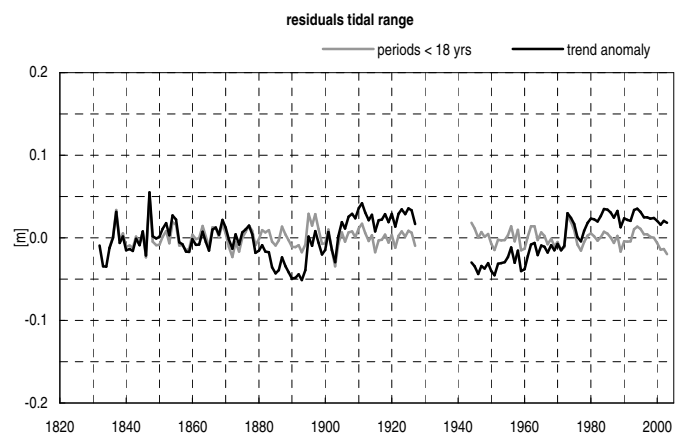
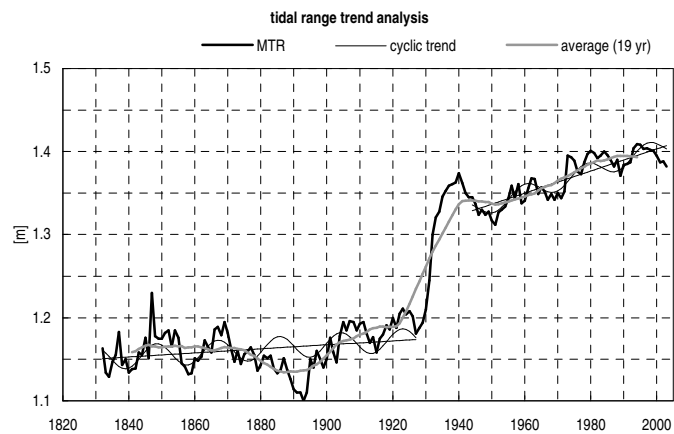
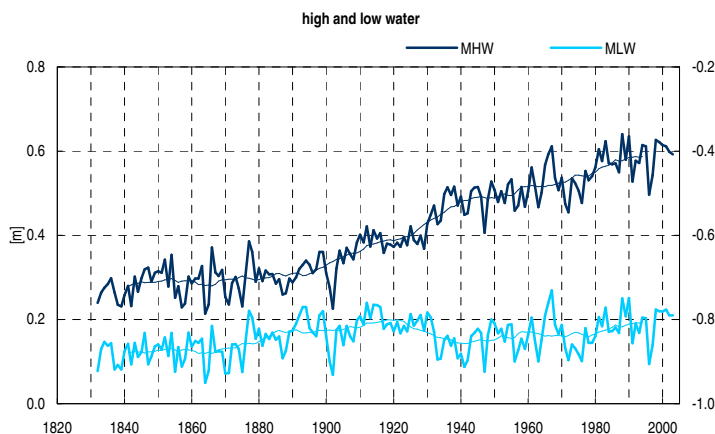
fact sheet station Scheveningen	
	1896..2003
mean tidal range [m]	1.67
linear trend [mm/100 yr]	187±10
nodal tide amplitude [mm]	9.6 (0.6%)
trend fit (R <sup>2</sup> )	0.79

5 IJmuiden



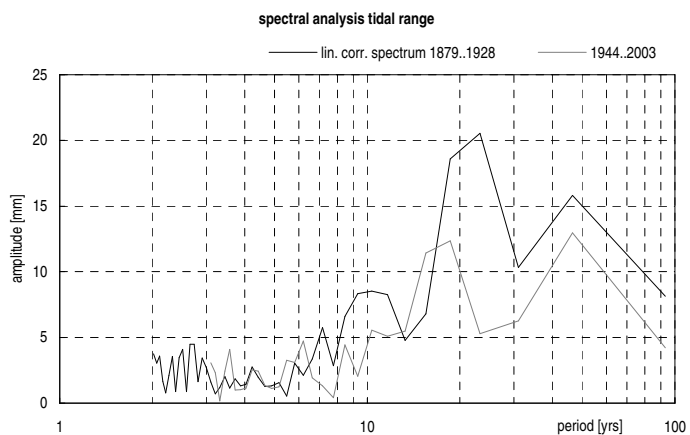
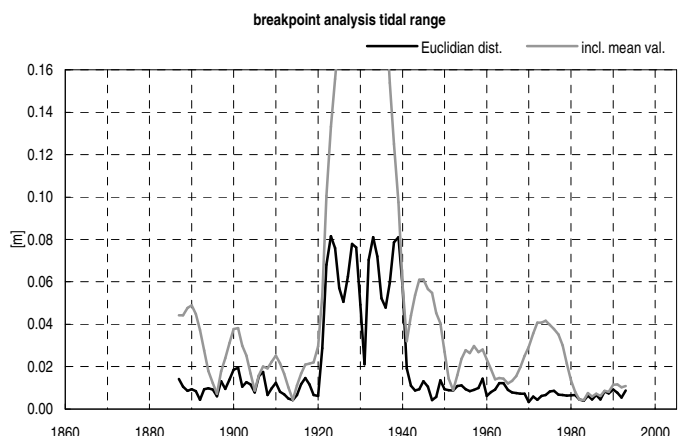
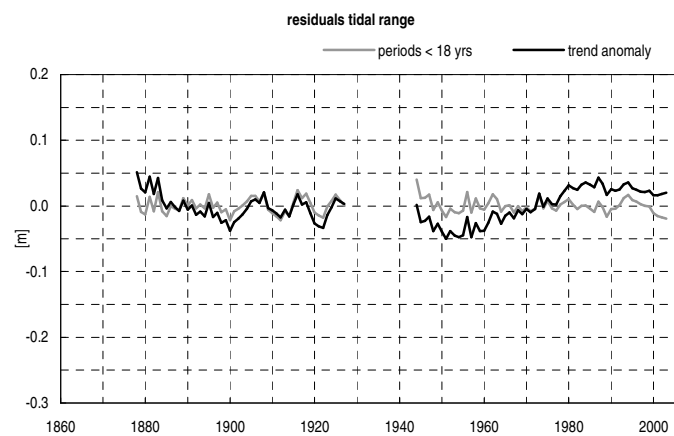
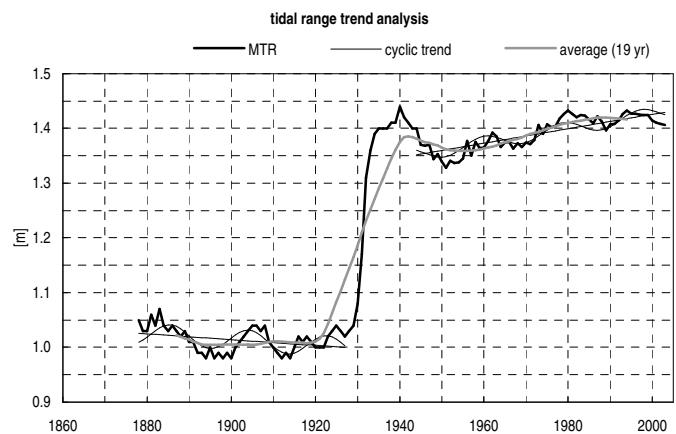
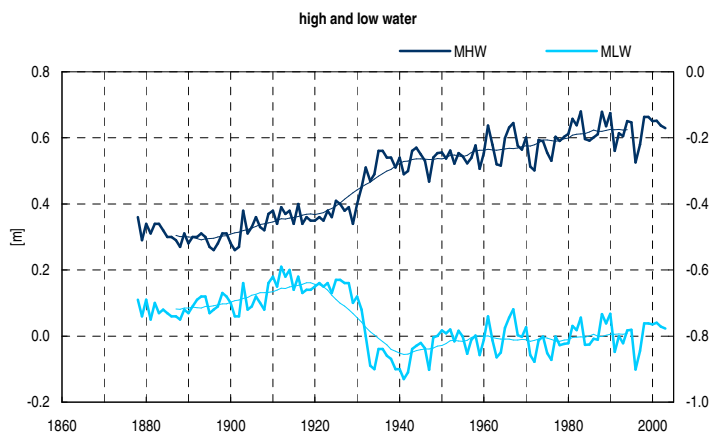
fact sheet station IJmuiden	
	1872..2003
mean tidal range [m]	1.64
linear trend [mm/100 yr]	51±9
nodal tide amplitude [mm]	16.9 (1.0%)
trend fit (R <sup>2</sup> )	0.26

6 Den Helder



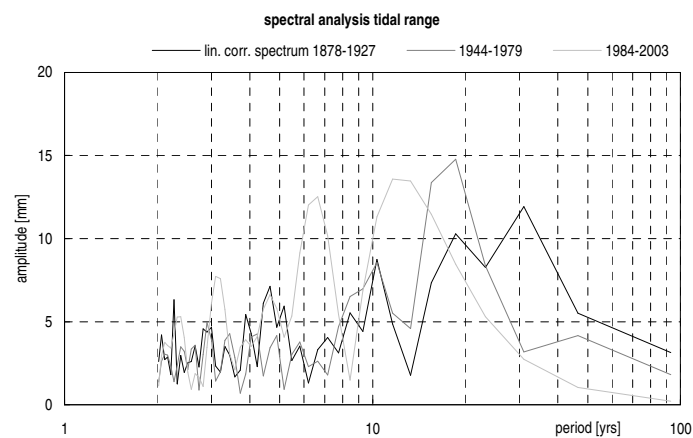
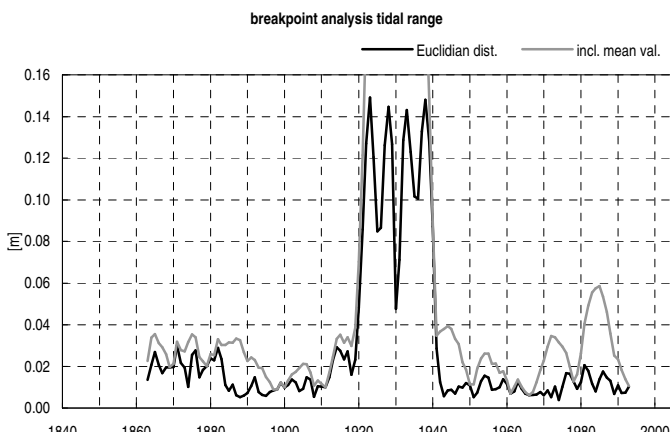
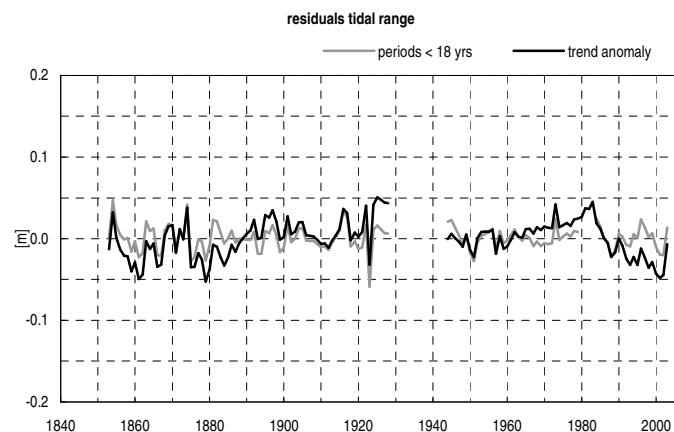
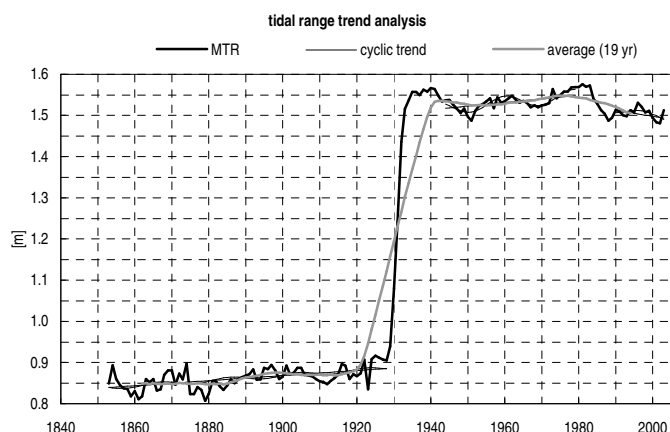
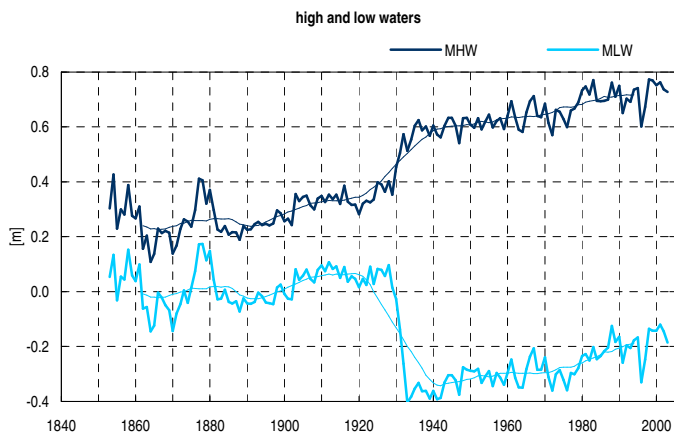
fact sheet station Den Helder		
	1832..1928	1944..2003
mean tidal range [m]	1.16	1.37
linear trend [mm/100 yr]	25±8	130±9
nodal tide amplitude [mm]	13.9 (1.2%)	10.8 (0.8%)
trend fit (R <sup>2</sup> )	0.24	0.83

7 Oudeschild



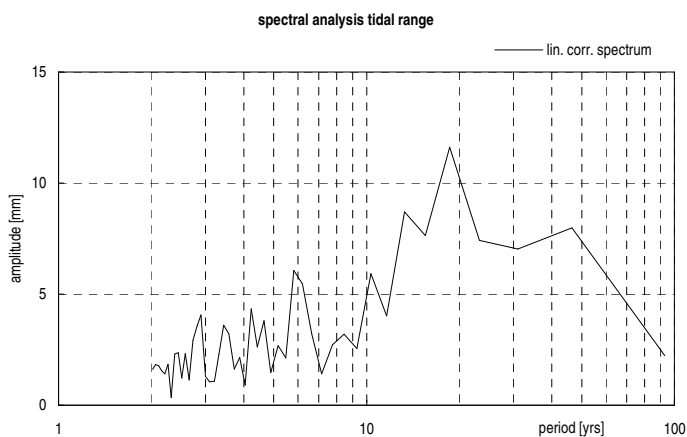
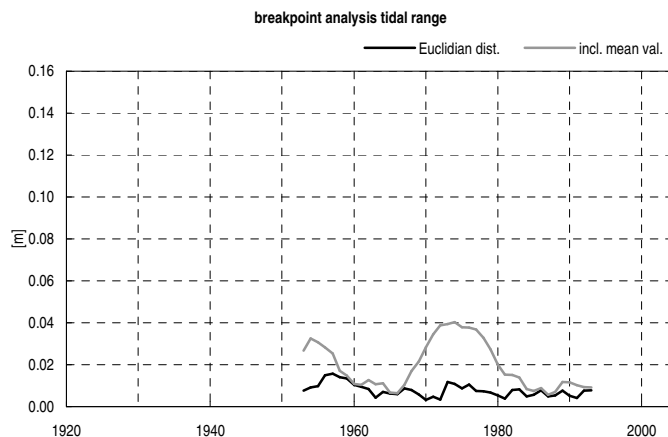
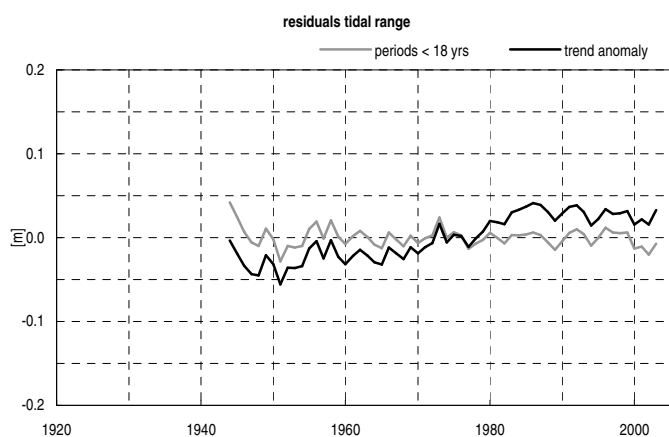
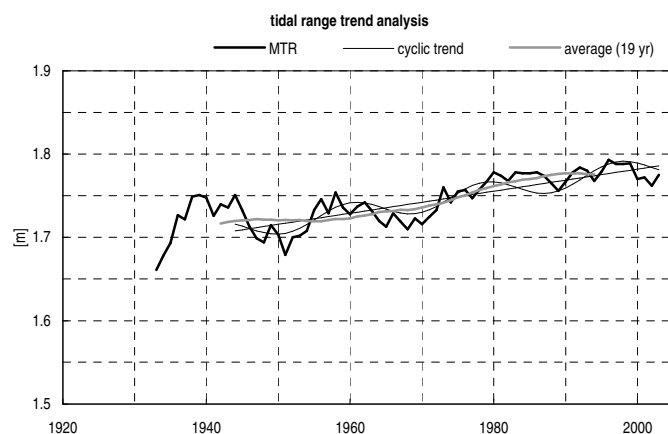
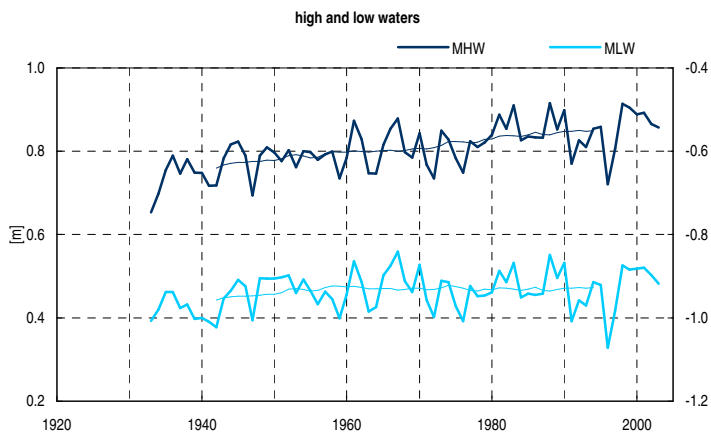
fact sheet station Oudeschild		
	1878..1928	1944..2003
mean tidal range [m]	1.02	1.39
linear trend [mm/100 yr]	-53±17	133±9
nodal tide amplitude [mm]	19.4 (1.9%)	12.6 (0.9%)
trend fit (R <sup>2</sup> )	0.43	0.77

8 Den Oever



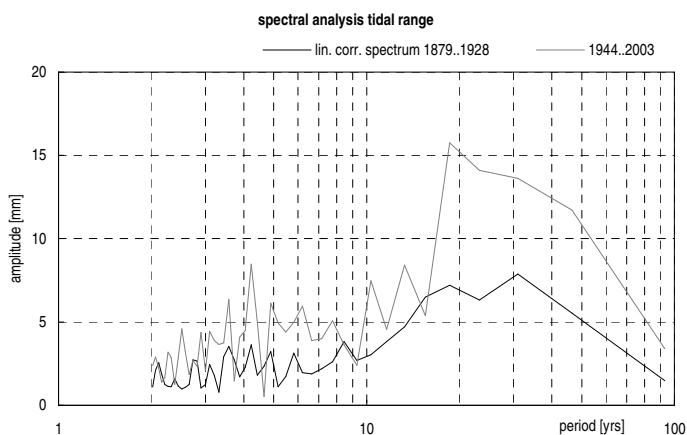
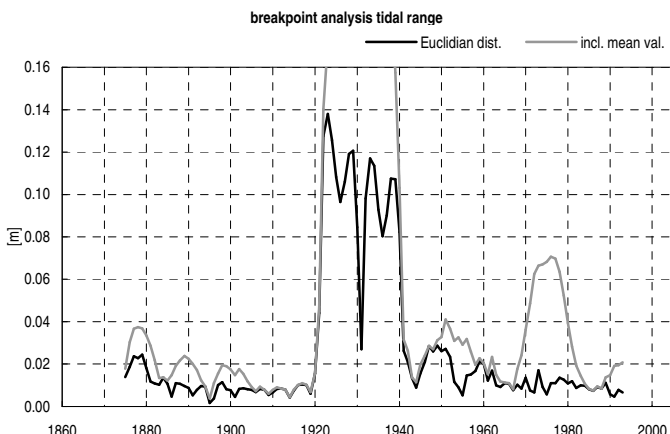
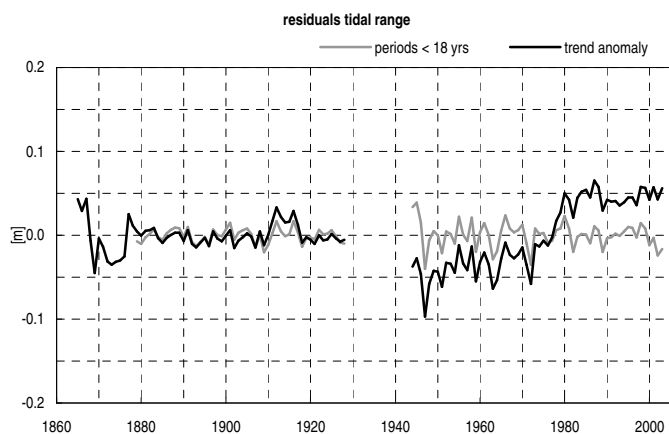
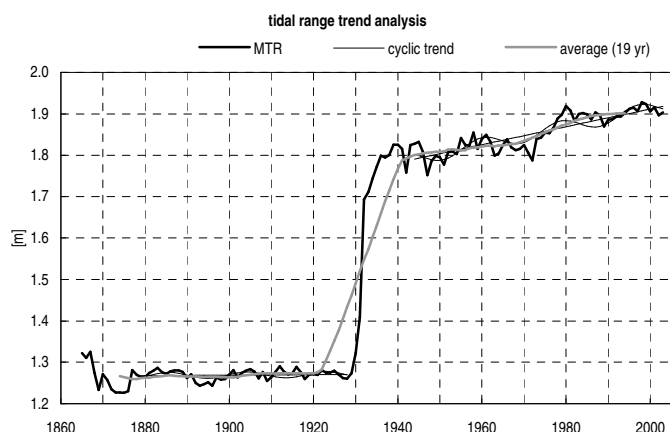
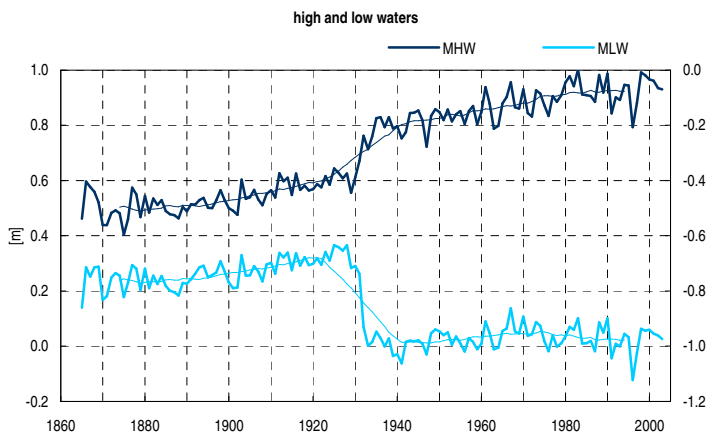
fact sheet station Den Oever			
	1853..1928	1944..1979	1984..2003
mean tidal range [m]	0.86	1.53	1.52
linear trend [mm/100 yr]	62±11	87±15	-170±50
nodal tide amplitude [mm]	4.9 (0.6%)	15.7 (1.0%)	13.1 (0.9%)
trend fit (R <sup>2</sup> )	0.34	0.74	0.26

9 Kornwerderzand



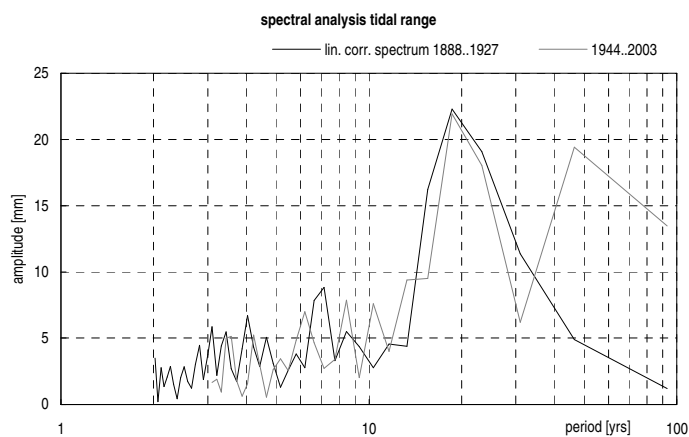
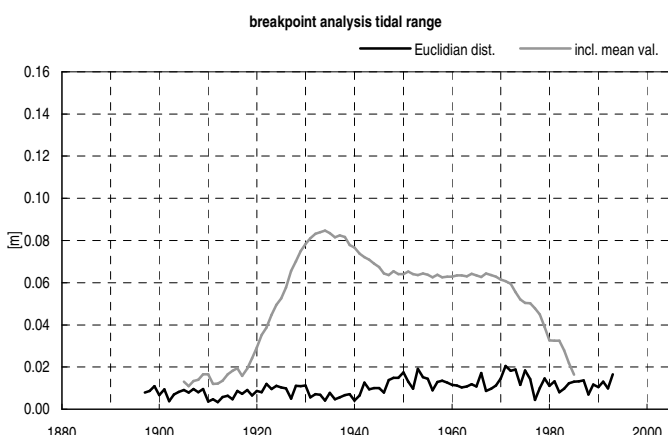
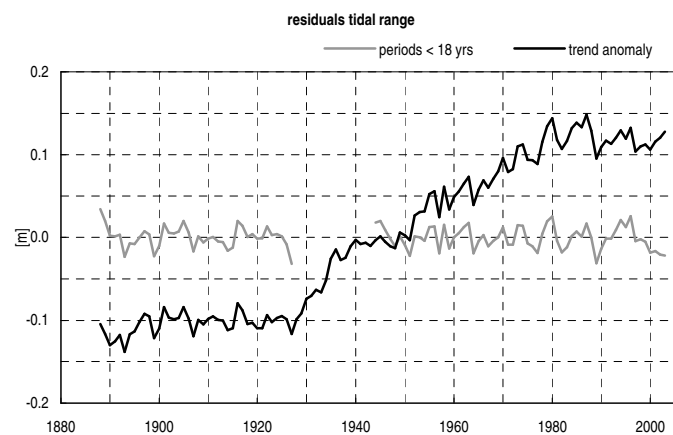
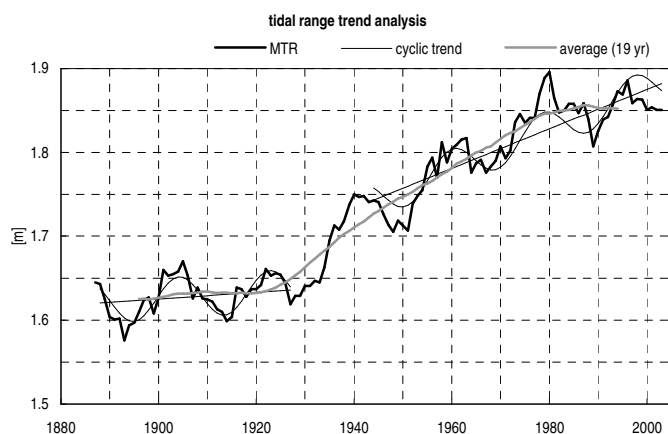
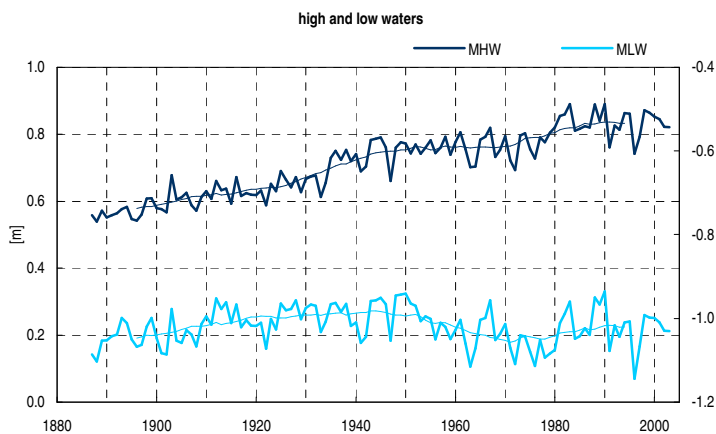
fact sheet station Kornwerderzand	
	1933..2003
mean tidal range [m]	1.74
linear trend [mm/100 yr]	132±10
nodal tide amplitude [mm]	12.5 (0.7%)
trend fit (R <sup>2</sup> )	0.79

10 Harlingen



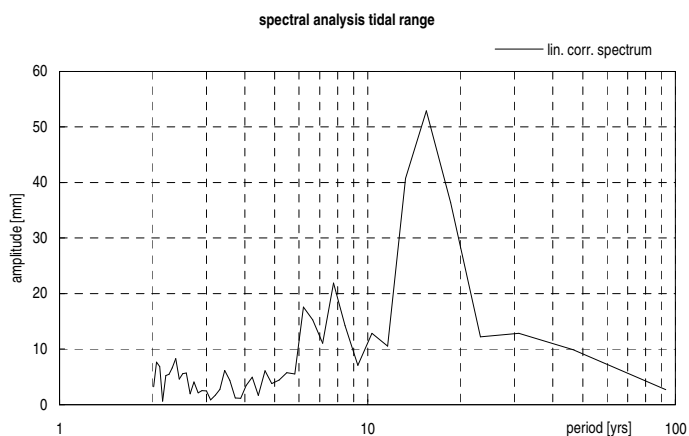
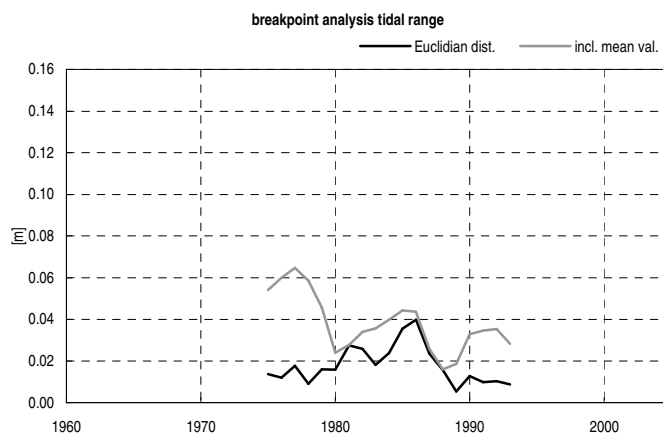
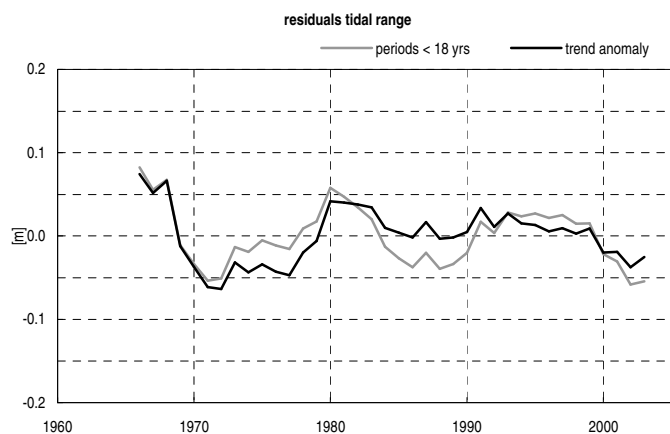
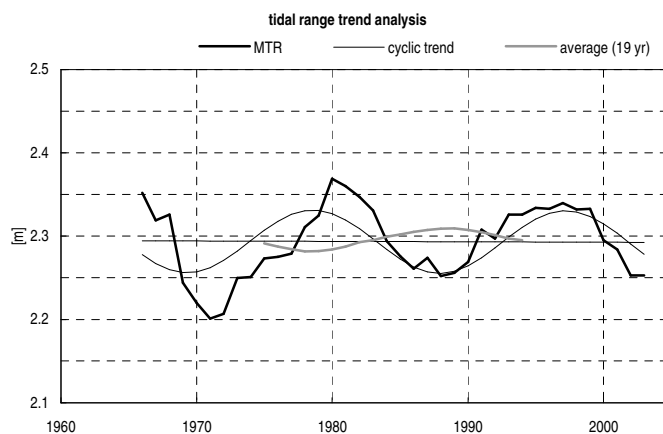
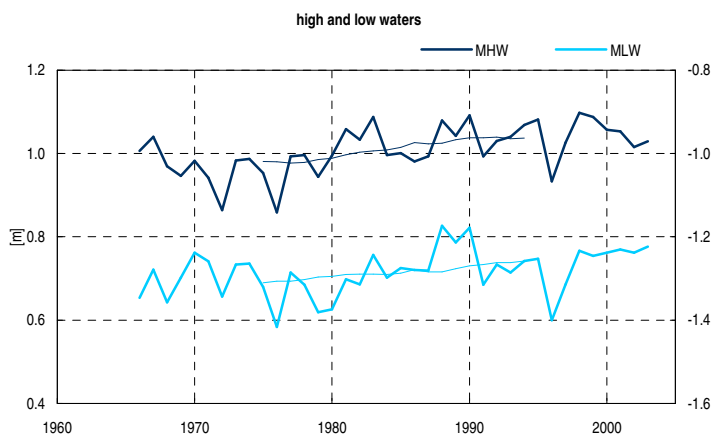
fact sheet station Harlingen		
	1879..1928	1944..2003
mean tidal range [m]	1.27	1.86
linear trend [mm/100 yr]	6±10	216±15
nodal tide amplitude [mm]	7.5 (0.6%)	16.5 (0.9%)
trend fit (R <sup>2</sup> )	0.22	0.82

11 West-Terschelling



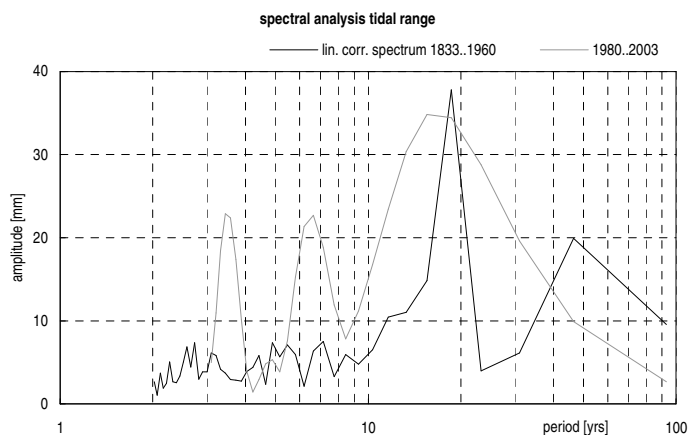
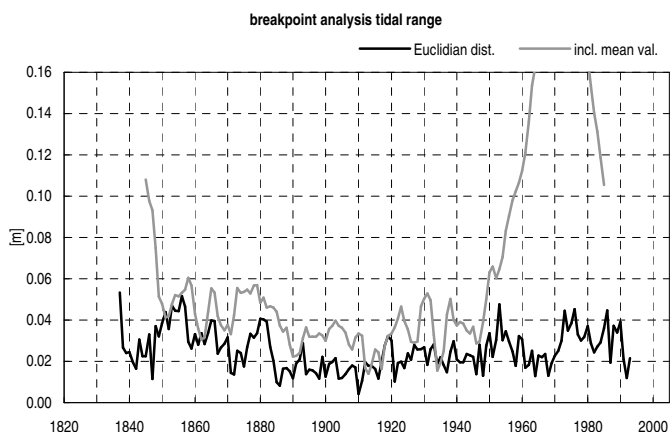
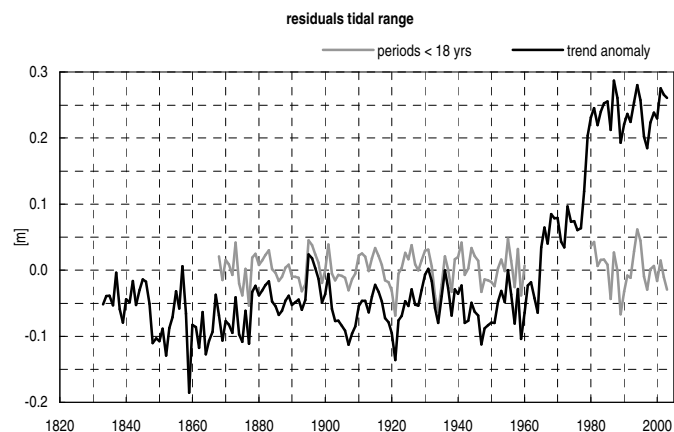
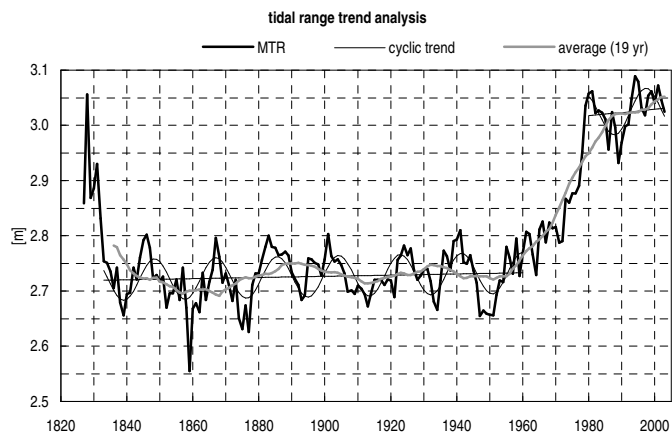
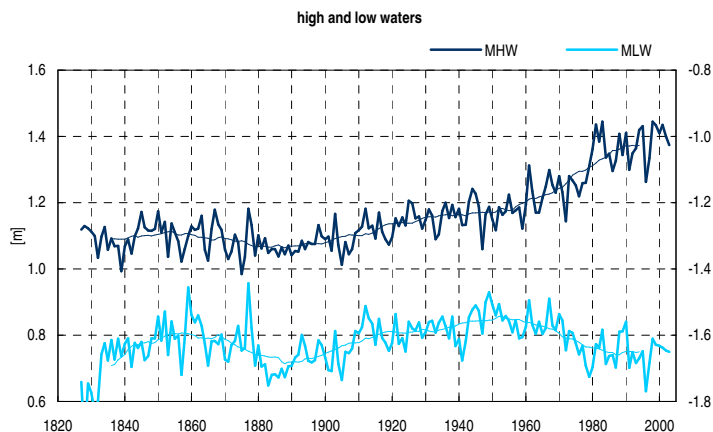
fact sheet station West-Terschelling		
	1888..1927	1944..2003
mean tidal range [m]	1.62	1.81
linear trend [mm/100 yr]	40±16	236±16
nodal tide amplitude [mm]	24.7 (1.5%)	22.9 (1.3%)
trend fit (R <sup>2</sup> )	0.73	0.83

12 Schiermonnikoog



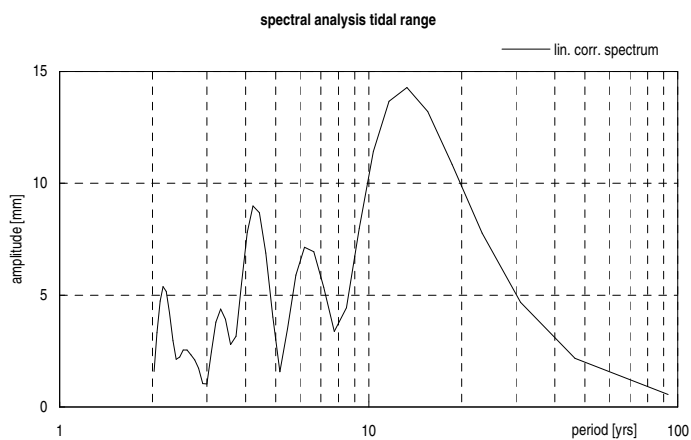
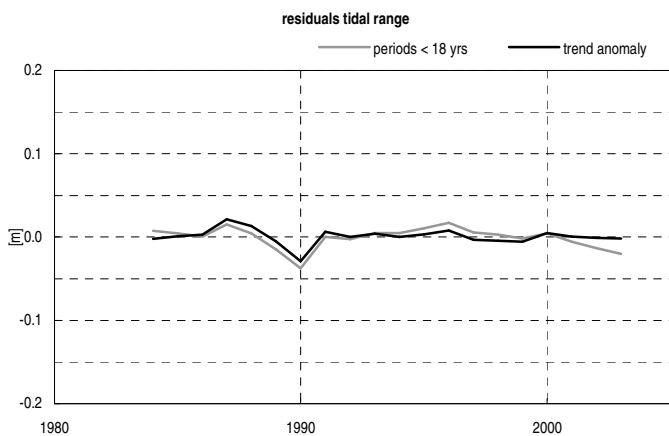
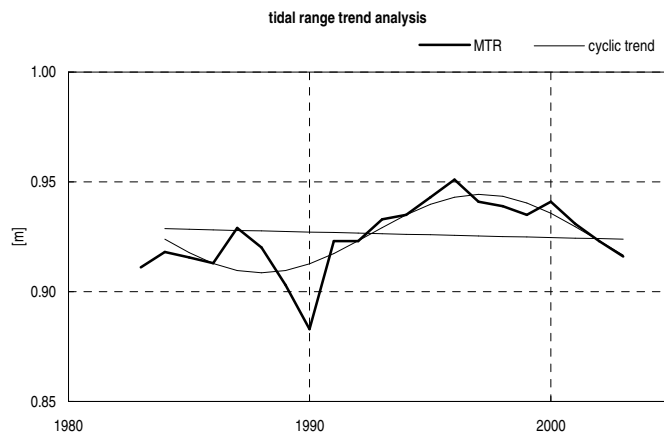
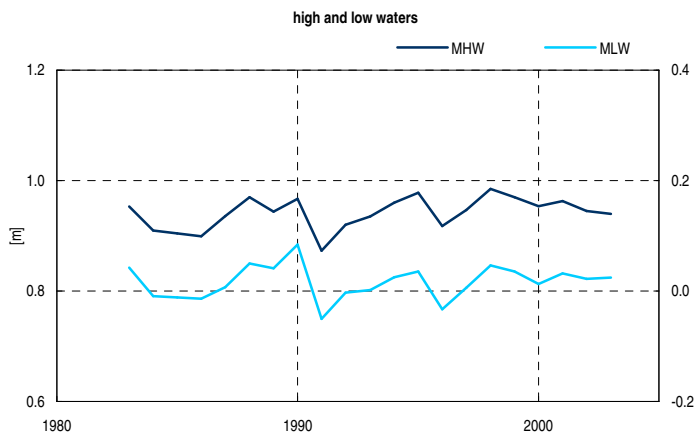
fact sheet station Schiermonnikoog	
	1966..2003
mean tidal range [m]	2.29
linear trend [mm/100 yr]	-2±51
nodal tide amplitude [mm]	37.1 (1.7%)
trend fit (R <sup>2</sup> )	0.39

13 Delfzijl



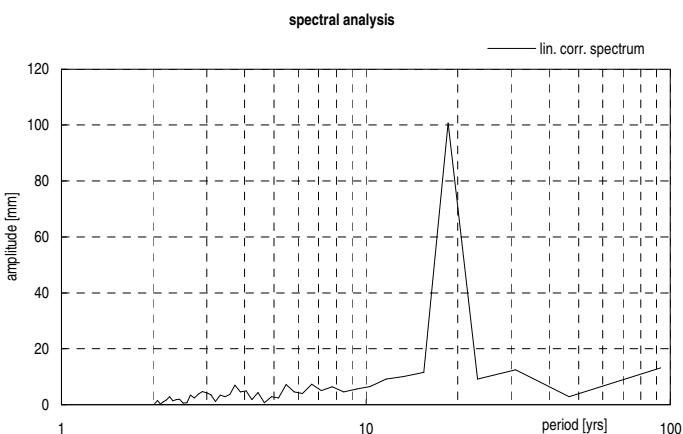
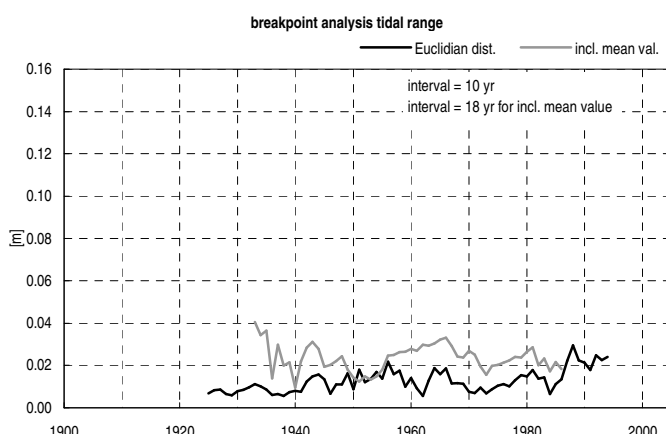
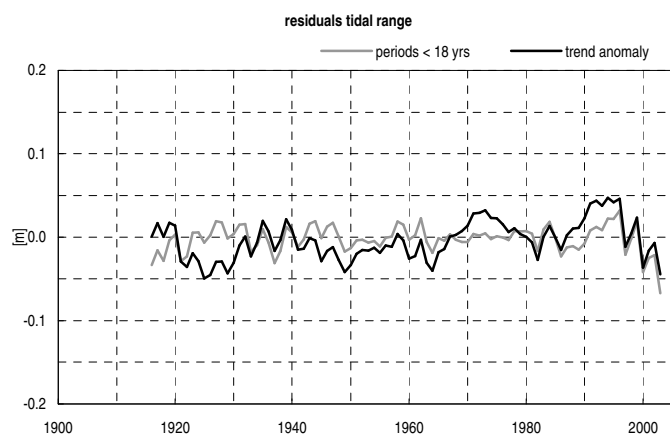
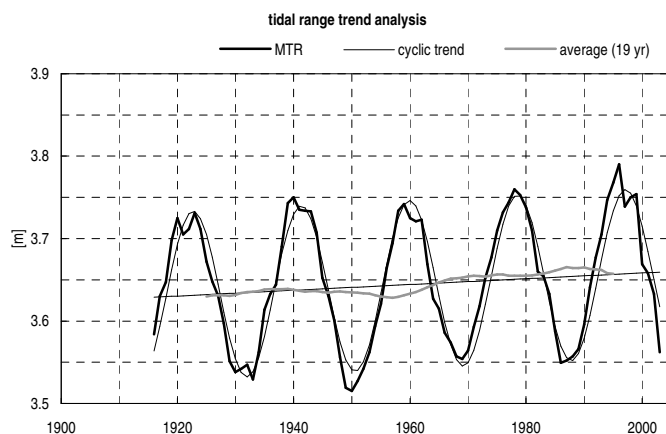
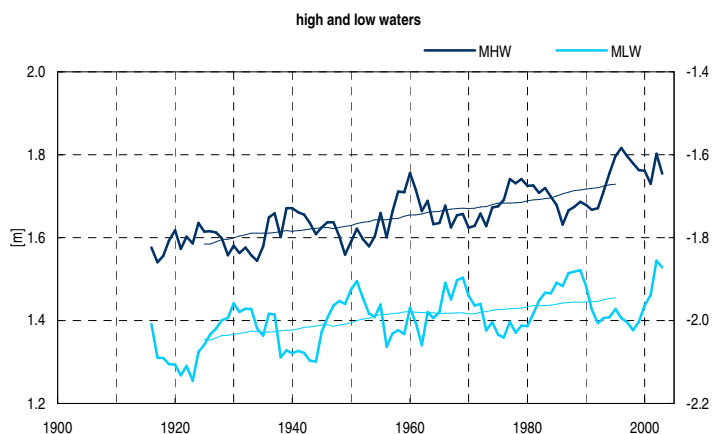
fact sheet station Delfzijl		
	1833..1960	1980..2003
mean tidal range [m]	2.73	3.03
linear trend [mm/100 yr]	11±8	60±78
nodal tide amplitude [mm]	37.4 (1.4%)	39.6 (1.3%)
trend fit (R <sup>2</sup> )	0.39	0.55

14 Euro Platform



fact sheet station Euro Platform	
	1984..2003
mean tidal range [m]	0.93
linear trend [mm/100 yr]	-21±38
nodal tide amplitude [mm]	19.1 (2.1%)
trend fit (R <sup>2</sup> )	0.64

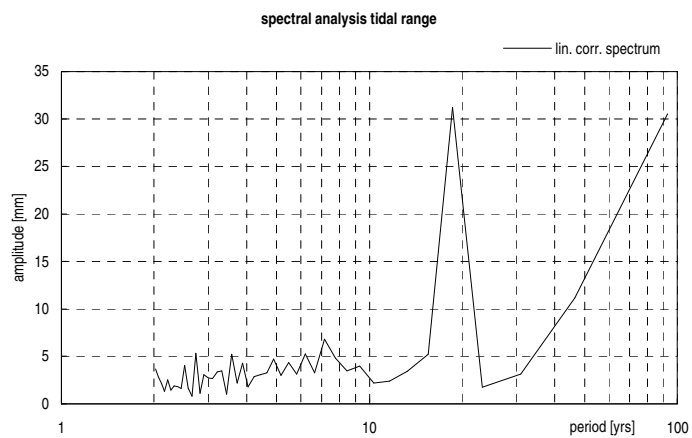
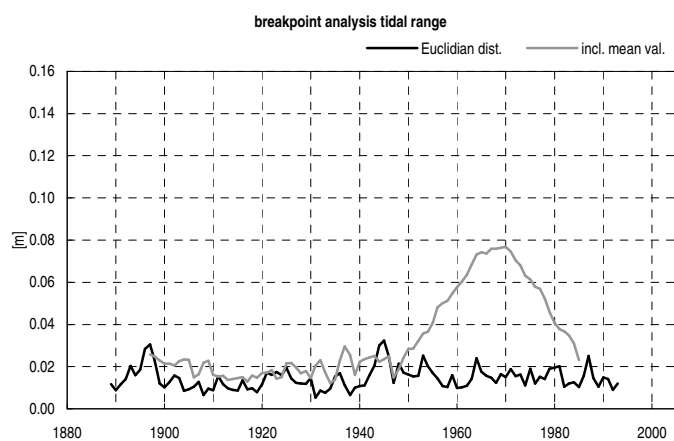
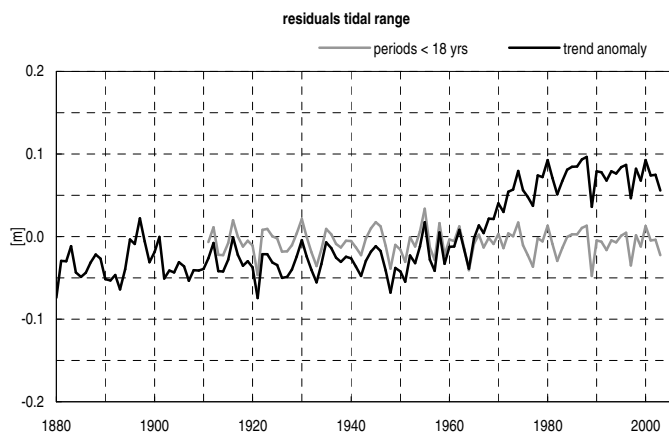
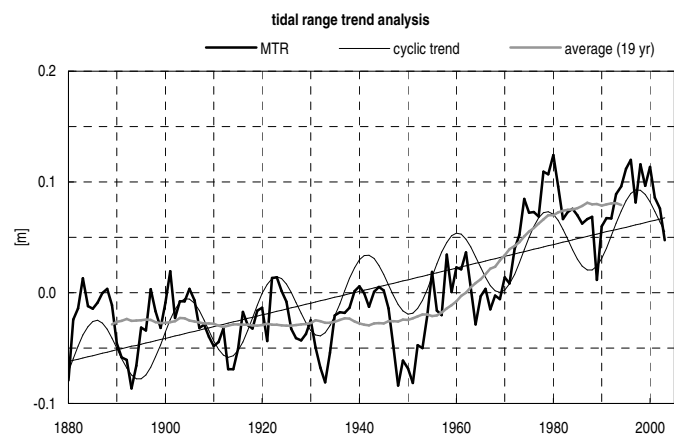
15 Newlyn



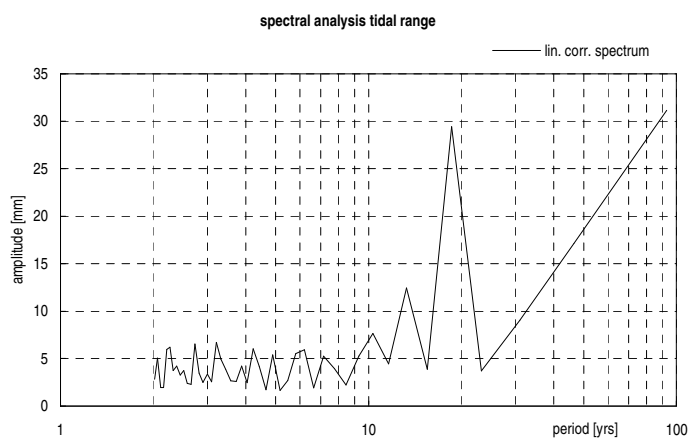
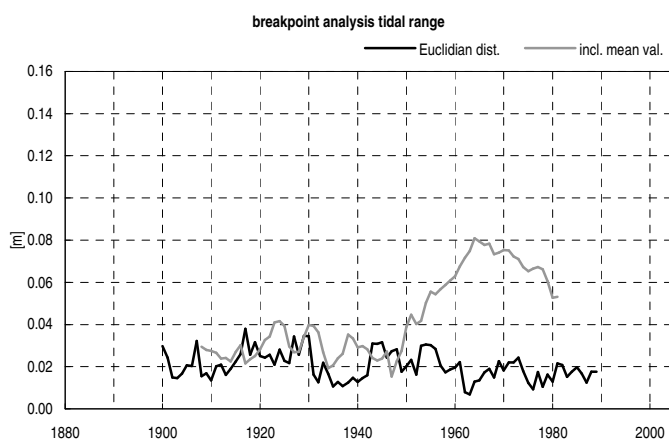
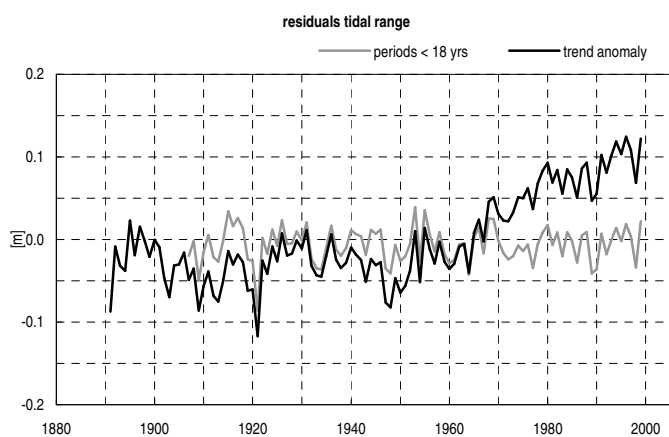
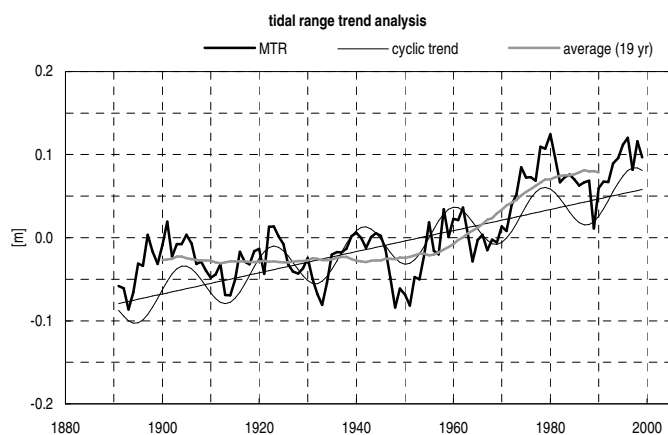
fact sheet station Newlyn	
mean tidal range [m]	1915.2004 3.65
linear trend [mm/100 yr]	35±9
nodal tide amplitude [mm]	102.2 (2.8%)
trend fit (R <sup>2</sup> )	0.92

16

## Average Netherlands (Vlissingen, Burghsluis, Hoek van Holland, Scheveningen and IJmuiden)



17 Average German North Sea islands (Borkum, Norderney, Lighthouse Alte Weser, Helgoland and Wittdün)



18

## All stations MTR trend anomaly

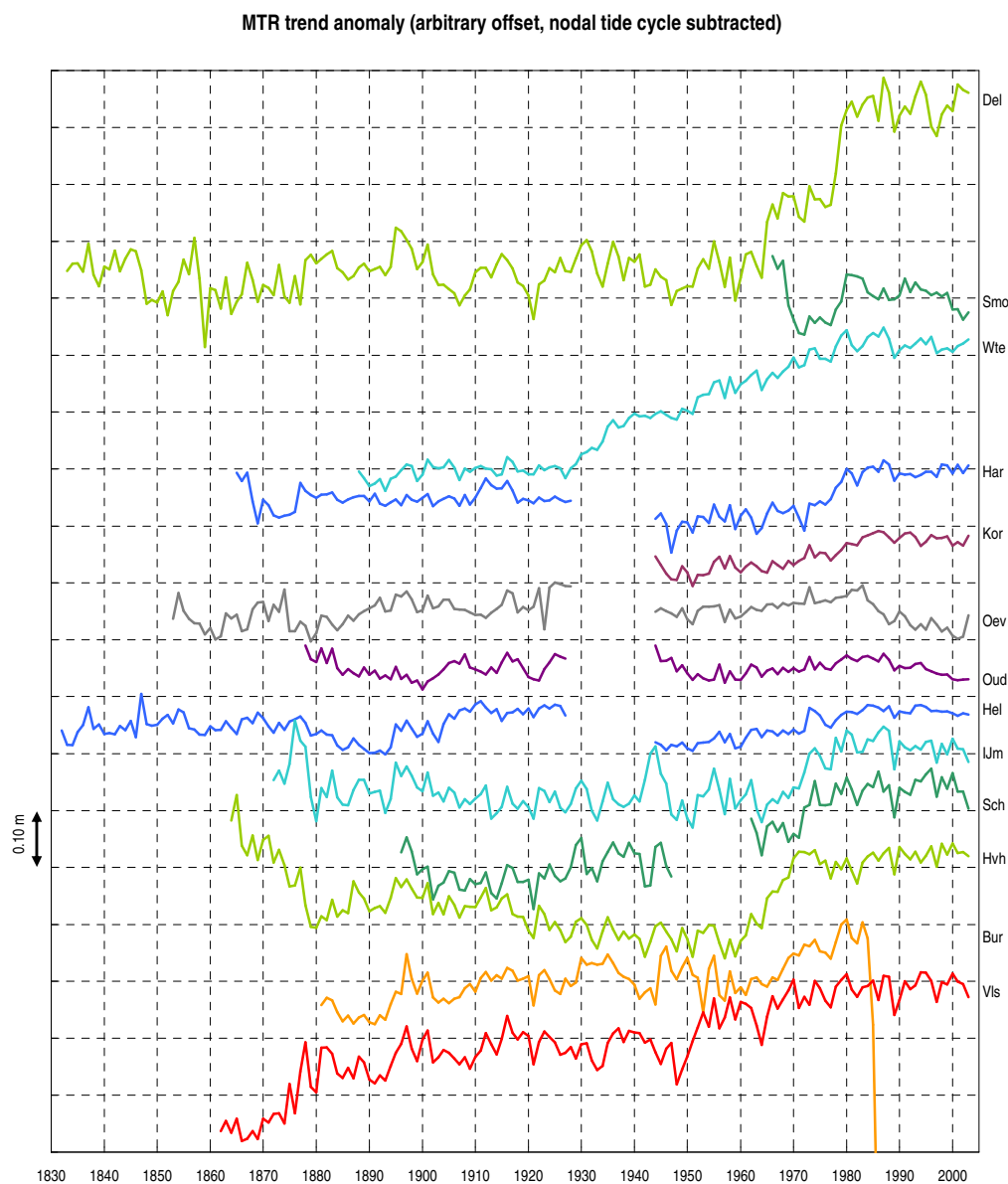


**Figure A6.18: MTR trend anomaly for all Dutch stations. This graph represents the annual mean tidal range after subtracting the nodal tide cycle. Vertical shift is arbitrary and vertical scale is shown in graph.**

## A7 Irregularities in tidal range records

This section describes the trends of the tidal range for all analysed Dutch stations. Here only major characteristics are given. For a more detailed explanation of irregularities in the trends and their causes see [Rakhorst, 2005]. The stations are given in order from South to North and grouped by tidal inlet if applicable.

### **Vlissingen**

In general the tidal range at Vlissingen shows a continuously increasing trend with the most rapid rises in the periods 1870-1900 and 1950-1970. The first increase is caused by a lowering of the low waters while the second period is characterised by increasing high waters and constant low waters. These relative rapid changes are also visible in the discontinuities graph [see appendix A6]. Langendoen [1987] and Rakhorst [2003b] ascribe this almost completely to changes in the morphological system of the Westerschelde.

### **Burghsluis**

The record for Burghsluis is fairly constant with a small increasing trend until c. 1965. After then the tidal range increases slightly and drops suddenly in 1983. This is caused by the closure of the Oosterschelde (Burghsluis is located behind the closure dam from then on). The residual signal for Burghsluis shows a large peak around 1945-1946. Unreliable recordings during the Second World War can possibly explain this [Rakhorst, personal communication, 2005] although this is not mentioned in [Rijkswaterstaat, 1985].

### **Hoek van Holland**

Hoek van Holland stands out for its decreasing trend from 1860 till c. 1960. This is caused by the construction of the Nieuwe Waterweg, the separation of the Maas and the Waal and the damming up of the Brielse Maas. During this period the low waters increased caused by a increase in the river discharge at Hoek van Holland. A rapid increase in tidal range can be seen during the period 1960-1970. This can be explained by the construction of the Europoort and the Maasvlakte and the extension of the breakwater Noorderhoofd. However, other neighbouring stations like Vlissingen, Burghsluis, Scheveningen and IJmuiden show all an relative strong increase during the same period. The increase at Hoek van Holland is much larger (0.3 m) compared to the other stations (roughly 0.1 m). It is likely that the increase at Hoek van Holland is a combination of the mentioned local changes and larger scale processes.

### **Scheveningen**

No data are available for the period 1948-1961 because of unreliable recordings [Rijkswaterstaat, 1989]. The measurements of the second sub-record are taken at a different location than the first one. The first record is more or less constant (within margin of 3%) while the second record shows a strong increase fading out between 1975 and 1985. This increase is caused by an increase of the high water levels.

### **IJmuiden**

IJmuiden is a station with a long constant record (1870-1960) with large peaks only at the beginning of the record and between 1940 and 1945. This latter peak is possibly caused by unreliable records during the Second World War [Rijkswaterstaat, 1985]. The tidal range increases rapidly during the period 1965-1980 and shows a flat course from then on.

### **Den Helder (Texel inlet)**

The record of Den Helder is fairly constant for the period 1830-1930. Only the period 1880-1910 shows a divergent trend. During this period the outer delta of the Texel inlet has changed considerably. In 1931 the tidal range increases suddenly with c. 0.2 m. This is caused by the closure of the former Zuider Sea. The tidal range stabilises around 1940 and shows a small gradually increasing trend between 1955 and 1980.

### **Oudeschild (Texel inlet)**

The temporal development of the tidal range at Oudeschild is comparable with Den Helder. Only the record before 1930 shows a slightly decreasing trend. This is, however, due to higher high waters at the start of the record (until c. 1890). The jump at 1931 is easily observed like at Den Helder.

### **Den Oever (Texel inlet)**

Den Oever shows the same trend as Den Helder and Oudeschild. Here the increase of the tidal range because of the closure of the Zuider Sea is c. 0.65 m, this is an almost 100% increase. Remarkable is the decrease of the tidal range between 1980 and 1985. At that time the harbour entrance was relocated affecting the discharges from the sluices in the closure dam. This has an effect on the low water levels [Rakhorst, 2003b].

### **Kornwerderzand (Texel inlet)**

The record of Kornwerderzand is very short (1930-present). The record is nearly constant till c. 1965 and shows a gradual increase till c. 1980. There are no peaks or other irregularities.

### **Harlingen (Texel inlet)**

This record is very similar to Den Helder and the other station of the Texel inlet. The record shows an odd course at the first 10 yrs. At this station a gradual increasing trend is observed between 1955 and 1980.

**West-Terschelling**

The record of West-Terschelling is constant until the closure of the Zuider Sea (1931). After then the tidal range increases but not as suddenly as at the stations of the Texel inlet. The rate of increase becomes lower since c. 1945 and becomes minimal since c. 1980.

**Schiermonnikoog**

The record of Schiermonnikoog starts only at 1966 and shows an almost perfect flat development (not considering the present 18.6-yr cycle).

**Delfzijl**

The tidal range record for Delfzijl is constant between c. 1835 and 1960. The first few years of the whole record (from 1827) show a rapid decrease of 0.3 m. Here the low waters show a jump which likely indicates changes in the gauge or its location. Between 1960 and 1980 the tidal range shows a sharp rise of 0.3 m and remains constant after 1980. This is caused by construction of a breakwater (1963-1966) and the damming of a harbour entrance (1978) [Rakhorst, 2003b].

## A8 Phases periodicities 8.85-18.6 yr

station	cycle period [yr]			
	8.85	11	13.3	18.6
Vlissingen	1977.8	1984.2	1981.7	1977.8
Burghsluis	1980.1	1984.3	1982.1	1977.8
IJmuiden	1976.1	1986.6	1984.4	1978.5
Den Helder	1977.2	1985.3	1983.0	1978.1
West-Terschelling	1979.1	1985.2	1988.8	1977.9
Delfzijl	1977.9	1983.0	1983.1	1977.8
std deviation [yr]	1.4	1.2	2.6	0.3
mean	1978.0	1984.8	1983.9	1978.0

Table A8.1: Phases calculated with individual MLRs for the 4 periods

station	cycle period [yr]			
	8.85	11	13.3	18.6
Vlissingen	1976.9	1986.2	1987.1	1977.8
Burghsluis	1975.8	1984.8	1986.3	1977.8
IJmuiden	1976.3	1986.7	1989.3	1978.4
Den Helder	1977.8	1985.0	1988.7	1978.3
West-Terschelling	1978.7	1984.7	1988.4	1978.1
Delfzijl	1978.3	1982.9	1985.1	1977.8
std deviation [yr]	1.2	1.3	1.6	0.3
mean	1977.3	1985.1	1987.5	1978.0

Table A8.2: Phases calculated with a single joint MLR

station	cycle period [yr]			
	8.85	11	13.3	18.6
Vlissingen	-0.9	2.0	5.4	0.0
Burghsluis	-4.3	0.5	4.2	0.0
IJmuiden	0.2	0.1	4.9	-0.1
Den Helder	0.6	-0.3	5.7	0.2
West-Terschelling	-0.4	-0.5	-0.4	0.2
Delfzijl	0.4	-0.1	2.0	0.0
absolute mean diff.	0.7	0.3	3.6	0.0

Table A8.3: Phase differences between the individual MLRs [table A8.1] and the joint MLR [table A8.2].

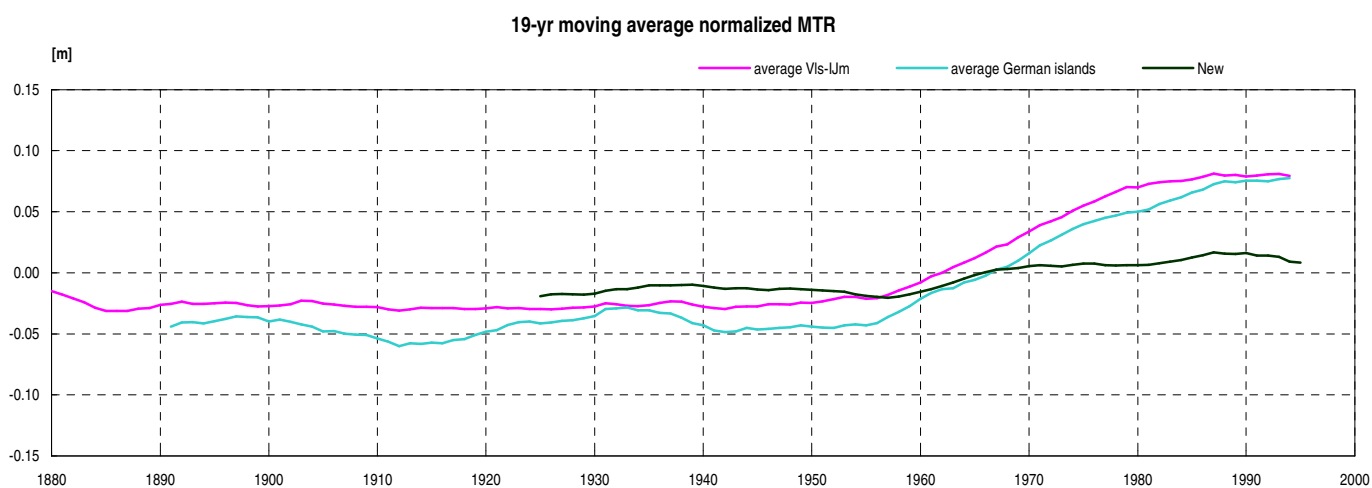
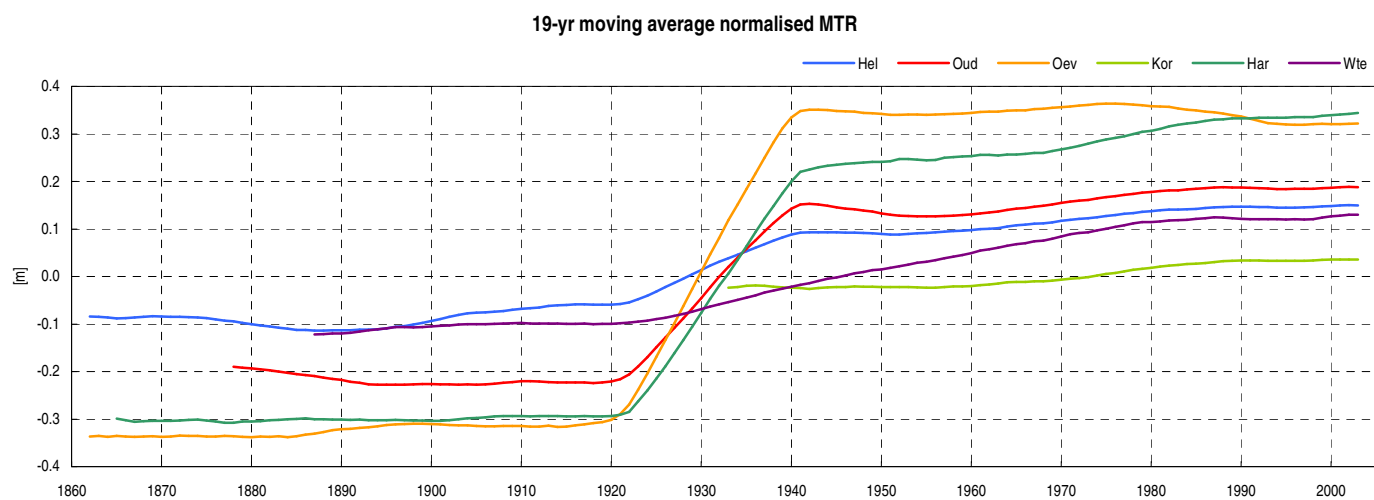
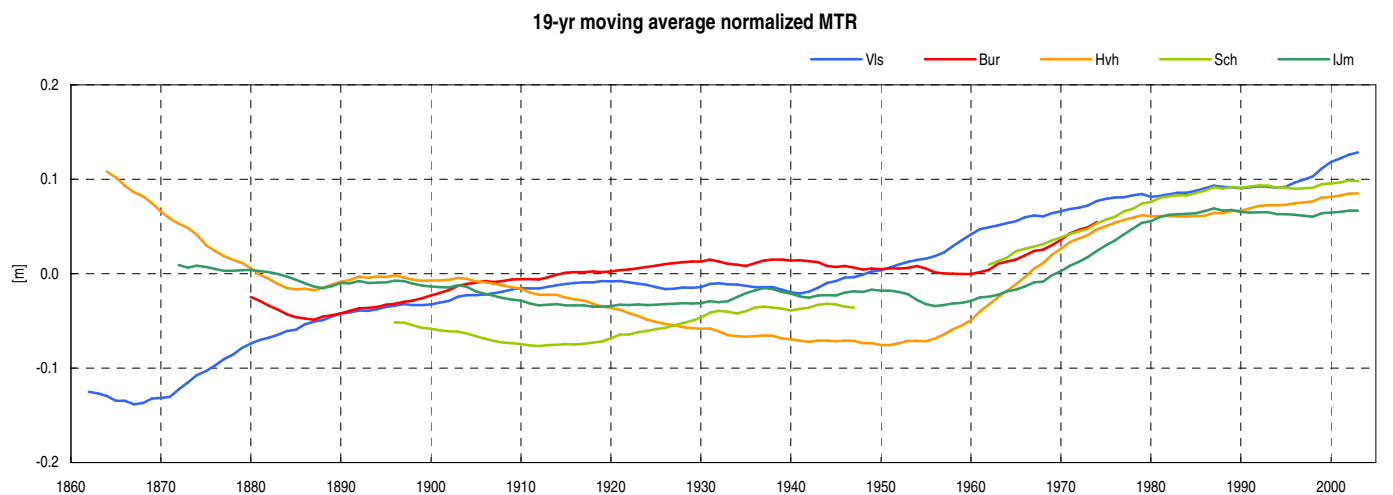
## A9 Results of MLR analysis of tidal ranges

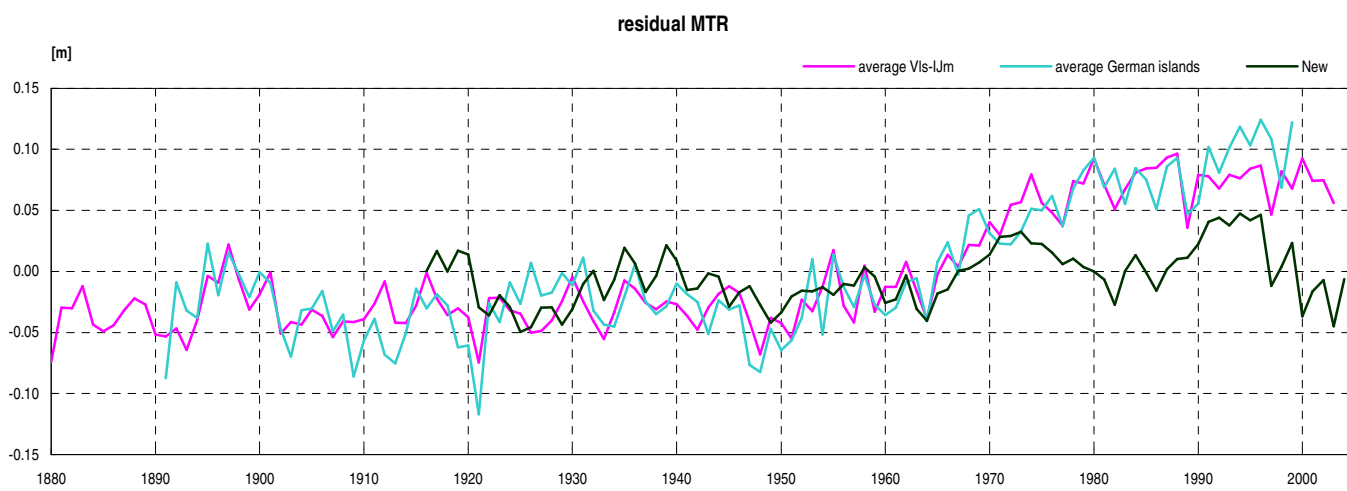
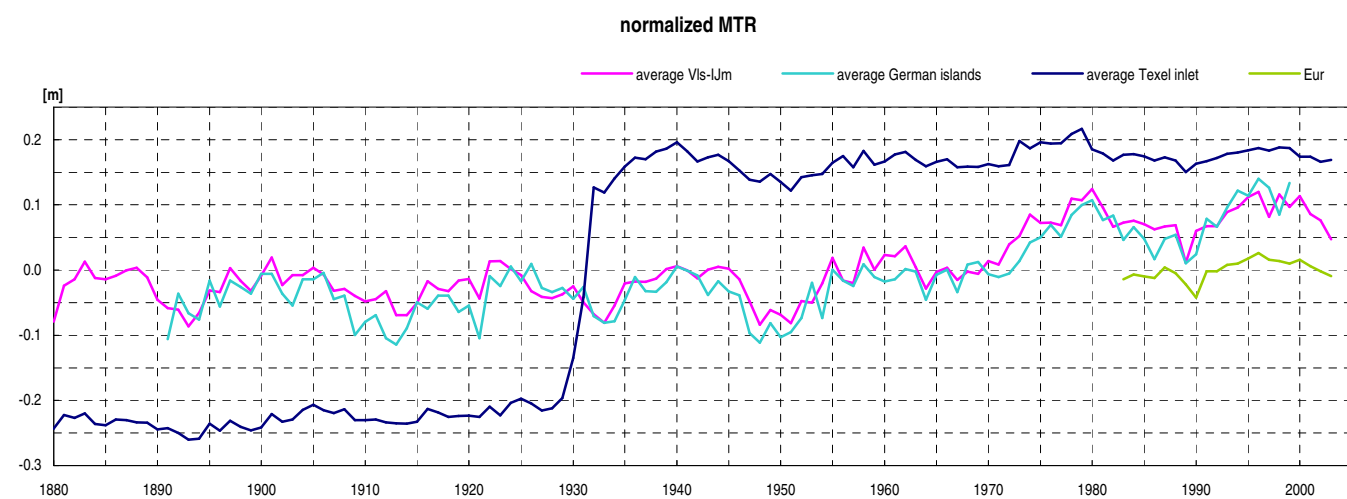
$$MTR(t) = a_0 + s \cdot t + a_{18.6} \cos\left\{\frac{2\pi}{18.6}(t - 1978.4)\right\}$$

station		mean MTR ( $a_0$ ) [m]	slope (s) [mm/yr]	amplitude ( $a_{18.6}$ ) [mm]    [%]		trend fit ( $R^2$ ) [-]
Euro platform		0.93	-0.21±0.38	19.1	2.1	0.64
Vlissingen		3.75	1.60±0.07	59.6	1.6	0.84
Burghsluis		2.76	0.92±0.09	39.9	1.4	0.67
Hoek van Holland	1883..1904	1.65	0.34±0.69	8.6	0.5	0.09
	1905..1956	1.61	-1.41±0.18	12.8	0.8	0.62
	1976..2003	1.72	1.16±0.35	16.2	0.9	0.49
Scheveningen		1.67	1.87±0.10	9.6	0.6	0.79
Ijmuiden		1.64	0.51±0.09	16.9	1.0	0.26
Den Helder	1832..1928	1.16	0.25±0.08	13.9	1.2	0.24
	1944..2003	1.37	1.33±0.09	10.8	0.8	0.83
Oudeschild	1878..1928	1.02	-0.53±0.17	19.4	1.9	0.43
	1944..2003	1.39	1.32±0.11	12.6	0.9	0.77
Den Oever	1853..1928	0.86	0.62±0.11	4.9	0.6	0.34
	1944..1979	1.53	0.87±0.15	15.7	1.0	0.74
	1984..2003	1.52	-1.70±0.50	13.1	0.9	0.26
Kornwerderzand		1.74	1.32±0.10	12.5	0.7	0.79
Harlingen	1879..1928	1.27	0.06±0.10	7.5	0.6	0.22
	1944..2003	1.86	2.16±0.15	16.5	0.9	0.82
West-Terschelling	1888..1927	1.62	0.40±0.16	24.7	1.5	0.73
	1944..2003	1.81	2.36±0.16	22.9	1.3	0.83
Schiermonnikoog		2.29	-0.02±0.51	37.1	1.7	0.39
Delfzijl	1833..1960	2.73	0.11±0.08	37.4	1.4	0.39
	1980..2003	3.03	0.60±0.78	39.6	1.3	0.55
Newlyn	1915..2004	3.65	0.35±0.09	102.2	2.8	0.92
<b>variance</b>		<b>0.50</b>	<b>1.1</b>	<b>232.3</b>	<b>0.2</b>	
<b>average</b>		<b>1.92</b>	<b>0.9</b>	<b>21.0</b>	<b>1.0</b>	

Table A9.1: Results of the multiple linear regression analysis of the mean tidal range (MTR). The parameters in this analysis are a constant value, a linear slope and the amplitude of the 18.6-year cycle. The phase of this cycle is set to 1978.4 (year with a maximum). See also equation above. For the calculation of the variances and averages only the most recent sub-record of split stations is used.

# A10 Long-term trends





## Delft3D-FLOW model description

Delft3D-FLOW is a flow model solving the unsteady shallow-water equations with a finite difference approximation. In this study a 2 dimensional, depth-averaged model is applied. The main physical processes simulated are:

- Free water surface gradients (barotropic effects)
- Effect of earth's rotation on water motion (Coriolis forces)
- Tidal forcing at an open boundary
- Shear-stress at the bed attenuating waves

The main assumptions in the Delft3D-FLOW model are:

- Shallow-water assumption: the water depth is small compared to horizontal length scales. This implies that the vertical acceleration can be neglected and that the vertical momentum equation reduces to the hydrostatic equation:

$$\frac{\partial p}{\partial z} = -\rho g \text{ with boundary condition } p(z = \text{surface}) = 0 \quad [32]$$

where  $p(z)$  is the pressure at vertical level  $z$ ,  $\rho$  is the density of water and  $g$  the gravitational constant.

- At the bed slip boundary conditions are applied with quadratic bed stress formula.
- Shear stresses at lateral closed boundaries are neglected (so called free slip condition).

The shallow water equations are a system of a continuity equation and horizontal momentum equations.

The continuity or water mass balance equation is given by:

$$\frac{\partial \zeta}{\partial t} + \frac{\partial(hU)}{\partial x} + \frac{\partial(hV)}{\partial y} = 0 \quad [33]$$

The horizontal momentum equations in  $x$  and  $y$ -direction are:

$$\frac{\partial U}{\partial t} + U \frac{\partial U}{\partial x} + V \frac{\partial U}{\partial y} - fV = -g \frac{\partial \zeta}{\partial x} - \frac{\tau_{b,x}}{h} + F_x \quad [34]$$

$$\frac{\partial V}{\partial t} + U \frac{\partial V}{\partial x} + V \frac{\partial V}{\partial y} - fU = -g \frac{\partial \zeta}{\partial y} - \frac{\tau_{b,y}}{h} + F_y \quad [35]$$

with the bed stress defined as:

$$\tau_{b,x} = \frac{\rho g U |U|}{C^2} \text{ and } \tau_{b,y} = \frac{\rho g V |V|}{C^2} \quad [36], [37]$$

where  $C$  is the Chézy bed smoothness parameter [ $\text{m}^{1/2} \text{s}^{-1}$ ].

The turbulent character of the flow is allowed for by the Reynold's stresses:

$$F_x = \nu \left( \frac{\partial^2 U}{\partial x^2} + \frac{\partial^2 U}{\partial y^2} \right) \text{ and } F_y = \nu \left( \frac{\partial^2 V}{\partial x^2} + \frac{\partial^2 V}{\partial y^2} \right) \quad [38], [39]$$

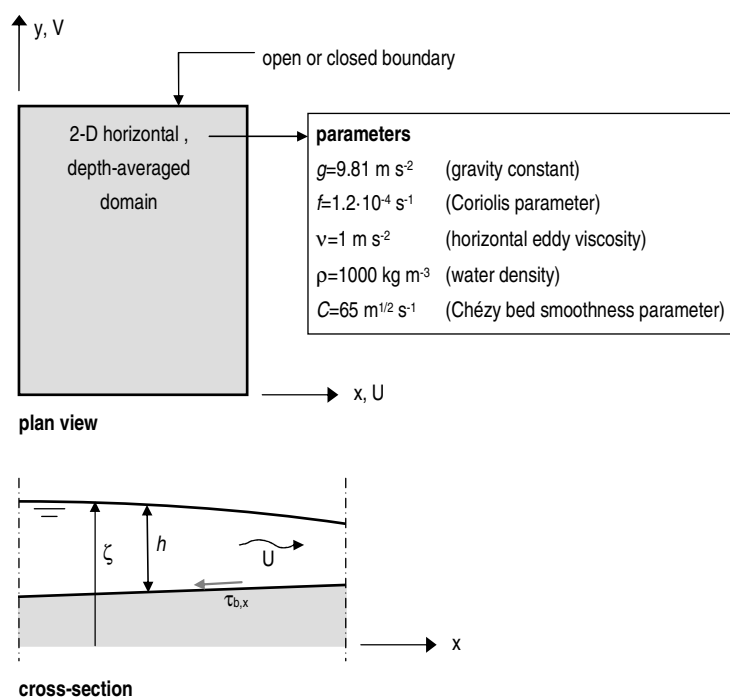
where  $\nu$  is the horizontal eddy viscosity [ $\text{m}^2 \text{s}^{-2}$ ].

The Coriolis accelerations are given by:

$$f = 2\Omega \sin \varphi \quad [40]$$

where  $f$  is the Coriolis parameter [ $\text{m}^2 \text{s}^{-2}$ ],  $\Omega$  is the earth's angular velocity and  $\varphi$  is the latitude.

See for the definitions of the variables and parameters the picture below.





## A12 Evaluation of model adjustment time

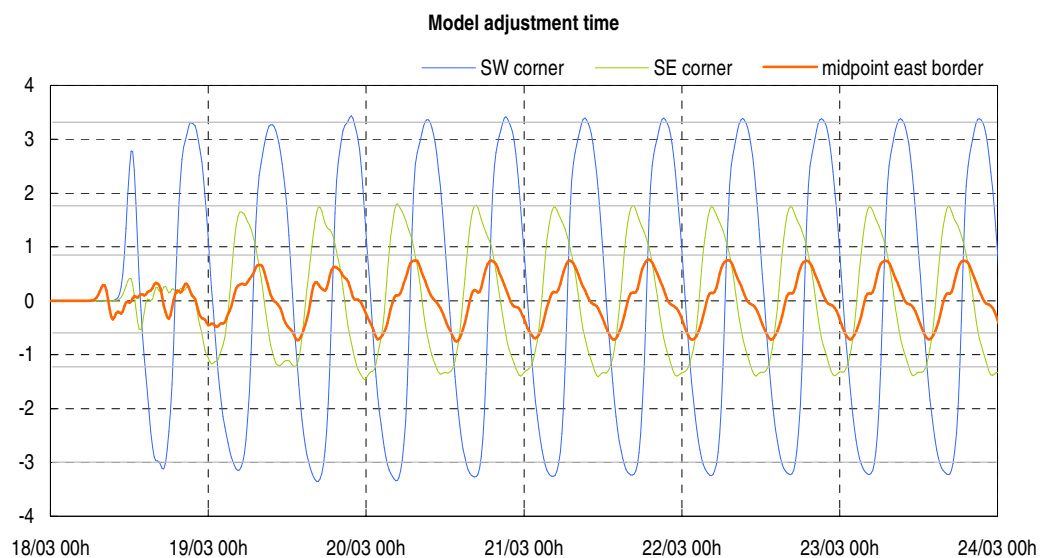
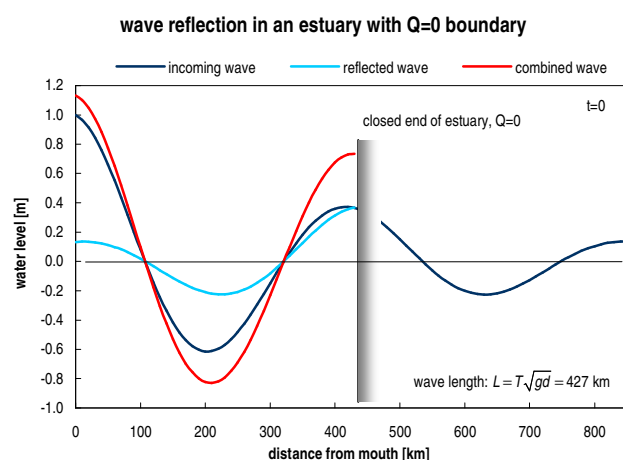


Figure A12.1: Time series of water levels at three locations in the basin in simulation 2 (reference case with sloping bed)

A stable situation is reached after maximum 4 days. This corresponds to a steady state in the frequency domain. The tidal ranges at each location are estimated by fitting an  $M_2$  tide in the simulated records. Although shallow water tides are present in the time series, the  $M_2$  tide can be used as a proxy for the tidal range.

## A13 Wave amplification in an estuary

Tidal waves progressing along a coastline can be attenuated by inlets. The attenuation is caused by the storage capacity of the tidal basin behind the inlet. When an inlet is closed no storage takes place any longer resulting in an increased tidal wave outside the inlet. There are hypothetical situations possible where the opposite occurs. In the case of a short (relative to the tidal wave length) estuary which is relatively deep, the tidal wave entering the estuary is reflected at the closed end. The water levels inside the estuary are a superposition of the incoming and the reflected wave [see figure A13.1]. When damping is small enough (i.e. in deep water or with a smooth bed) the tidal wave at the mouth of the estuary is larger than the incoming wave. This is of course not possible since the surface is continuous. This means that the estuary tries to increase the tidal wave outside the mouth. After the closure of the estuary the process of amplification is no longer present, this results in a decrease of the tidal range. This has been observed in early simulations of the conceptual model [see figure A13.2]. The decrease is only observed in the close vicinity of the closed inlet, and the regular pattern of increasing tidal ranges is observed



**Figure A13.1: Reflection and amplification of a tidal wave in an estuary [adapted from Boon, 2004].** In case the estuary length is not equal to the wave length, the left boundary in the graph is shifted. The right boundary remains at the same further away.

In this study we have excluded the amplification effects by increasing the bed roughness and decreasing the depth of the estuary. Non-reflecting boundaries are possible in the flow model used but they allow discharge through the boundary. This has a significant effect on the tidal prism and therefore this boundary type has not been applied.

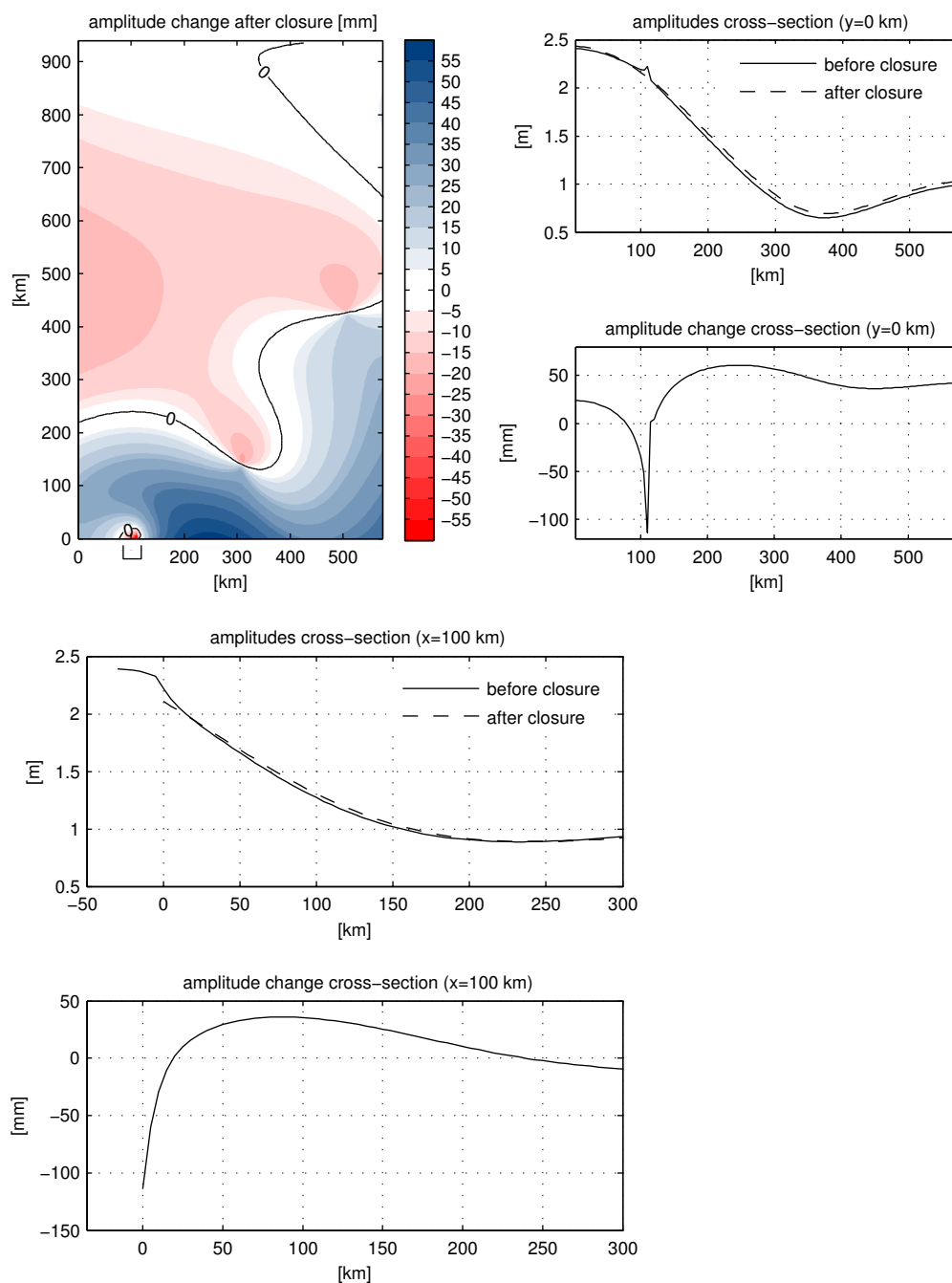


Figure A13.2: Amplification at the end of the estuary ( $L=30$  km,  $D=50$  m,  $P=1.8 \cdot 10^9$  m<sup>3</sup>)

Figure A13.2 shows the results of a simulation of a closure of a 30 km short and 50 m deep estuary with a prism of  $1.8 \cdot 10^9$  m<sup>3</sup>. The incoming tidal wave is reflected at the closed end of the estuary with a  $Q=0$  condition. The reflected wave is not damped inside the estuary and increases the tidal wave outside the mouth. After closure this process of amplification is stopped and the tidal range decreases locally.

## A14 Simulation results

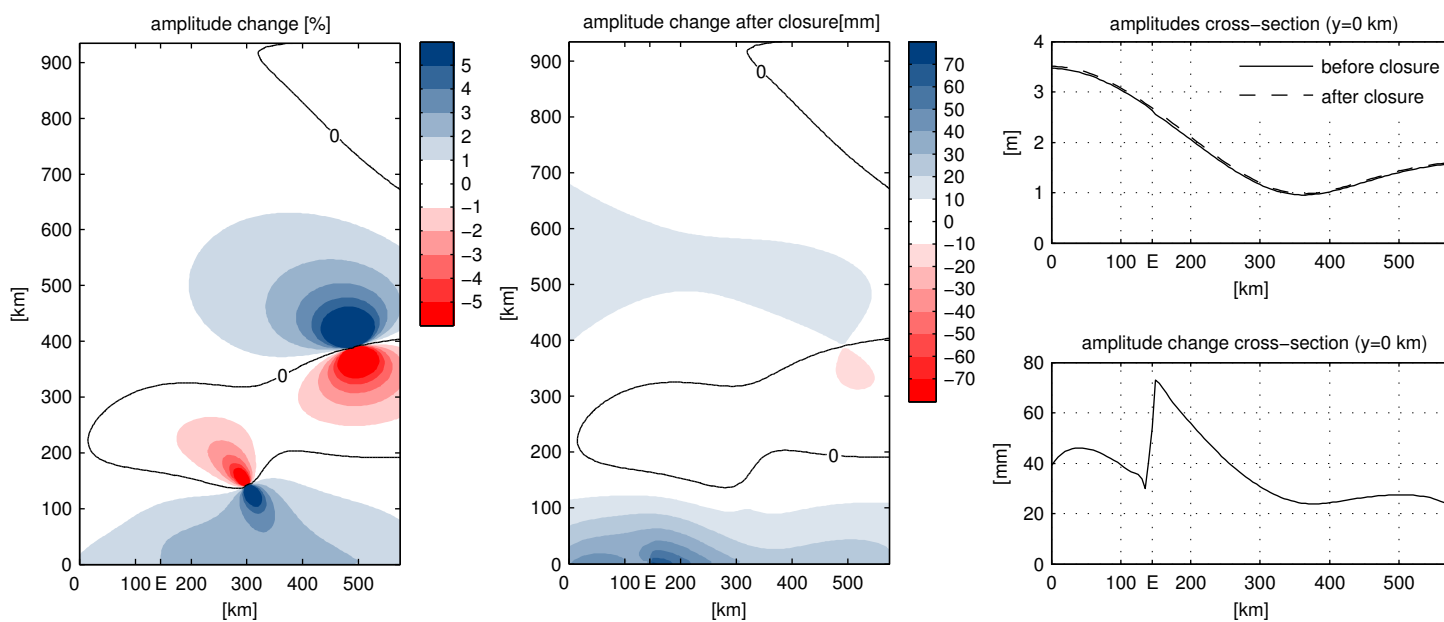


Figure A14.1:  $M_2$  amplitude change after closure of an estuary with  $P=3.3 \cdot 10^9 \text{ m}^3$  located at E (simulation 5)

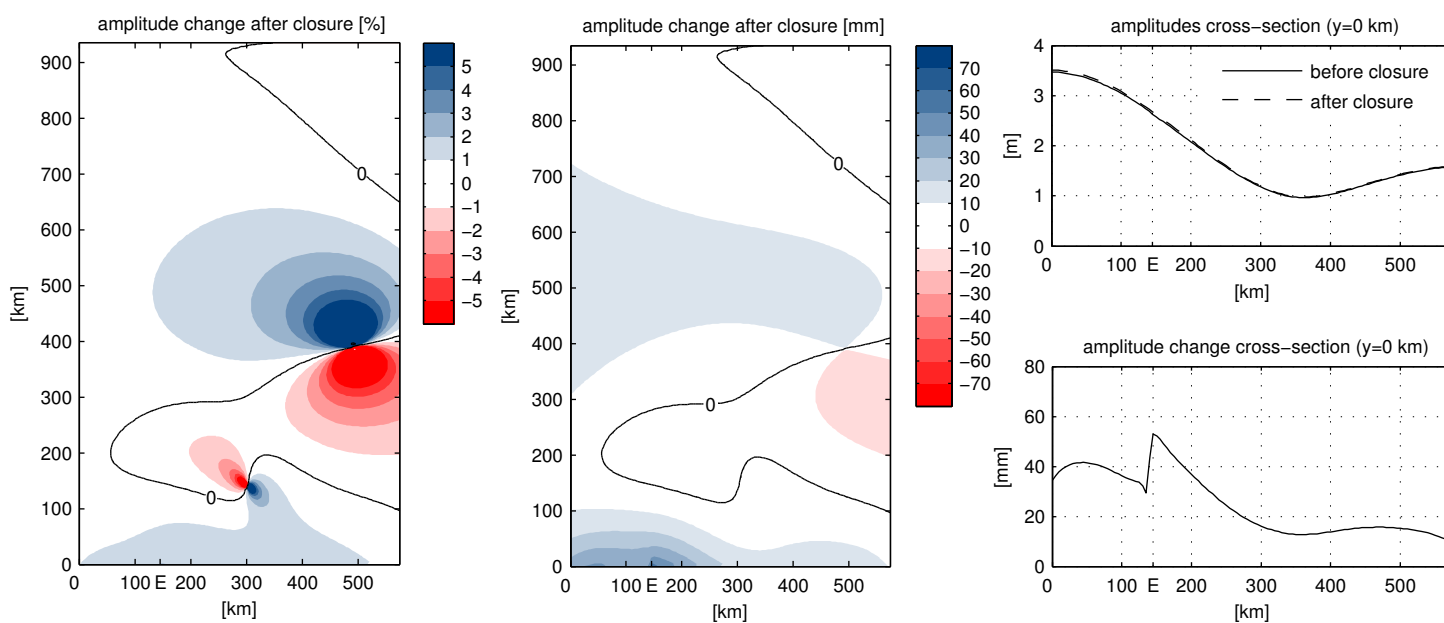


Figure A14.2:  $M_2$  amplitude change after closure of an estuary with  $P=1.3 \cdot 10^9 \text{ m}^3$  located at E (simulation 6)

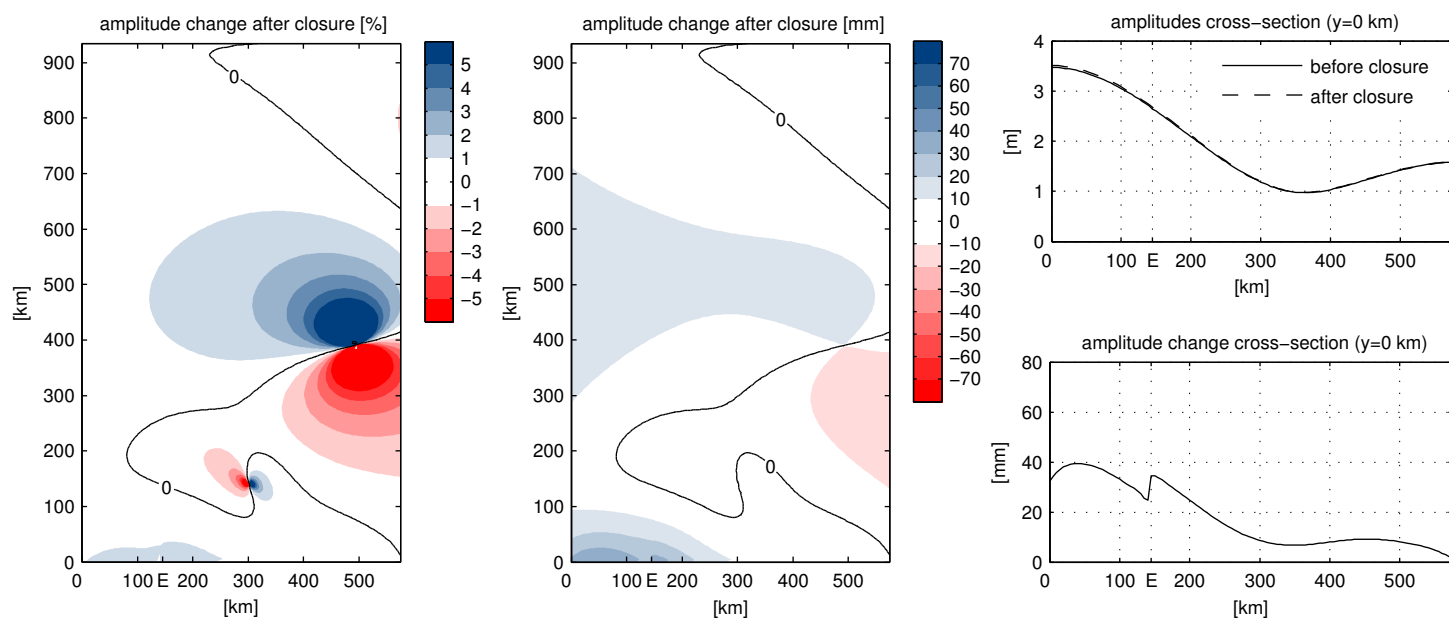


Figure A14.3:  $M_2$  amplitude change after closure of an estuary with  $P=0.7 \cdot 10^9 \text{ m}^3$  located at E (simulation 7)

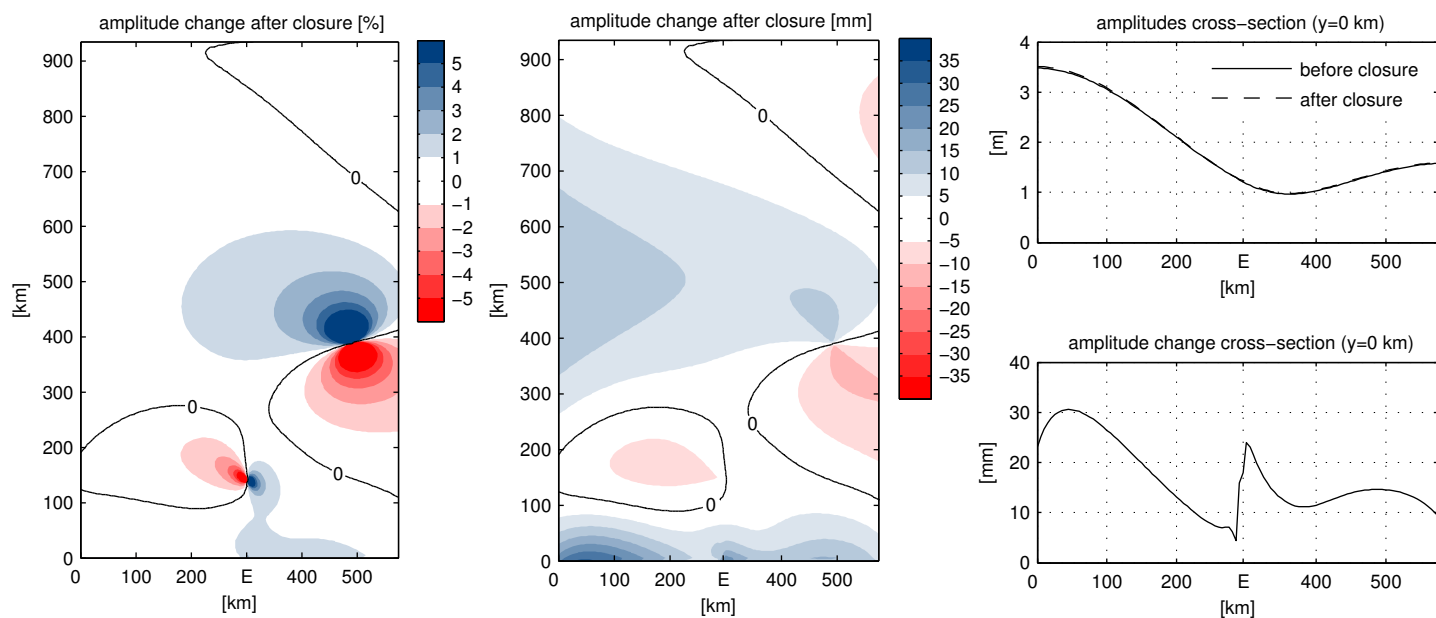


Figure A14.4:  $M_2$  amplitude change after closure of an estuary located at E (simulation 8)

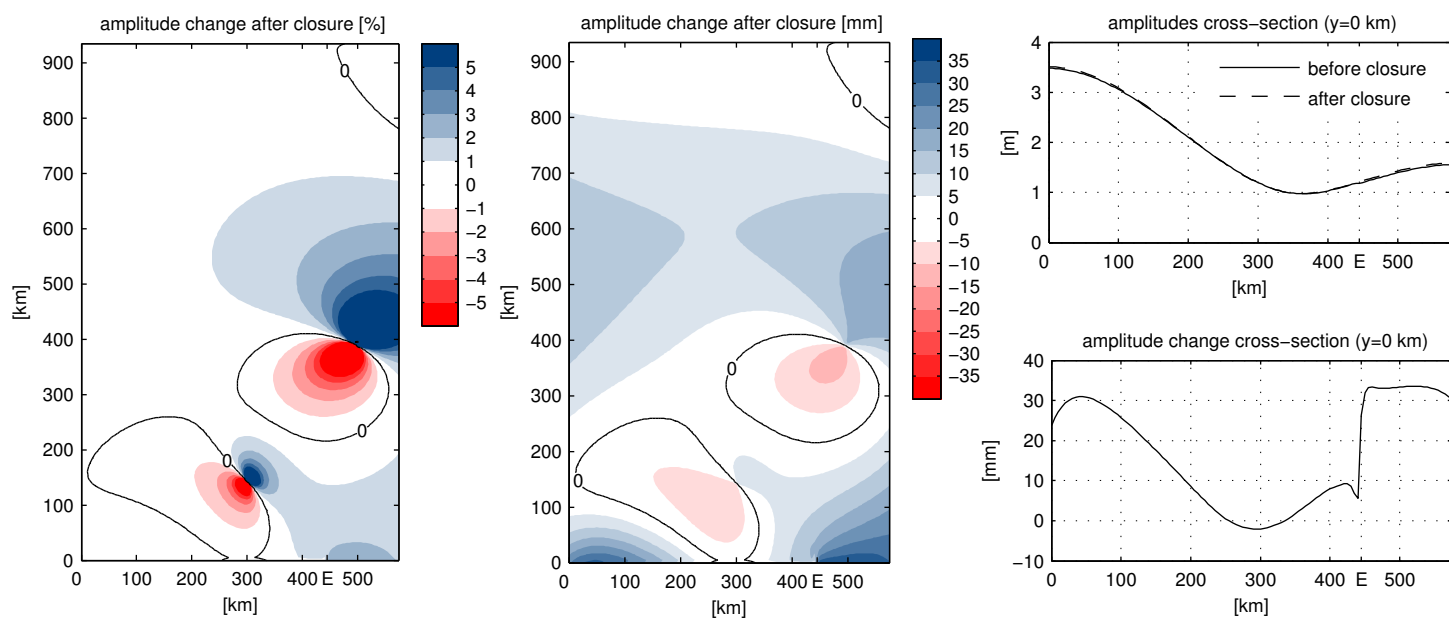


Figure A14.5:  $M_2$  amplitude change after closure of an estuary located at E (simulation 9)

